NANYANG TECHNOLOGICAL UNIVERSITY

CONTINUOUS MICROFLUIDIC PLATFORMS FOR OIL-IN-WATER (O/W) EMULSIONS FOR ENVIRONMENTAL MONITORING APPLICATIONS

DHIMAN DAS

SCHOOL OF CHEMICAL AND BIOMEDICAL ENGINEERING

2016

CONTINUOUS MICROFLUIDIC PLATFORMS FOR OIL-IN-WATER (O/W) EMULSIONS FOR ENVIRONMENTAL MONITORING APPLICATIONS

DHIMAN DAS

School of Chemical & Biomedical Engineering

(SCBE)

A thesis submitted to Nanyang Technological University in partial fulfillment of the requirement for the degree of

Doctor of Philosophy

2016

Acknowledgement

This work could not be completed without help from many people. I would like to thank my supervisor, Professor Vincent Chan, for his visions, support and encouragement throughout the duration of my research. Moreover, I would also like to express my utmost and sincere appreciation to my co-supervisor, Professor Charles Yang Chun, without whose directions, constant support and mentoring, I would not have reached this far. The frequent discussions and his advisory comments from both my supervisors have helped me in shaping my ideas tremendously and have been a valuable experience for me. I would also like to thank my collaborator Professor Kang Yuejun for helping with the cleanroom facilities for the fabrication works.

I also like to thank my lab mates and friends, namely, Mr. Yan Zhibin, Mr. Zhao Yugang, Dr. Zhou Yi, Dr. Jiao Yan Mei, Dr. Phan Dinh Tuan, Dr. Nishanth V. Menon, Mr. Shreyas Kuddannaya, Dr. Muneesh Maheshwari and Dr. Suhanya Duraiswamy, for the fruitful discussions at the crucial junctures. All the good moments we shared while doing experiments are treasures for me.

Lastly, I would like to thank my parents: Mr. Bijit Das, Dr. Nilakshi Das and my sweet sister, Ms. Prerana Das for putting their faith in me and encouraging me to work harder.

Abstract

Microfluidic devices for diagnostic applications are of critical importance to environmental monitoring agencies. In this work, continuous flow microfluidic platforms are designed and evaluated for environmental applications with respect to oil-in-water (O/W) emulsions. O/W emulsions are encountered in an aftermath of oil spills. Use of surfactants can break down the oil spill into droplets of sizes less than 70 microns which are then carried by winds, waves, etc to long distances and are hard to detect. Moreover, the presences of toxic polycyclic aromatic hydrocarbon (PAH) species, such as phenol in oil spills, are readily released by the smaller droplets with enhanced surface area to the surrounding vicinity. This has grave consequences for the environment. Hence, portable diagnostic devices for fast on-site detection of micron-sized oil droplets and PAHs in O/W emulsions are extremely important. In all the experiments reported in this work, a stable emulsion of monodisperse oil droplets in water is generated by using a cross-flow junction and by using surfactants in the water phase.

Now, real-world samples from the field are very complex and require a sample preparation step for solvent extraction and detection. So first, a droplet-based high throughput sample preparation method is presented using a poly (methyl methacrylate) (PMMA)-based microfluidic device for investigating the continuous liquid-liquid extraction (LLE) of phenol from oil. A suspension of phenol in silicone oil is used as a simulator of real-time oil samples containing PAH ions. It is found that for the higher extraction efficiency of the target analyte species like PAH from a highly viscous organic donor phase such as silicone oil droplets onto a less viscous fluid, a lower flow rate ratio

of continuous to dispersed phase is to be preferred. Finally, a hydrophobic polypropylene membrane is integrated into the device for liquid-liquid-liquid extraction (LLLE) of phenol molecules from silicone oil droplets onto the bottom phase via continuous phase.

Second, a novel microfluidic device is developed for the continuous trapping and detection of micron-sized oil droplets using AC electroosmosis (ACEO). An electric field is applied through optically transparent indium tin oxide (ITO) electrodes fabricated on a glass substrate to enable direct visualization of the trapped oil droplets in water. The continuously flowing oil droplets in water are trapped by the opposing AC-driven electroosmotic (ACEO) flow due to the formation of electric double layers because of the deposition of polyelectrolytes. The deposition of these polyelectrolytes is done via a layer-by-layer (LbL) flushing technique and is necessary for the hydrophilization of the polydimethylsiloxane (PDMS) and glass device. An array of SU8 micro-pillars is fabricated within the oil droplet entrapment zone to reduce the hydrodynamic drag force of the incoming fluids. The entrapment efficiency of oil droplets in water is studied as a function of the applied frequency of the electric field. The results suggest the presence of a size-dependent negative dielectrophoretic (DEP) force as the droplets exit the entrapment zone which implies that the entrapment efficiency of the device will be further improved for larger sized droplets as the strength of the DEP force would be higher.

Finally, a multi-module PDMS-based microfluidic device with gold electrodes is presented for achieving two objectives, namely, the continuous pre-concentration of fluorescein ions in the water phase of O/W emulsions and the separation of micron-sized

oil droplets from the same. Fluorescein ions, in the water phase, are used to simulate the presence of PAH ions in O/W emulsions. Once again, PDMS microchannels are hydrophilized using the same LbL technique via flushing with polyelectrolytes. A positive DC-biased AC electric field is employed in both the modules. In the first module, a nanoporous Nafion membrane is used for activating the concentration polarization effect on the fluorescein ions, resulting in the formation of stable ion enrichment zones. In this module, the main inlet is also split into two using a Y-junction so that there are two outlets for the oil droplets. Further downstream, the second module is present which consists of two oil droplet entrapment zones at the two outlets. By activating the appropriate electrodes, anyone of the two oil droplet entrapment zones can be activated and the droplets can be blocked in that outlet. As a result, the oil droplets are released from the other outlet only. In summary, the conclusions from these projects are expected to facilitate the development of microfluidic devices for O/W emulsion systems for emerging technologies concerning portable environmental diagnostic applications.

TABLE OF CONTENTS

Table of Figures

Nomenclature

D_w	Diffusion coefficient in the continuous phase [m^2/s]
D_o	Diffusion coefficient in the dispersed phase [m^2/s]
v	Velocity [m/s]
Q	Volumetric flow rate [m^3/s]
Q_c	Continuous phase flow rate [m^3/s]
Q_d	Dispersed phase flow rate [m^3/s]
V_d	Volume of the droplet [m^3]
V_c	Volume of the continuous phase [m^3]
r_H	Hydrodynamic radius [m]
D_H	Hydrodynamic diameter [m]
R_H	Hydraulic resistance [m^2s/kg]
g	Gravitational acceleration $9.8 m/s^2$
d_H	Dielectric thickness [m]
L	Length of the droplet [m]
W	Width of microchannel [m]
H	Height of microchannel [m]
k	Boltzmann constant, 1.3806488×10^{-23} J/K
A_i	Area of the oil-water interface [m^2]
n	Number of chemical species [mole]
J	Diffusive flux [$moles/m^2.s$]
P	Pressure [Pa]

K	Partition Coefficient
a	radius of particle [m]
t	time[s]
T	Temperature [K]
V	Volume [m^3]
C	Concentration [mol/m^3]
$\vec{E}$	Electric field [V/m]

Greek Symbols

α	dispersed to continuous phase fraction
β	mass transfer coefficient [m/s]
μ	dynamic viscosity [Pa.s, kg/m.s]
γ	Interfacial surface tension [N/m]
$\dot{\gamma}$	Shearing rate [s^{-1}]
θ_Y	Young's contact angle [°]
θ_Y	Effective Young's contact angle [°] under an applied electric field,
ρ	Density [kg/m^3]
t	Residence time [s]
δ	Thickness of the oil-water interface [m]
λ_D	Debye length [m]
ε	Permittivity [F/m]
ε_o	Permittivity of free space, $8.9 \times 10^{(-12)}$ [F/m]
ε_p	Permittivity of the particle [F/m]
σ_m	Conductivity of the medium [S/m]

σ_p	Conductivity of the particle [S/m]
e	Elementary charge [coulomb]
z	Valency of the species.
ζ_P	Zeta Potential [Volt]
ω	Frequency [Hz]

1. Introduction

1.1 Research background and objectives

Microfluidic devices with sensing capabilities for toxic water soluble ions and oil droplets in oil-in-water (O/W) emulsions are of immense importance to the environmental monitoring agencies. In this work, the focus has been on the potential applications of continuous flow "lab-on-a-chip" microfluidic devices for environmental monitoring applications with respect to these emulsions which are formed from oil spills[1]. In the ideal scenario, it would be desirable to have such a portable and accurate device on which real samples can be directly introduced and investigated. This would greatly reduce the sample analysis time as target analyte species would be tested on the site itself. Other advantages of miniaturization[2] using such devices include low sample consumption, precise manipulation and control of small volumes(µL, nL, pL, fL) of fluids due to the laminar flow profile in the microchannels, higher data quality , low risk of contamination by eliminating the need for transportation of samples, reduced reaction times due to enhanced surface area-to-volume ratio, low waste production, etc. Such devices can also be rapidly prototyped.

According to the economists, the microfluidics market is expected to reach $7.5 billion USD by 2020 from $3.1 billion in 2015[3]. There is a strong sense of optimism in the microfluidics/ micro-electro-mechanical (MEMS) research community and industry that someday cheap and disposable cartridges, with microfluidics-based systems, will be readily available which can perform a whole range of *in situ* real-time operations like sample preparation, preconcentration, isolation, separation, detection, etc[2] on the same

platform itself for complex real-world samples. Automated cartridges would offer the advantage of simplicity as the need to use bulky, expensive and complicated instruments would be eliminated. As a result, regular and untrained third parties will also be able to perform diagnostic tests in remote locations as all it will require is the contact or injection of the sample into the cartridge.

In this work, the focus has been on the environmental monitoring applications for O/W emulsions using microfluidic devices. These O/W emulsions are formed from oil spills after surfactants or dispersants have been used to break down the oil slick floating on the surface of water. Usually surfactants such as Corexit EC9500A[4] are used to break down the oil slicks which eventually reduce to oil droplets of sizes less than or equal to 70 microns. Among the compounds present in crude oil, the greatest concern has been the presence of the polycyclic aromatic hydrocarbons (PAHs). The smaller micron-sized oil droplets with enhanced surface area can readily release the PAHs to the surrounding vicinity. Presence of these harmful polycyclic aromatic hydrocarbon (PAH) species in oil spills has grave consequences for the environment. PAHs in these oil spills can permeate the food chain through zooplanktons[5]. Subsequently, these species can also permeate into the higher tropic levels. Even two years after the spill of the Deepwater Horizon (DWH)[1], a study initiated by the National Institute for Occupational Safety and Health, USA has concluded that the workers and the residents involved in the clean-up efforts oil spill[1] are still suffering long-term health consequences such as cancers, liver and kidney diseases, mental health disorders, birth defects and developmental disorders because of the exposure. These problems have continued through 2015. Hence, these hydrocarbon species are extremely dangerous and so early detection from complex oil-in-

water emulsions is essential. Moreover, the micron-sized oil droplets travel a large distance due to the turbulence caused by waves, winds, underwater currents, etc and are hard to detect.

Figure 1: a tugboat moving through the oil slick on May 6, 2010 in the Gulf of Mexico (Reprinted from reference [6] which is in the public domain)

After an oil spill, the standard practice has been to use sample preparation methods for homogenizing the real water samples which is followed by gas chromatography-mass spectrometry(GC-MS) and high-pressure liquid chromatography (HPLC)[7] for finally analyzing the presence of PAHs. The whole process is done in batches and the overall analysis speed is slow. The sample preparation methods are necessary because most analyses are carried out on samples which contain complex mixtures of very small amounts of chemicals that need to be identified. However, real-time samples from the field such as oil spills and waste water are very complex in nature and cannot be analyzed

directly in common analytical instrumentation equipments such as GC, HPLC, capillary electrophoresis (CE) and atomic absorption spectroscopy (AAS). This calls for a need for effective and fast sample pre-concentration method so as to make them more suitable for analysis. With taxing environmental policies and tightening international policies, development of high throughput novel methods of detecting aromatic hydrocarbons in oil-water emulsions is a highly important issue. In this research, a novel way of incorporating a pH gradient-based [8, 9] sample preparation technique using a continuous flow droplet-based microfluidic device for the extraction of phenol (PAH) in oil is reported. For the solvent extraction of polyaromatic hydrocarbons (PAHs) in an aqueous medium, the pH gradient is employed between a donor and acceptor phase. Several works have been published where batch reactors [8, 9] were used for this purpose. Hence, we utilized the same existing pH gradient mode for extracting these hydrocarbon species from oil-in-water emulsions in a microreactor device using droplet-based microfluidics.

As far as the detection of oil droplets in water is concerned, the most commonly used instruments are based on the fluorescence [10-12] properties of the oil. These fluorescence-based oil detectors depend on the absorption-emission spectrum of the oil droplets and are not reliable as the fluorescent signal generated by the equipment does not truly reflect the actual concentration of the oil. Since the equipment is calibrated using specific oils, the concentration yield is relative to those specific oils only. Besides, these equipments are bulky, expensive and process the fluids in batches so overall throughput is slow. Using microfluidic devices, the possibility of trapping micron-sized oil droplets in designated entrapment zones using the forces generated by alternating current

electroosmotic (ACEO) flow field using transparent electrodes has been explored. Using ion concentration polarization (ICP)[13] techniques, pre-concentrating the ions present in the water phase of the O/W emulsion at designated zones of the microfluidic device by using a direct current (DC) biased AC electric field has also been explored. Fluorescent salt dye was used to simulate the presence of PAHs and to observe the enriched ion concentration zones in the water phase of the O/W emulsion flowing through the microchannels.

We used two of the most commonly used polymers for the fabrication of our microfluidic devices: poly methyl methacrylate (PMMA) and polydimethylsiloxane (PDMS). The former requires laser cutting for etching the microchannels using while the later requires soft photolithography. However, both polymers are hydrophobic in nature and it is difficult to perform experiments using O/W emulsions as the oil droplets will stick to the microchannel walls and will eventually choke the device. Hence, appropriate surface modification techniques were implemented for hydrophilizing the surfaces prior to doing our experiments. It would be worthwhile for the researchers to have permanently hydrophilized polymer surfaces in the future so that such steps may be avoided.

1.2 Scopes and Expectations

The main objective of this study is design and fabrication of continuous flow based microfluidic devices for environmental monitoring applications with regard to oil spills. Since the oil spills eventually break down into stable O/W emulsions, an O/W emulsion system will be developed for experimental investigation in this study. To accomplish the objective of environmental monitoring applications, the scopes of the thesis include are the following:

- To fabricate droplet-based microfluidic reactors for continuous liquid-liquid extraction of analyte species such as phenol from oil-in-water (O/W) emulsions as a high throughput sample preparation method for real-time applications.

- To develop a continuous flow microfluidic device for the trapping of micron-sized oil droplets in water in designated oil entrapment zones with micro-pillars using an ACEO flow field.

- To develop an electrokinetic valve for micron-sized oil droplets in O/W emulsions. It acts an oil droplet separation module by incorporating a Y-junction where a positive DC-biased AC electric field is imposed to generate electric forces for blocking the oil droplet flow in the water phase at one of the two outlets of the Y-junction and releasing the same from the other.

- To develop a microfluidic ion enrichment module wherein a novel design is reported for pre-concentrating the ions present in the water phase of the O/W emulsion using the same DC-biased AC electric field in a continuous flow device.

1.3 Organization of the thesis

The complete thesis comprises of the following main sections:

In Chapter 1, an introduction of the background and motivation for this work is given. The environmental concerns regarding oil spills and the need for high throughput continuous flow microfluidic devices for diagnostic applications are briefly reviewed. The objectives and the scope of this thesis research are clearly stated.

In Chapter 2, a diverse literature review for the fundamentals necessary for carrying out this work is given. In this work, the focus has been on the design and fabrication of high throughput microfluidic platforms for oil-in-water (O/W) emulsions for environmental monitoring applications. A cross-flow junction has been used for the monodisperse generation of oil droplets for all the experiments. Hence, initially a detailed literature review to explain the details of droplet-based microfluidics has been provided. Following that; a brief review of the relevant sample preparation techniques and a background study of electrokinetics are presented. Popular microfluidic technologies for environmental monitoring applications are also briefly explained. Finally, the surface modification technique for PDMS hydrophilization has been elaborately discussed.

In Chapter 3, a low width-to-height aspect ratio polymethylmethacrylate (PMMA)-based microfluidic device is reported. The extraction efficiency of phenol from the dispersed phase consisting of silicone oil to the external continuous water phase is studied as a

function of the flow rate ratio of the two immiscible phases. Thereafter, a multilayered membrane-based device is used for liquid-liquid-liquid extraction (LLLME) of phenol molecules from silicone oil droplets (donor) onto the bottom (acceptor) phase via the continuous phase by using the pH gradient between the continuous phase and the bottom phase.

In Chapter 4, a microfluidic device for high-throughput trapping of oil droplets in water by using an AC electric field in a continuous flow is reported. The electric field is applied through optically transparent indium tin oxide (ITO) electrodes fabricated on a glass substrate to enable direct visualization of the trapped oil droplets in water over time. The continuously flowing oil droplets in water are trapped by the opposing AC-driven electroosmotic (ACEO) flow due to the formation of electric double layers because of the deposition of polyelectrolytes. The deposition of these polyelectrolytes is necessary for the hydrophilization of the polydimethylsiloxane (PDMS) reactor. An array of SU8 micro-pillars was fabricated within the oil droplet entrapment zone to reduce the hydrodynamic drag force of the incoming fluids.

In Chapter 5, a microfluidic device is reported wherein a nanoporous nafion membrane is integrated for the pre-concentration of ions present in the water phase of the O/W emulsion near the nafion membrane. A positive DC-biased AC electric field is used instead of the conventional DC electric field for inducing the ion concentration effect as the oil droplets come under the influence of the EOF force and saturate the region between the nafion membrane and the anode under the DC field. This device is also equipped with an oil droplet separation module using a Y-junction where the same DC-

biased AC electric field is used for blocking the oil droplet flow in the water phase at one of the two outlets. This oil droplet separation module essentially acts as an electrokinetic valve for the micron-sized oil droplets in the O/W emulsion.

In Chapter 6, a summary of the major findings and contributions of this work is provided. Directions for further studies are briefly addressed.

2. Literature Review

2.1Droplet-based microfluidics

In our work, we use a cross-flow junction for the generation of oil-in-water droplets. Hence, a literature study of droplet-based microfluidics is given first. Droplet-based microfluidics[14, 15], in itself, is an exciting field of research wherein micro-emulsions are formed by two immiscible fluid phases. Droplets at the micro-scale offer high surface to volume ratios which enhances the heat and mass transfer rates; diffusion distances are shorter as well which makes the reaction rates much faster than ordinary batch reactors. Usually, discrete volumes of the dispersed are obtained by shearing one immiscible fluid into another, forming an interface at a junction. Unlike continuous flow systems, droplet-based microfluidics can create discrete volumes using immiscible liquid which allows us to perform a large number of reactions on a simple platform. The biggest advantage of droplet-based microfluidics is the production of monodisperse droplets with a predetermined size at a controlled frequency. The microfluidic platforms also offer great advantages in reducing the consumption of reagents. The flow of the two liquids, i.e, the continuous and the dispersed phase, is controlled either by volume, using, e.g., syringe pumps or by pressure, using, e.g., hydrostatic reservoirs. This branch of microfluidics has a wide range of applications and has innumerable advantages as the movement of the droplets, once generated, can be manipulated in the sense that it can sorted, merged, splitted and so on; on a microscale platform to a great degree of control and precision. These devices are characterized by the low-Reynolds number flow regime which implies that the mixing by molecular diffusion is rather slow [16] at typical microfluidic channel widths. A continuous flow of droplets formed by an immiscible fluid phase contain

convective flow profiles[17] within them. This enables better mixing profiles and only axial dispersion can be avoided. Droplet microfluidics also offers greater potential for increased throughput due to increased interfacial area of contact and scalability than continuous-flow systems.

Droplet-based microfluidic devices have already been used for a diverse list of applications in the past decade. It has been used in the fields of biology, material science and chemistry. It has been used for the production of polymer particles[14, 18]. Minseok et. al[18]. used a UV-light source for photo-polymerization of monomer droplets and controlled the rate of monomer polymerization by varying the concentration of photo-initiator in the monomer droplets . Having the right concentration of photo-initiator in the monomer droplets will result in polymer particles with a reduced mean diameter than that of the corresponding droplets, a rigid outer "skin" and a liquid inner monomer core. A higher content of photo-initiator, however, led to particle "explosion" due to the large amount of heat released during the polymerization reaction which is not useful. Droplet-based microfluidics has also been used for the production of biological micro-gels[19]. Previously, microgels are obtained by emulsifying solutions of low viscosity monomers or oligomers, which is accompanied by their photo-induced in-situ (on chip) cross-linking or polymerization. Now, microfluidic strategies for the production of polymer particles have offered precise control over the shapes, morphologies, and size distributions of polymer colloids.

2.1.1 Modes of droplet generation

There are two modes of droplet generation- passive and active modes. There are several inlet configurations such as the co-flowing, cross-flowing and flow focusing streams (Fig.2), all of which are passive modes of droplet generation wherein the local flow field is used to break the dispersed phase into droplets. In all cases, the continuous phase liquid preferentially wets the microchannel walls while the dispersed liquid barely touches the micro-channel walls due to the presence of a thin film of the surrounding continuous phase. Liquids are usually Newtonian because it makes the viscous stress exerted at the junction in proportional to the flow field applied. The geometry of the flow field also determines the local flow field that breaks the dispersed phase into discrete droplets. We will discuss the two modes in detail.

2.1.1a Passive mode

In this mode, a shear force is exerted on the emerging droplet by the continuous phase stream. This drag force must overcome the interfacial tension between the two immiscible fluids at the junction, which resists the deformation of the droplet. A number of studies have characterized the droplet breakup in microfluidic T-junctions. This geometry is popular due to the ease with which droplets can be formed and the uniformity of the resulting droplets. Over a wide range of flow rates, the droplet formation is periodic and regular as long as a single T-shaped channel is used. Most T-junction studies fall into one of two groups: those in which the emerging droplet rapidly fills the junction region and is influenced by its confinement within the micro-channel,

and those in which the emerging droplets do not interact with the downstream micro-channel walls and remain unconfined by the micro-channel.

Unconfined droplets do not disrupt the continuous phase flow significantly, and thus their size is primarily controlled by the local shear stress. Confined droplets restrict the flow of the continuous phase liquid to the thin film between the liquid interface and the micro-channel walls. This obstruction leads to increased upstream pressure in the continuous phase liquid, driving pinching of the interface. Nominally, unconfined breakup occurs when the width of the continuous phase channel is much larger than that of the dispersed phase channel. It is likely that both the pinching pressure and the shear stress are important for many microfluidic flow conditions[14].

There are **two distinct break-up regimes** observed both in co-flowing, cross flowing and flow focusing streams: the dripping regime and the jetting regime[20, 21]. In the dripping regimes, the pinch-off occurs near the capillary tip but in the jetting regime, the pinch-off occurs from an extended thread downstream of the capillary tip.

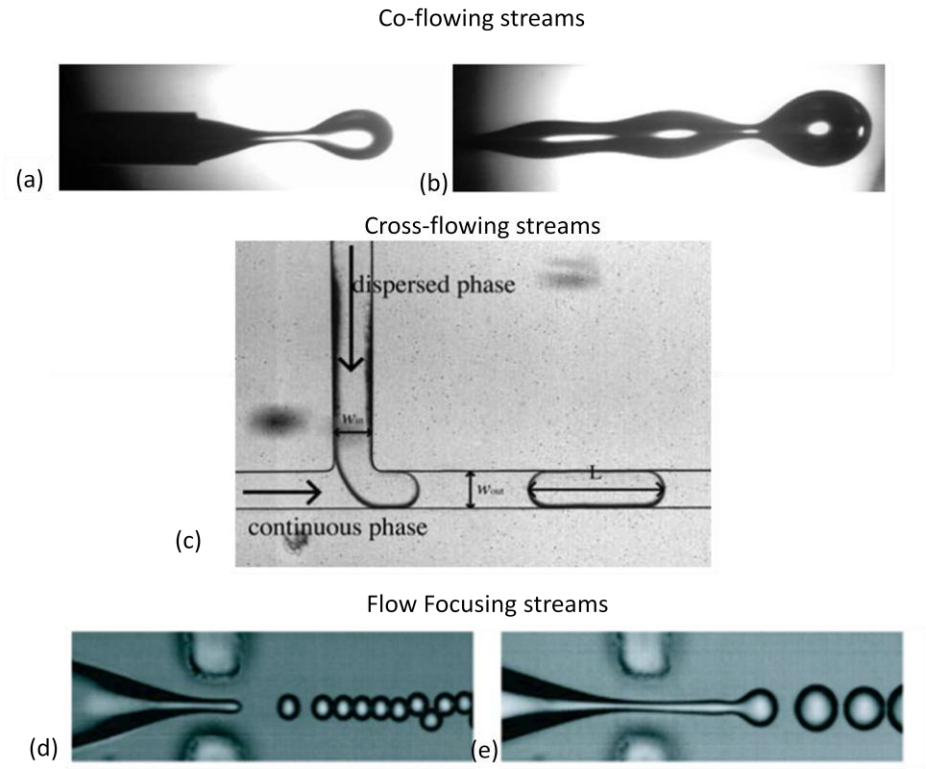

Figure 2: Passive modes of droplet generation: (a), (b) the dripping and jetting droplet break-up regimes in co-focusing streams (Reprinted from reference [20] with permission from Elsevier), (c) the break-up regime in confined T-geometries (Reprinted from reference [22] with permission from Elsevier), (d) dripping and (e) jetting regimes in flow-focusing geometries (Reprinted from reference [23] with permission from American Institute of Physics).

Guillot, et.al [24] predicted a transition from dripping to jetting regime with increase of continuous flow rates above a critical value. Nearly all experimental studies have reported some type of dripping and jetting regimes, and a few studies have reported the observation of other breakup regimes. Within each regime, the droplet size and frequency of breakup also vary with the flow parameters. Hence, the most important outcome of these flow regimes is that it has a significant influence on the droplet volume which is

very important from the reaction engineering aspect. Unlike in co-flowing and cross-flowing configurations, no simple model exists that can predict the droplet size as a function of control parameters in microfluidic flow focusing, in which capillary pressure and viscous stresses are generally significantly more important than inertia.

2.1.1b Active mode

External forces offer additional handles for control over the droplet size and pinch-off frequency. A typical example is the "Drop-on-demand" technology used in inkjet printers. Inkjet printers use a piezoelectric material in an ink-filled chamber behind each nozzle. When a voltage is applied, the piezoelectric material changes shape, which generates a pressure pulse in the fluid forcing a droplet of ink from the nozzle. The ink system requires active solvent regulation to counter solvent evaporation. Viscosity is monitored and a solvent (or solvent blend) is added to counteract solvent loss.

One way of controlling droplets is by actuating the dispersed phase channel by using membranes across a T-junction[25] or by pinching off the channel walls using an electromagnetic valve switch across a cross flow junction[26]. The resulting droplet size is a strong function of actuation frequency and the flow rate ratio used to create the fluid thread. Electric field provides another alternative for generating a monodisperse array of continuous droplet streams. When the electric field is turned on, for sufficiently large voltage differences the oil-water interface begins to deflect and subsequently ruptures. The flow undergoes an interfacial instability in a finite size channel leading to the formation of drops [27, 28]. In this case, the droplet size is dependent on the flow rates and the strength of the electric field. It was reported that as the voltage difference

increases, the drops become smaller. However, as long as the voltage difference and flow rates are held constant, not only the drop size but also the speed of the drops and the distance between consecutive drops remain constant over time.

2.1.2 Dimensionless parameters

There are several fluid forces involved for droplet break up in the passive mode such as viscous stress, capillary pressure, inertia, buoyancy and interfacial surface tension. Several key dimensionless numbers are used to characterize the relative importance of each of these fluid forces. The most important of these is the capillary number, $\mathbf{Ca=\mu v/\gamma}$ [21]where $\boldsymbol{\mu}$ is the kinematic viscosity and $\boldsymbol{v}$ is the characteristic mean velocity of the fluids and $\boldsymbol{\gamma}$ is the interfacial tension between the two phases. This number highlights the ratio of the viscous stresses to the stress imposed by the interfacial tension between the two immiscible fluids. The Reynold's number, $\mathbf{Re=\rho v D_H/\mu}$ [14] where $\boldsymbol{D_H}$ is the hydraulic diameter of the micro-channel. This number highlights the ratio of the inertia to the viscous stresses. Typically, microfluidic length scales lead to Re<<1. Another dimensionless number is the Weber number, **We=Re.Ca** which is a measure of the relative importance of the fluid's inertia compared to its surface tension. Another important parameter is the Bond number, $\mathbf{Bo=D_\rho g w^2/\gamma}$ where $\mathbf{D_\rho=\rho_d-\rho_c}$ is the density difference between the two immiscible fluids, **w** is the micro-channel width. This number characterizes the relative importance of buoyancy and the surface tension. For oil-water emulsion systems in microfluidics, the density difference is usually very small. Hence, the Bond number, Bo is significant in droplet formation in microfluidic devices[14].

2.1.3 Droplet-based microfluidic extraction

Droplet-based microfluidics offer great control over reaction kinetics. Factors which can influence reactions rate are droplet size, velocity and temperature. Reactions can be performed much more quickly due to short diffusion and heat and mass transfer distances. Mixing inside micro-droplets also benefits from the internal vortex circulation directed by channel geometry. Moreover, as the interface is continuously regenerated between continuous and dispersed phase, this help in further improving the mass transfer process. In particular, several studies have been conducted to quantify the mixing in droplets. The mixing dynamics was typically analyzed by fluorescence microscopy but lately fluorescence lifetime imaging was also employed to reconstruct mixing patterns with upto 5 μs[29] and 1 μs [30] time resolution.

A study of microfluidic droplet-based liquid-liquid extraction[31] was reported between continuous(octanol) and dispersed phase(water) using fluorescent dyes. Mass transfer driven by the chemical potential difference of fluorescent dyes was analyzed. The study was conducted without the involvement of any chemical reactions. They studied the extraction of fluorescein from the external phase as well as the rejection of rhodamine from the droplets onto the external phase and established a law that determines the time it takes to reach the equilibrium, a crucial quantity for the extraction technique. It was established experimentally that the characteristic time of diffusion for reaching equilibrium between the immiscible phases is given by $\mathbf{t_D = h^2/D_w}$ where h is the height of the channel and D_w is the diffusion coefficient of the continuous phase obtained from

Wilke-Chang equation[32], a result apparently independent of the diffusion constant within the droplet. For each experiment, the final radius of the droplet is kept constant.

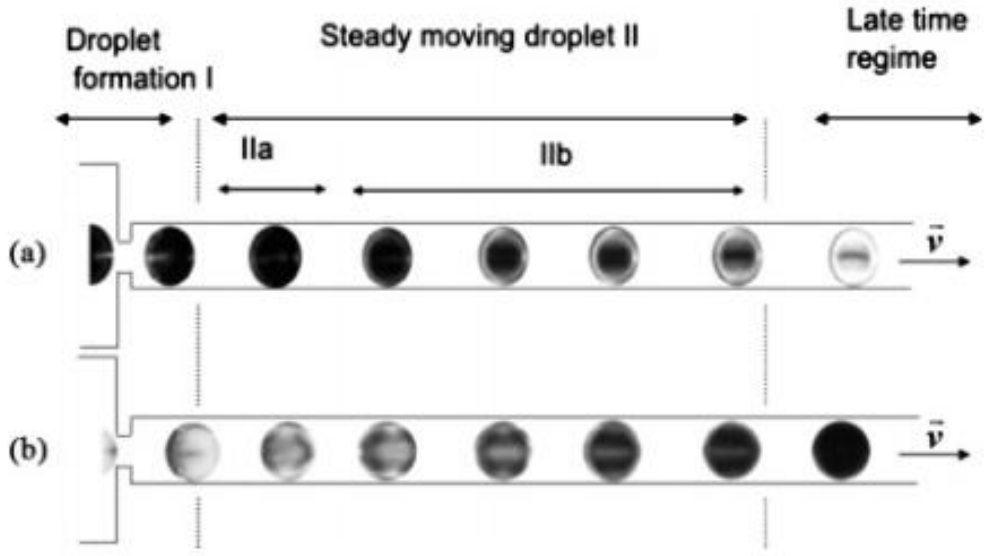

Figure 3: Fluorescence image of droplets at different times in the channel in configuration A: respectively, extraction, droplet composed of a mixture of water/60 wt % glycerol wherein ions are extracted from the continuous phase to the droplet, and B: purification, wherein ions are extracted from the water droplet to the continuous phase (Reprinted from reference [31] with permission from American Chemical Society).

Burns, et.al [33] studied the diffusion rate between immiscible slugs by monitoring the extraction of acetic acid from kerosene slugs as they moved along the reactor channel. The slugs were created in a T-junction geometry. The aqueous phase having molecules of NaOH or KOH reacted with acetic acid in an organic phase as the latter diffused across the interface. Analysis of the titration within the microreactor was performed through measurements of the distance along the channel at which the pH indicator in the aqueous phase changed its color. It was observed that increasing the flow speed reduced the time

required for color change. The reaction rates were also found to depend on both the concentration ratios of the acid and bases, and the length of the alternating segments. Smaller segments are expected to have a higher reaction rate due to their greater surface area to volume ratio, which will enhance the diffusion- dependent reaction process.

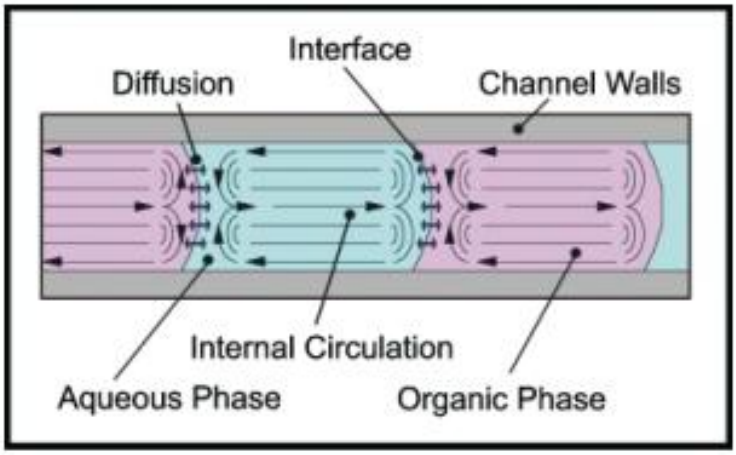

Figure 4: Internal circulations between immiscible phases along the interface (Reprinted from reference [33] with permission from Royal Society of Chemistry).

They also reported[34] the nitration of benzene and toluene in a microreactor having the same configuration. Slug lengths of around 1.6 mm were generated in this device using a mixture of silicone oil and kerosene (dyed dark blue) for the organic phase having benzene and toluene or water for the aqueous phase having HNO_3 and H_2SO_4. The basic mechanism uses H_2SO_4 to catalyze the generation of NO_2^+ ions from HNO_3. These attack organic molecules passing across the interface into the aqueous phase, producing nitrated product that diffuses back into the organic phase. Analysis of the microreactor performance was measured by looking at the color change behaviour along the aqueous

and organic phase interface under the microscope. Output from the reactor was collected in a sample bottle containing aqueous and organic solvents.

2.2 Effect of viscosities on microfluidic emulsification

Nie et.al[21] reported the role viscosities in emulsification. It was noted that highly viscous liquids emulsified into larger droplets with lower polydispersity and although it was not possible to provide a unified scaling for the volumes of the droplets, the break-up dynamics of the lower viscosity fluids resembled the rate-of-flow-controlled break-up more accurately. They examined the effect of viscosity of the dispersed phase on the droplet formation by emulsifying silicone oils with viscosities 10, 20, 50, 100 and 500 cP. Depending on the flow rates of the two immiscible liquids and on the properties of the dispersed (inner) phase, emulsification occurred in two different modes - a dripping and a jetting mode.

Three regimes of droplet formation were observed by increasing the flow rate of the inner phase progressively- (a) the dripping regime (R1) in which the droplet thread covered most of the cross-section of the microchannel. After each break-up the thread broke in the orifice, and after each break-up the tip of the discontinuous stream retracted upstream of the orifice, to the end of its inlet channel. (b) The dripping regime (R2) in which the break-up occurred either in the orifice, or slightly upstream of it, but the tip of the discontinuous stream did not retract to its inlet, but stayed at the inlet to the orifice and immediately reentered it for a successive break-up. In this mode, the thread of the inner phase did not always occupy the entirety of the cross-section of the orifice. (c) In the

jetting regime (R3), a continuous thread of the inner phase extended into the outlet channel and broke far (several widths of the orifice) downstream of the orifice.

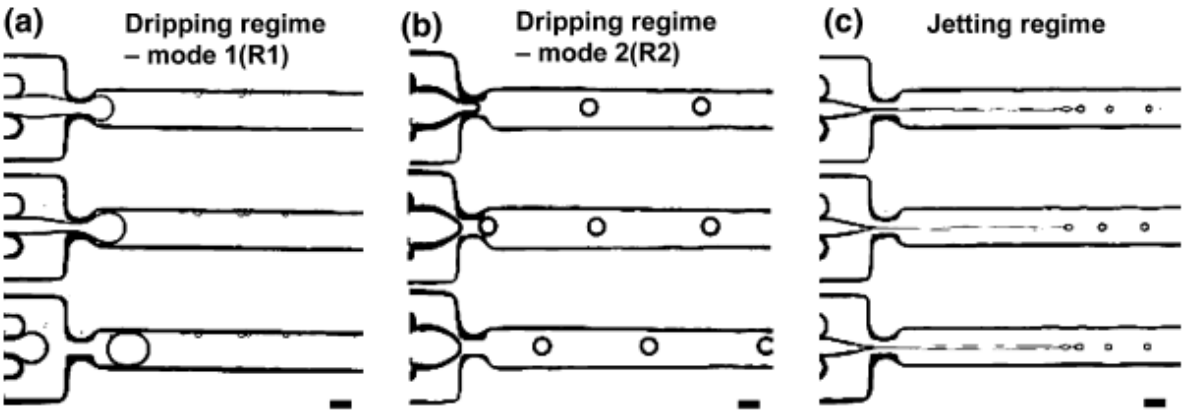

Figure 5: Snapshots of the three different stages of droplet formation (Reprinted from reference[21] with permission from Springer).

The major features of these three regimes of droplet formation are featured in the table[21] (with permission from Springer) given below:

Significant features	Dripping regime—mode 1 (*R1*)	Dripping regime—mode 2 (*R2*)	Jetting regime
Flow rates	Low Q_o and Q_i	Moderate Q_o and Q_i	High Q_o and Q_i
Breakup point	*Inside* the orifice	*Inside* or *behind* but close to the orifice	*Behind and far away* the orifice
Size distribution	Narrow, CV < 3%	Depends on viscosity of droplet phase. In a particular window of flow rates CV < 1.8–2%;	In a particular window of flow rates 1.5 < CV < 8%. Droplets with broad size distribution can be formed
Droplet size and shape	Much larger than the orifice width; discoid shape	Comparable to the orifice width; discoid or spherical shape	Comparable or smaller than the orifice width; spherical shape

It was explained that low viscosity oils followed the rate of flow controlled mechanism i.e volume of the droplet, $\mathbf{V_d = aQ_d/Q_c}$ where a is a constant and Q_d, Q_c are the flow rates of the dispersed and continuous phase, respectively. However, fluids with higher viscosity departed from the rate-of-flow mechanism, that is, the larger the viscosity, the smaller the dependence of droplet volume on the ratio of the rates of flow. Also, the coefficient of variation (CV) is more for the higher viscosity oils as the droplets were significantly larger and inconsistent. To explain the variability in experiments with similar viscosity ratios, it was concluded that the gradients of the concentration of surfactant on the interface impacted the dynamics of the drop formation process.

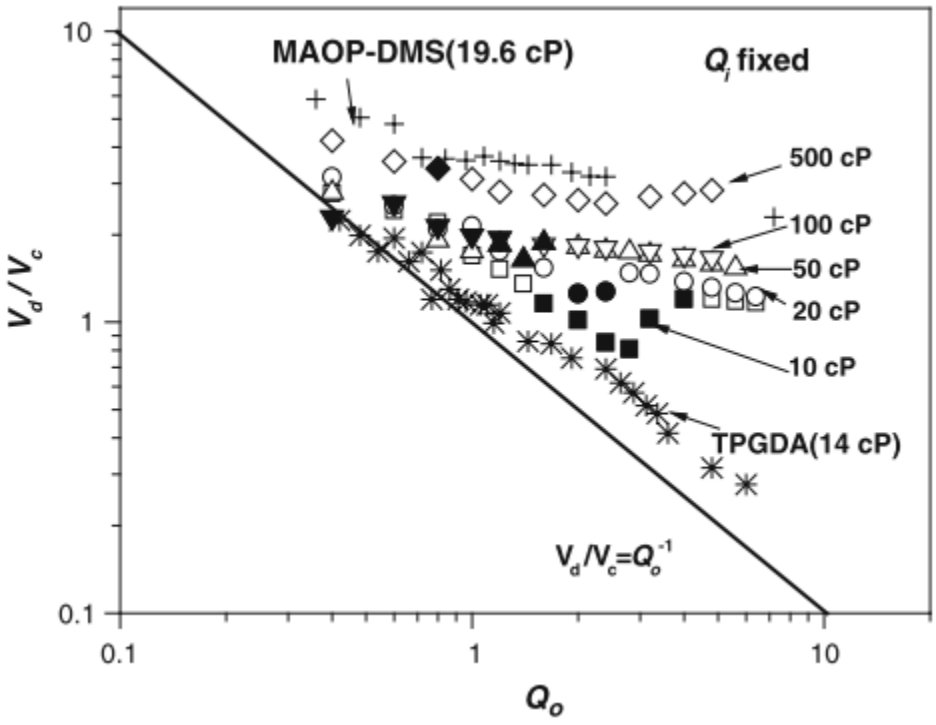

Figure 6: Rate-of-flow controlled mechanism (Reprinted from reference[21] with permission from Springer). A log-log plot of the variation in the dimensionless droplet volume, Vd/Vc (defined as droplet volume Vd divided by the cube of orifice width Vc) of dispersed phase plotted as a function of water flow rate, Qo , for constant flow rate 0.04 ml/h of the droplet phase for the following dispersed phase fluids in 2.0 wt% SDS aqueous solution: Monomers tripropyleneglycol diacrylate (TPGDA), dimethacrylate oxypropyldimethyl siloxane (MAOP-DMS) and the rest were silicone oils of varying viscosities: from 10 to 500 cP.

The Weber number (We = Re.Ca) which is defined as the ratio of the fluid's inertia to the interfacial tension was approximately 0.0015~0.40; since We < 1, it was implied that the interfacial tension forces dominate inertia.

Finally, the dimensionless droplet volume was plotted as a function of capillary number, Ca for a fixed value of continuous to dispersed phase velocity of 60. The capillary number (Ca) represents the relative effect of viscous forces versus interfacial tension acting across an interface between two immiscible fluids. It can be clearly observed from the figure below that the volume of droplets for higher viscosity fluids were independent of the flow rates such as for 100 and 500 cP. However, for lower viscosity fluids, it was observed that $\mathbf{V_d/Vc \propto Ca^n}$, where n<1. Overall it was observed that the volume of all droplets in a region where the value of exponent **n** varied between 0 and (-1/2).

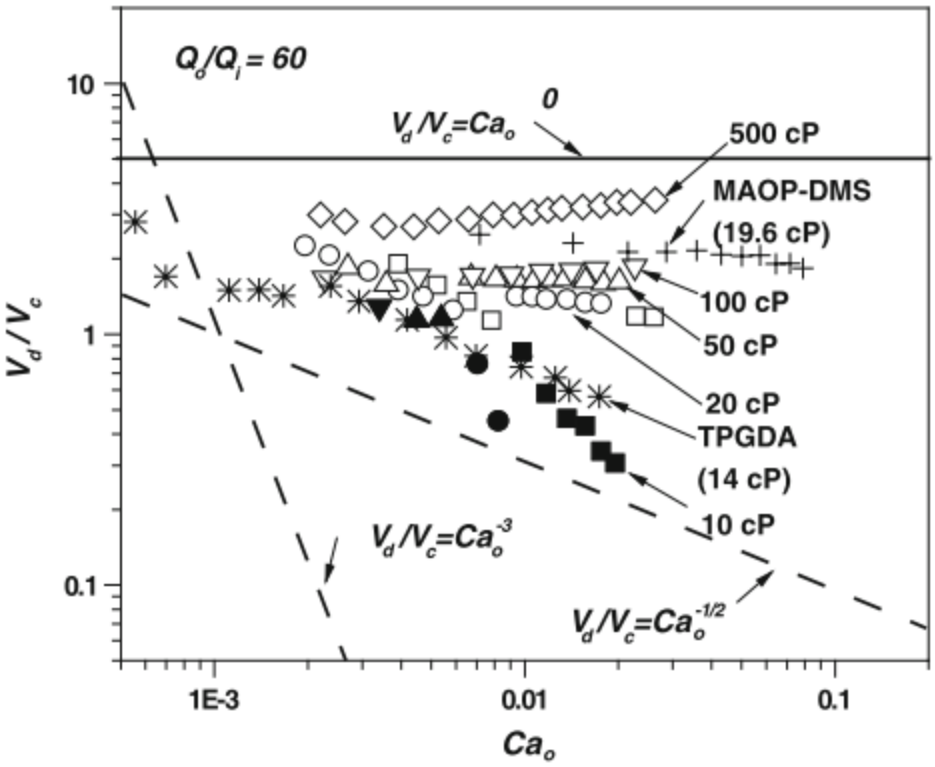

Figure 7: A log–log variation in the dimensionless droplet volume, Vd/Vc plotted as a function of capillary number Cao of the continuous phase (Reprinted from reference [21] with permission from Springer).

2.3 Pressure drop hydrodynamics in droplet-based microfluidics

In microfluidic flow-focusing[35] and T-junction devices[36], it has been established that the length of the droplets and slugs is primarily determined by the flow rate ratio between the continuous and dispersed phases. In other words, the most dominant parameter which influences the size of the droplets is the inlet pressure exerted by the two phases. However, there is another parameter which influences the length of the plugs or size of the droplets which is the contribution to the overall pressure drop due to the individual phases downstream of the capillaries[37]. Hence, the total length of the microchannels also plays a role.

There are two regimes[37] of droplet formation along the microchannel length – one where a thin film is deposited along the channel wall (if the continuous phase does not wet the microchip material completely) and the other without the film (if the continuous phase wets the microchip material completely.

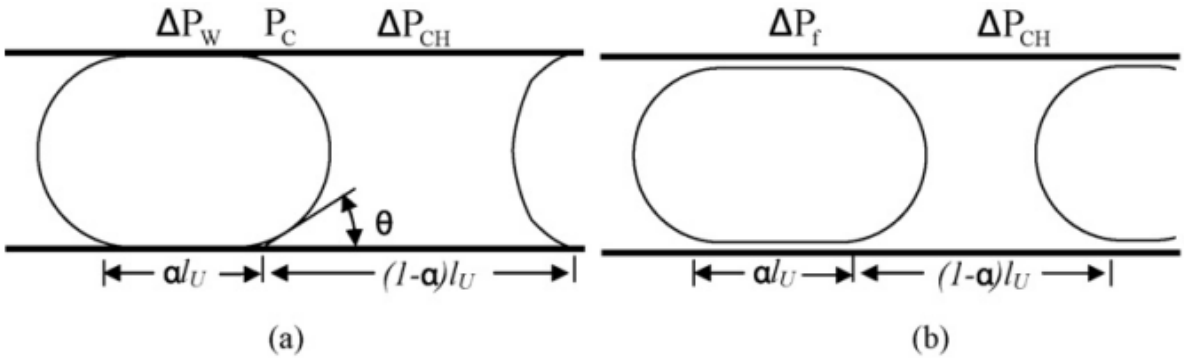

Figure 8: Pressure drop along the side view of a single droplet a. without and b. with film (Reprinted from reference [37] with permission from Elsevier).

In fig.8, Kashid et.al [37] demonstrated the formation of water plugs in cyclohexane and explained the pressure drop model along the length of PTFE micro-capillaries. The overall pressure drop for case (a) along its length can be written as:

$$\Delta P_v = \Delta P_H + \Delta P_C = \Delta P_W + \Delta P_{CH} + \Delta P_C$$

ΔP_H denotes the hydrodynamic pressure drop calculated from the Hagen–Poiseuille equation, while ΔP_C denotes the capillary pressure drop obtained from the Young–Laplace equation for a cylindrical tube. The hydrodynamic pressure drop term, ΔP_H can be further split into the continuous and dispersed phase which is water (W) and cyclohexane (CH).

$$\Delta P_W = \frac{8\mu_w u \alpha l_u}{r_H^2}, \Delta P_{CH} = \frac{8\mu_w u(1-\alpha) l_u}{r_H^2}, \Delta P_C = \frac{2\gamma}{r_H^2} cos\theta$$

μ_W and μ_{CH} is the viscosity of water and cyclohexane, respectively ; u is the flow velocity while α is the water phase fraction. Dynamic contact angle θ must be calculated from the side view of the droplets. The equations for the pressure-drop above are defined for circular cross-section. The flow-pressure relation in pressure-driven channels is simplified as $Q = \Delta p / R_H$ where R_H is the hydraulic resistance and defined for a cylindrical cross-section given as $R_H = \frac{8\mu l}{\pi R^4}$. In microfluidic networks, however, most channel geometries are rectangular. For non-circular channels, the channel radius R is replaced with the hydraulic radius r_H or diameter $D_H = 2r_H$. The hydraulic radius of the channel r_H [m] is a geometric constant defined as $r_H = 2A/P$, where A [m^2] is the cross-sectional area of the channel and P [m] is the wetted perimeter. However, this estimate gives about 20% error and thus it isn't much satisfying. Another solution for obtaining

the hydraulic resistance is by solving the incompressible Navier-Stokes equation for uniform-viscous Newtonian fluids which comes out as

$$R_H = \frac{12\mu l}{wh^3\left(1 - \frac{h}{w}\left(\frac{192}{\pi^5}\sum_{n=1}^{\infty}\frac{1}{(2n-1)^5}tanh\left(\frac{(2n-1)\pi w}{2h}\right)\right)\right)}$$

When the aspect ratio (h/w<1) is high[38], the Fourier series can be truncated at the first harmonica (n = 1) since the other terms become negligible and the simplified formula is obtained as .

$$\mathrm{R_H} = \frac{12\mu l}{wh^3}\left[1 - \frac{192}{\pi^5 w}\tanh\left(\frac{\pi w}{2h}\right)\right]^{-1}$$

This equation is accurate to within 0.26% for any rectangular channel that has h/w > 1, provided that the Reynolds number Re is below 10^3. Inserting this into the flow-pressure relation in pressure-driven channels $Q = \Delta p/R_H$, the pressure drop term is obtained as

$$\Delta p = \frac{12\mu l Q}{wh^3}\left[1 - \frac{192}{\pi^5 w}\tanh\left(\frac{\pi w}{2h}\right)\right]^{-1}$$

which is the Hagen-Poiseuille's law used to describe the flow in rectangular microfluidic channels.

Anna et.al[39] exploited the relationship between pressure drop and the length of the microfluidic channel to facilitate the break-up of droplets with controlled polydispersity. Under typical operating conditions, polydispersities of less than 5% and usually between 1% and 3%, was achieved. A T-junction was placed further downstream of the microchip which introduced a high pressure stagnation point splitting the droplets into two daughter droplets. Sufficiently long droplets always break at the T junction independent of the flow rate. In his experiments, the main microchannel was split into two side-arms further

downstream and the asymmetric breakup of droplets was accomplished by adjusting the relative lengths, l_1 and l_2, of the side channels.

To explain this behaviour, an analogy was drawn between microfluidics and electric-current-splitting device where the flow rate in each channel, q_1 and q_2 are analogous to an electric current, and the pressure drop Δp is analogous to a voltage.

To find the analog of resistance for a fixed flow rate q down a channel of width w, height h, and length l, the pressure drop is first calculated as $Dp = \beta ql$ where β is a constant directly proportional to $\eta(3/4)[1/(wh^3)][1-6(2/P^5)(h/w)]^{-1}$. The electric circuit analog to the resistance is then given by βl. Hence the shorter arm offered lower resistance and could accommodate longer droplets and vice versa. That is, the ratio of the flow rates in the arms is then inversely proportional to the ratio of lengths q_1/q_2 is directly proportional to l_2/l_1. In addition, the ratio of volumes of the two daughter droplets, V_1 and V_2, is proportional to the ratio of volume flow rates. However, it was observed that smaller droplets do not break if they are traveling too slowly down the channel, and instead flow alternately into each of the side channels. This technique had the advantage that it is passive, requiring no moving parts.

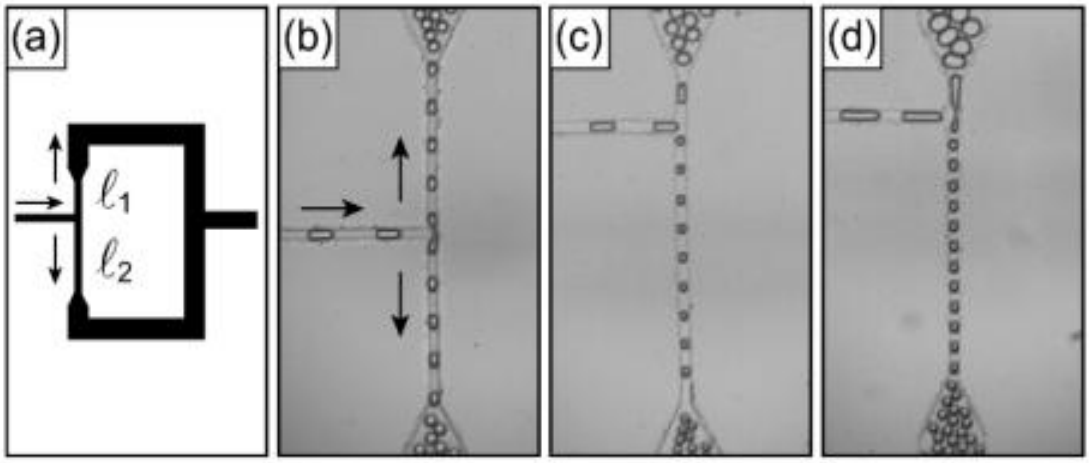

Figure 9: Passive breakup of the droplets at the T junctions as droplets flow into a T-junction. Breakup shows that the volume of the daughter droplets are a function of the side-arm lengths (Reprinted from reference [39] with permission from American Physical Society).

In fig.9 (a), the flow is split into two side-arms. The narrow portion of the two side arms, of lengths l_1 and l_2, control the relative flow resistance of the paths and, hence, each droplet splits into two daughter drops as shown in the fig. (b),(c) and (d).

The ratios of arm lengths are, respectively, l_1:l_2 are 1:1, 1:5:2, and 1:8:1, corresponding to daughter drop volume ratios of (b) 1:1,(c) 1:5:2, and (d) 1:7:5. This method offers much flexibility in adjusting the size of the droplets as daughter droplets with a pre-determined size ratio can be generated.

Simon et.al [40] used a net Laplace pressure on the droplet by the front and back curved surface so as to passively trap the droplets. This net force is balanced by the hydrostatic pressure exerted on the droplet by the flowing continuous phase from the back side.

The Laplace pressure for a given interface is defined by the Young-Laplace equation is given by $\Delta P=2\gamma/r$ where γ is the interfacial tension between the two phases and r is the radius of curvature at the interface. If a droplet enters a narrowing channel, the front of the droplet will experience a different Laplace pressure than the back of the droplet due to the changing cross-sectional area of the channel. This difference induces a net force on the droplet as a result of the difference in the radius of curvature between the front and back of the droplet. This impedes the droplet's forward progress. When this force is balanced by the hydrostatic pressure (Hagen-Poiseuille pressure drop for rectangular channel) which is the force applied to the droplet by the continuous phase that is pushing the droplet forward, the droplet will slow down dramatically and eventually stop, as the two forces become equal and opposite to each other.

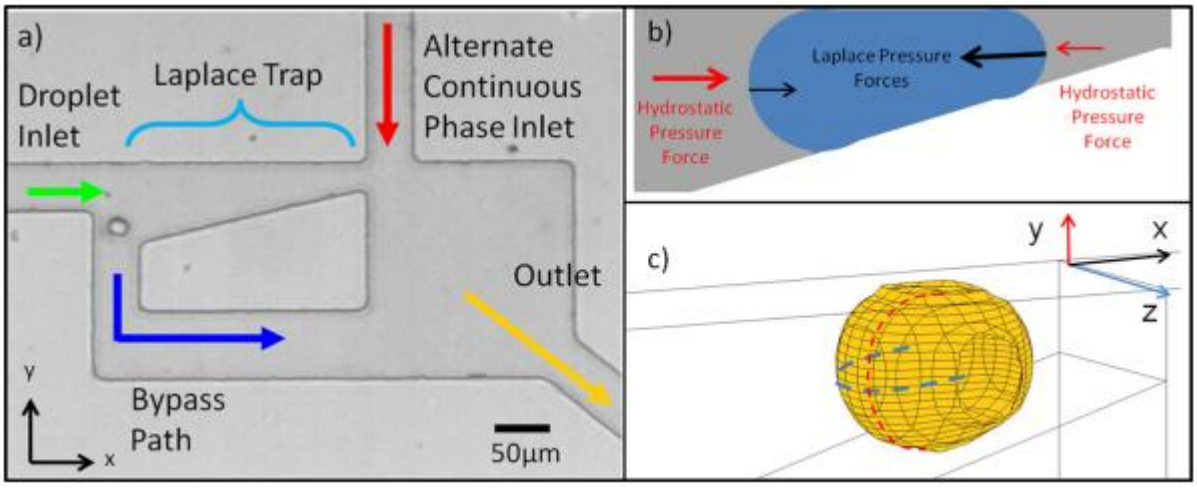

Figure 10: Laplace pressure trap (a) depicts the direction and location of the forces on a droplet inside the trap. (b) illustrates the balancing of the direction of the Laplace pressure forces acting across the interfaces of both the front and back of the droplet (black) and hydrostatic pressure forces, supplied by the continuous phase in the microfluidic channels (red). Arrow size shows relative magnitudes of the forces. (c)

illustrates the axis system of Laplace pressure forces on a droplet constricted in the trap (Reprinted from reference [40] with permission from American Institute of Physics).

If there is a change in the dimensions of microfluidic channels, as for instance in Fig3(a), the droplet is no longer a sphere which causes a change in the radius of curvature at the junction. This induces a net Laplace pressure in the direction of the larger dimension. The intention of the current work is to investigate the feasibility of sample preparation techniques as well as detection of analyte species in oil droplets on a microfluidic chip. The next chapter reports a literature review of Solvent Micro-Extraction (SME) most of which is reported, thus far, in batch reactors.

2.5 Background study of liquid-liquid micro-extraction (LLME), a solvent micro-extraction method (SME)

In the Chapter 3 of the report, the two processes, namely, liquid-liquid microextraction (LLME) and continuous membrane separation process were implemented together on a PMMA chip for continuous and droplet-based extraction of target analyte species from oil as a high-throughput sample preparation method. In that chapter, however; we used silicone oil droplets moving over a membrane, instead of crude oil, for the simplicity of experiments and also studied the effects of viscosity of the oil droplets on the microextraction efficiency of the process. The need for sample preparation via solvent micro-extraction (SME) methods come from the fact that most analyses are carried out on samples containing complex mixtures of very small amounts of chemicals that need to be identified. However, real-time samples from the field such as oil spills and waste water

are very complex and cannot be analyzed directly. Hence, elimination of unnecessary solvents is required via microextraction techniques. SME is a fairly recent development and has been successfully complemented with most common analytical instrumentation equipments such as gas chromatography (GC), high-performance liquid chromatography (HPLC), capillary electrophoresis (CE) and atomic absorption spectroscopy (AAS). However; so far, Solvent Micro-Extraction methods (SME) have been done offline and off the chip. To achieve, the true potential of portable microfluidic devices, SME methods must be integrated on the microfluidic platform itself for quantifying the analytes in complex mixtures which may be followed by standard electrokinetic detection techniques[41].

The different modes of Solvent Micro-Extraction (SME) have been discussed in detail by John et.al [42]. Within the scope of our work for employing SME with respect to O/W emulsions on microfluidic platforms, the most relevant mode is liquid-liquid microextraction (LLME). LLME is essentially a variation of the two-phase liquid-liquid direct contact immersion mode. There are several variations of the direct immersion mode which have been published in literature. Three of the most common direct immersion modes include : single drop microextraction (SDME)[43], hollow fiber protected microextraction (HFME) and dispersive liquid-liquid microextraction (DLLME). These three modes will be discussed briefly. Thereafter, liquid-liquid microextraction (LLME) will be discussed and compared to these methods.

The first paper on **single drop microextraction (SDME)** was published in 1997 by Jeannot et.al [44] which involves the extraction of sample with a single microdrop of

solvent suspended at the tip of a syringe. A microdrop (organic solvent) is suspended at the end of a needle, which is immersed in a aqueous phase having the analyte species. At the end of the experiment, the microdrop is pulled back into the needle by withdrawing piston of the syringe. It is then injected into GC/HPLC for quantification depending on the analytes which are being investigated. The extraction of several organic species has been proven to be defined by first order rate law kinetics [44]. In addition, the effects of stirring rate and sample diffusion coefficient on the mass transfer coefficient have also been investigated. The microdroplet can be assumed to be the receiver phase and the surrounding aqueous solution can be considered to be the donor phase.

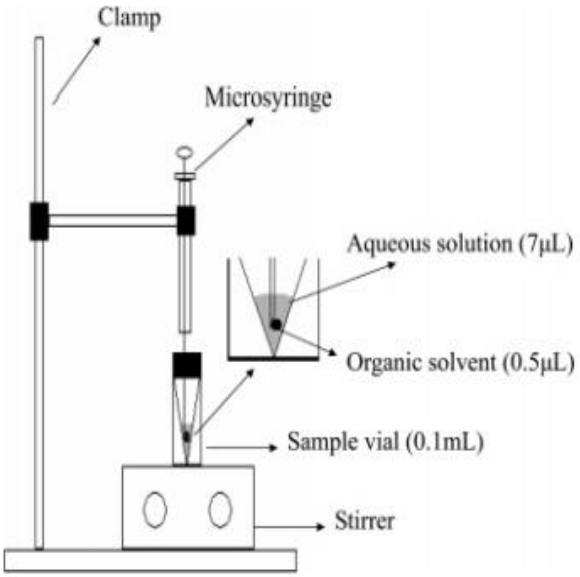

Figure 11: Illustration showing the mass transfer of solvent extraction into a Single Drop at the tip of a syringe Needle (Reprinted from reference[43] with permission from American Chemical Society).

Now, the mass transfer of analytes from the donor to the receiver phase occurs by convective-diffusive mechanism, however, it is limited by the presence of a thin film

adjacent to the interface. This theory was first proposed by Nernst [45]. At a distance, δ_{aq}, away from the liquid-liquid interface , complete convective mixing occurs in the bulk solution. This thin film is known as the Nernst diffusion film. Mass transfer across thin film is a purely diffusive process. At steady state, the aqueous phase mass transfer coefficient is given by $\beta_{aq}=D_{aq}/\delta_{aq}$. [44]. At faster stirring rates in the aqueous phase, the thickness of the Nernst diffusion film decreases, as a result, the overall mass transfer coefficient also increases. Microextraction reactions carried with and without stirring the donor phase is referred to as dynamic and static extraction mode, respectively[42]. However, a major issue with the SDME mode is the stability of the droplet attached to the needle. Also, surface area of a single droplet is quite small.

In **hollow-fiber based microextraction,** an organic solvent impregnated in the pores of a hollow fiber membrane is used as an interface between the donor and the receiver phase [46, 47]. The obvious advantage of this method over the SDME mode is that the solvent cannot be dislodged from the needle and a larger surface area can be provided. Moreover, the selectivity of the membrane can also be utilized for screening out certain analyte species from the donor phase because of the small pore size.

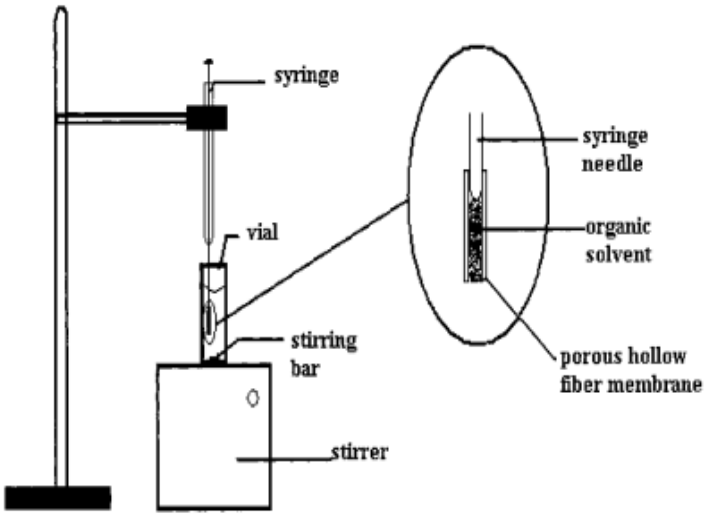

Figure 12: Illustration of the hollow fiber-protected liquid-phase microextraction set-up (Reprinted from reference [47] with permission from American Chemical Society).

Dispersive liquid-liquid microextraction [48] is another mode of microextraction wherein initially, a 5 to 10 ml of water sample is initially spiked with analyte species. Thereafter, between10 to 50 µl of a water-insoluble extractant solvent (such as carbon tetrachloride or carbon disulphide) dissolved in 0.5 to 2 ml of methanol, acetone or some other water soluble solvent is added to the above mentioned water sample. The mixture is then centrifuged which results in a cloudy solution. The extractant solution being heavier than water deposits at the bottom, which is removed by a syringe and analyzed. This extraction mode is very effective for the extraction of analytes such as PAHs and PCBs, which have a large organic solvent – water partition coefficient K_{ow}. A separate study was done [49] using a solvent lighter than water which solidified the sample in an ice bath. The sample was then removed, re-liquefied and analyzed.

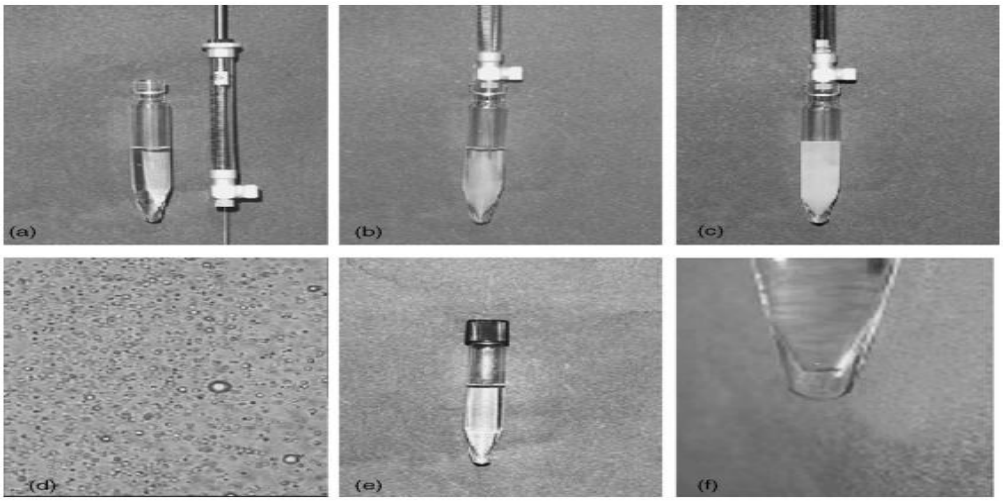

Figure 13: Dispersive Liquid-Liquid Microextraction (DLLME) (Reprinted from reference [48] with permission from Elsevier) (a)before injecting disperser solvent(acetone)having extraction solvent(C2Cl4) into sample solution, (b)beginning of injection, (c)end of injection, (d)optical microscopic photography, (e)end centrifuging, (f) enlarged view of sedimented phase.

In all the methods described briefly above, the analyte extraction was performed from the aqueous phase to an organic solvent, relying solely on the partition coefficient. Another method of solvent microextraction is the liquid-liquid extraction[8, 50] which exploited the effect of pH gradient on the microextraction process. In this process, there are two distinct phases; the donor and the acceptor, separated by a membrane. For the extraction of weak acids such as PAHs, the dissociation constant, pKa is to be very high for the process to work effectively. A low pH is maintained in the donor phase so that pH<<pKa. As a result, the analytes get protonated. Thereafter, the analyte species in order to get ionized (high pKa) migrate to the receiver phase, across the membrane, maintained at a pH>>pKa. This allows accumulation of analytes in the receiver phase over time.

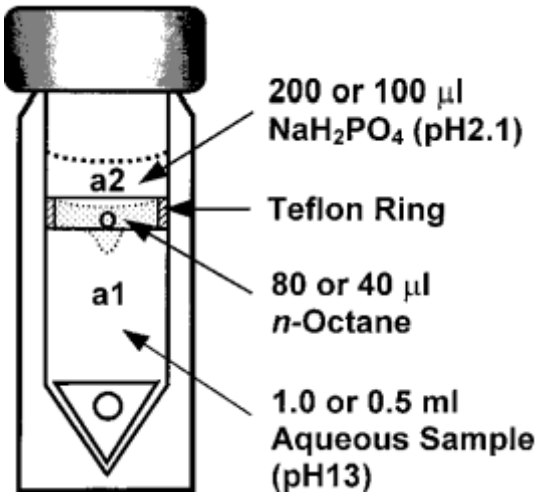

Figure 14: Schematic diagram of liquid-liquid-liquid microextraction (Reprinted from reference [50] with permission from American Chemical Society).

2.5a Continuous membrane extraction

In a separate study[51], continuous separation of phenol from crude oil was performed using a silicone membrane. This was the first work of its kind that employed two non-miscible phases for liquid-liquid extraction. However, this was not performed on a micro-scale and the efficiency of the process solely relied on the selectivity of the membrane. The acceptor line was directly coupled with a chromatographic system for online detection via HPLC.

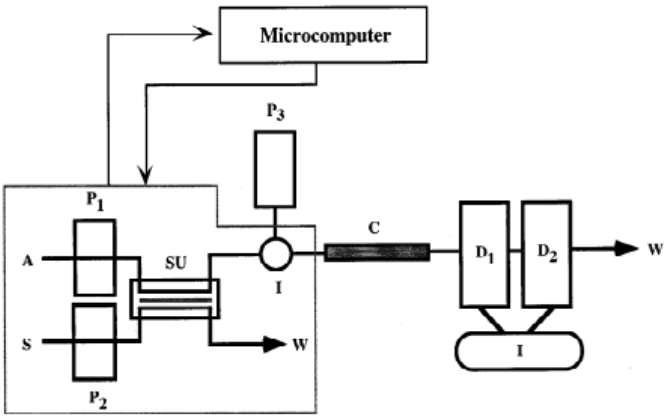

Figure 15: Overall scheme of extraction–separation system and arrangement of different components. S: sample; A: acceptor; P1: piston pump; P2: peristaltic pump; SU: Separation unit; P3:chromatograph pump; I: injection valve; C: chromatographic column; D : UV detector; D : electrochemical detector; W: waste; I: integrator (Reprinted from reference [51] with permission from Elsevier).

In the figure [15] above, two peristaltic pumps P_1 and P_2 were used to push the sample, S and acceptor, A, respectively. The separation unit, SU with the silicone membrane ensures the transfer of analyte species which then goes directly into the injector valve, I, for analysis. Fig [16] below shows a more detailed view of the membrane separation unit.

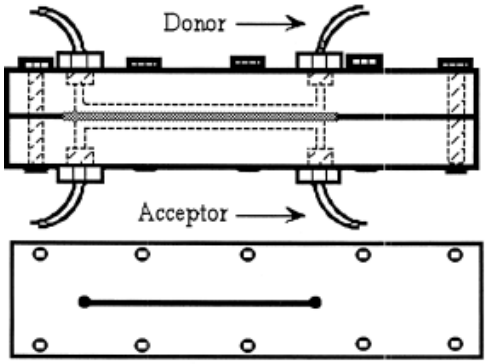

Figure 16: Membrane Separation Unit wherein the membrane is flanked by the donor and acceptor phase (Reprinted from reference [52] with permission from Elsevier).

2.6 Fundamentals of electrokinetics

This sub-chapter is dedicated to electrokinesis which consists of different phenomena namely, electroosmosis, electrophoresis, dielectrophoresis, ion concentration polarization, streaming potential and sedimentation potential. Electrokinesis occurs when an electrolyte solution acquires a net charge at the interface while in contact with another phase. This net charge at the interface is known as electric double layer (EDL)[53]. Electrophoresis is caused by electric field which leads to the relative motion of dispersed particles in liquid phases[53]. Particles in electrolytic solutions are meant for those entities whose dimensions are so large that they may be considered to form separate phase. Some examples may be O/W emulsion or vice versa. If electric field is applied to solid body-solution interface, considering that the solid body represents the immobile wall, the solution itself begins to move. The nature of the phenomena – the relative motion of particles to that of the solution and the relative motion of the solution to that of the immobile wall – is essentially the same. This motion of the solution is termed as **electroosmosis**. Electrophoresis and dielectrophoresis is of particular importance in biological studies and has been extensively used for facilitating rapid micro-analysis of real-time samples such as detection of foodborne pathogens[54], etc. In microfluidics, the scaling of the electrokinetic force is done keeping in mind the electrode size and particle size, in order to determine the ultimate size limits for controlled manipulation of the analytes.

The **electrophoretic force** of a charged particle through an electrolyte solution induced by the external electric field is given by $\mathbf{F_{EP}= qE}$ where E is the applied electric field and q is the net charge between the charge particle and the concentric Debye length (λ_D).

Debye length, λ_D (also called Debye radius), named after the Dutch physicist and physical chemist Peter Debye, is the measure of a charge particle's net electrostatic effect in a solution. The quantity,$1/\kappa$, called the Debye-Huckel parameter[55] quantity, is used to measure the thickness the Debye length (λ_D) or in other words the thickness of the electric double layer (EDL). The Debye length, λ_D is given by

$$\lambda_D = \left[\frac{\varepsilon kT}{e^2 \sum n_i^o z_i^2}\right]^{\frac{1}{2}}$$

where the summation term in the denominator is over all the species of ions present in the electrolyte and the valency, z_i , may take positive or negative values; E is the dielectric constant and *e* is the charge of an electron.

For analytes with a thin double layer [such that $a>>(1/\kappa)\Rightarrow \kappa a>>1$] where a is the radius of analyte, the solution of determining the local flow in a double layer is the same as the electroosmosis problem. Helmholtz-Smoluchowski[56] concluded that the relationship between particle velocity and electric field has the form

$$U_{EP} = \left[\frac{\varepsilon \zeta_P}{\mu}\right] E$$

where $\boldsymbol{\mu_E = \varepsilon\zeta_P/\mu}$ is the electrophoretic mobility (EP) of the particle**.** Here, $\boldsymbol{\zeta_P}$ is the zeta potential of the particle in that solution and $\boldsymbol{\mu}$ is the viscosity of the solution. EP mobility for thin EDL is not dependent of the shape and size of the particle. The size effect is implicitly contained in the zeta potential. However, this relationship can be violated at high zeta potentials.

For analyte species with thick electric double layers [such that κa<<1], the electric field lines are almost unaffected by the presence of the particles and the electric force on the particle on the particle is balanced by the viscous drag force on the fluid[56]. The expression is as follows:

$$qE = 6\pi\mu U_{EP} a$$

The potential of surface charge can be written as[56]:

$$\zeta_p = \frac{q}{4\pi\varepsilon(a + \lambda_D)}$$

Combining the previous two equations, the particle velocity may be written as:

$$U_{EP} = \frac{2}{3}\frac{\zeta_p \left(1 + \frac{a}{\lambda_D}\right) E}{\mu} \approx \frac{2}{3}\frac{\zeta_p \varepsilon E}{\mu}$$

The **dielectrophoretic force** is generated by the dipole moment of a dielectric particle in a non-uniform electric field[57]. The dielectrophoretic force (DEP) does not require a net charge on the particle but what it involves is brought about due to the relative difference in polarizability of the particle and surrounding medium through the complex dielectric particle permittivity (ε_p) and a dielectric medium permittivity (ε_m)to induce the particle dipole moment. The effective dipole moment or polarizability for a spherical particle with radius a is expressed by[57]:

$$p = 4\pi\varepsilon_m a^3 \left(\frac{\varepsilon_p^* - \varepsilon_m^*}{\varepsilon_p^* + 2\varepsilon_m^*}\right) E$$

where $\varepsilon^* = \varepsilon + \frac{\sigma}{j\omega}$ is the complex dielectric constant, σ is the electrical conductivity, ω is he electric field frequency, and j the imaginary number. The term in parenthesis is also known as the Clausius-Mossotti factor (f_{CM}). The DEP force can be described by[57]:

$$F_{DEP} = (p.\nabla)E$$

Hence, the effective DEP force is expressed by[57]:

$$\langle F_{DEP} \rangle = 2\pi\varepsilon_m a^3 Re[f_{CM}]\nabla|E|^2$$

Ion concentration polarization (ICP) is another electrokinetic phenomenon which occurs when a DC electric field is applied across a nanochannel and simultaneously, connected to two larger microchannels. ICP is a dynamic process and a schematic of this phenomenon is shown below. The nanochannel usually comprise of the nafion membrane [58-60].

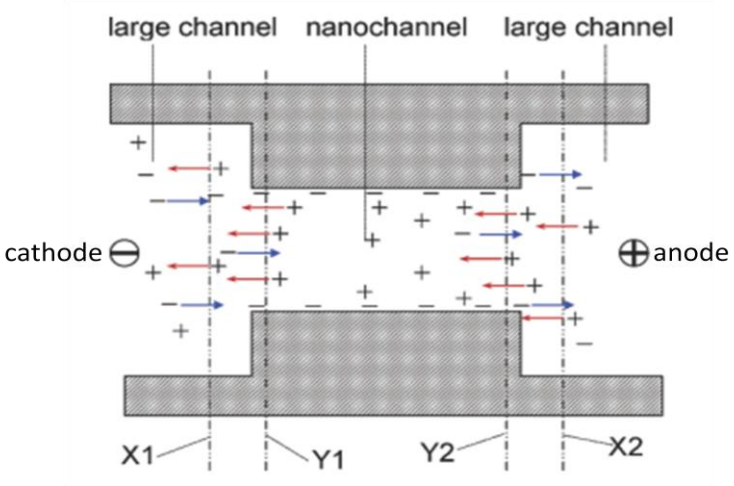

Figure 17 Schematic of ICP phenomena showing movement of cations towards the cathode and movement of anions towards the anode in the nanochannels which results in the formation of depletion and enrichment zone at the interface of microfluidic and nanofluidic interface (Reprinted from reference [13] with permission from American Chemical Society).

When an electric field is turned on, cations (counter-ions) migrate towards the cathode and as the nanochannels are negatively charged, it becomes cation-selective due to the

overlap of the negatively charged EDL in the nanochannels. Subsequently, the thickness of the EDL increases. As a result of this, the anions (co-ions) are increasingly expelled by cation-selective nanochannels [Fig. 18] via an enhanced EDL and this causes an accumulation of co-ions on the cathodic side of the nanofluidic junction over time. Eventually, to maintain electroneutrality in the region, an ion enrichment effect is observed on the cathodic side and an ion depletion effect is observed on the anodic side of the nanofluidic junction. The first experimental demonstration of the ion enrichment/depletion using nanochannels was shown by Pu et.al [13] in 2004 which is shown in the figure below.

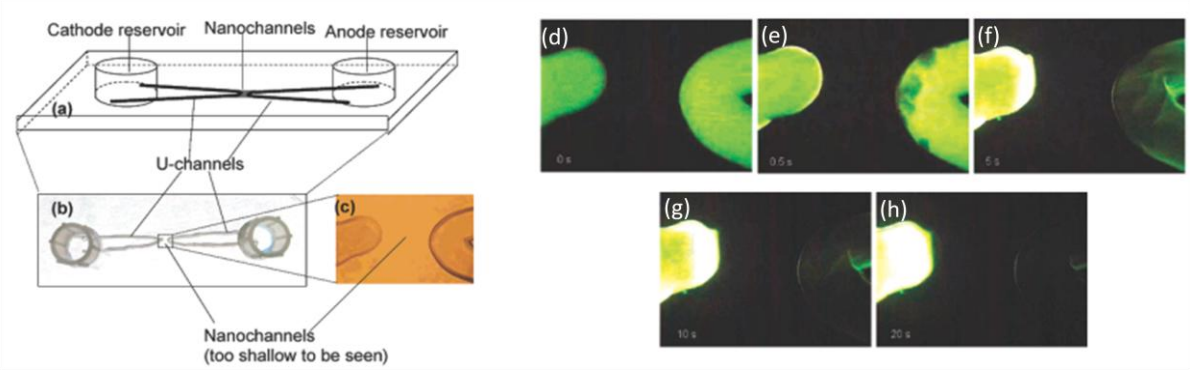

Figure 18 (a), (b), (c) Schematic diagram and zoom-in view of the two large U-shaped channels connected by nanochannels. (d) Fluorescein ions in the two large channels when no electric field is applied and gradual accumulation of the same when a DC voltage of 1000 V is applied after (e) 0.5s, (f) 5s, (g) 10s (h) 20s on the cathode side of the nanochannels(Reprinted from reference [13] with permission from American Chemical Society).

Streaming potential[61] is different from other electrokinetic phenomena listed above because unlike applying a potential for generating a force or an effect (such as ion enrichment in case of ICP), a potential is the effect or outcome of a pressure gradient flow. At steady state, the streaming potential built up across the flow system is given by $U_{str} = \frac{\varepsilon\varepsilon_o\zeta_p}{\eta K_L}\Delta P$ where ΔP is the pressure difference across the capillary and K_L is the specific conductivity of the bulk liquid. In the case of sedimentation potential, the motion of sediments in a solution relative to that of the solid phase results in the appearance of an electric field. Similarly, **electroviscous effects**[62] are the effects of the surface particle charge on fluid's viscosity given by $\eta=\eta_o(1+fE^2)$ where f is the viscoelectric coefficient of the fluid and E is the electric potential gradient. Other applications of electric potential include electrowetting (EW) and electrowetting-on-dielectric (EWOD) principles which can control the wettability of liquids on solid substrates. Both involve the spreading of a droplet over a larger surface area due to change in surface energy caused by an electrostatic field.

2.7 Microfluidic devices for environmental monitoring

Several works have been reported in the past decades which utilized separation of the samples using capillary electrophoresis (CE) [2, 63] based on the migration of ions from the sample reservoir to the detection reservoir under the influence of a DC electric field. The CE step is coupled with a spectroscopic [2, 64] or electrochemical detection [2, 63, 65] system. As ions different have different electroosmotic mobilities, they have different migration rates across the separation channel. They also have unique signatures on the spectrogram or electropherogram and identification is achieved due to the different optical (absorption-emission wavelength spectrum) or amperometric properties of the

ions to be detected. The schematic of a typical CE microfluidic device is shown in Fig. 20. As shown in the figure below, the most common configuration of CE devices is such that the sample reservoir (S), buffer reservoir and the sample waste reservoir (SW) are connected to a high voltage power supply. So, the ions migrate to the detection reservoir at a lower voltage via the separation channel where a suitable detector is employed. Sample preparation methods are also necessary in addition to the conventional CE based detection protocol as real samples have complex matrices. However, very little work has been done to incorporate the sample preparation schemes within the microfluidic device itself and till date, most of it is being done offline and off-the-chip via filtration[65], centrifugation[66], etc. To exploit the full potential of microfluidic devices in the form of hand-held portable devices with a wide range of applications, it is desirable that all the steps can be performed on the microchip itself which will enable faster analyses.

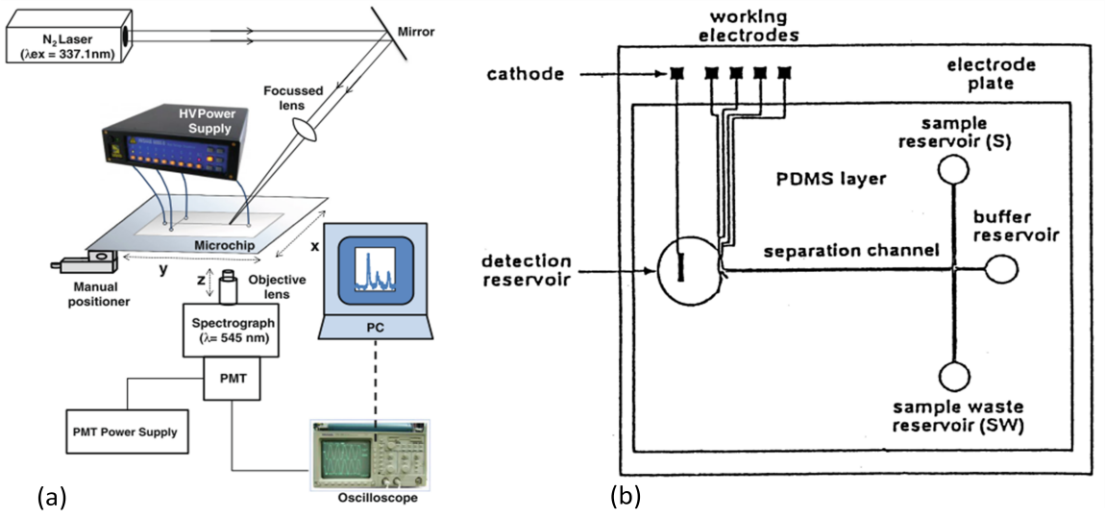

Figure 19: Typical configuration of a CE microfluidic device with (a) spectroscopic (Reprinted from reference [64] with permission from Springer) (b) electrochemical detector (Reprinted from reference [63] with permission from Elsevier).

Similarly, a lot of work has also been done using electroosmosis (EO) and dielectrophoresis (DEP). In contrast to CE where the design of the microfluidic device is pretty standard and stays roughly the same [Fig. 20], detection using EO and DEP relies more on the unique design of the device itself as the electrode and microchannel configuration have a stronger influence on these forces. We will report on some of the more popular works using these techniques for environmental applications. In 2005, Wu et.al [67] reported an alternating current electroosmotic (ACEO) based mechanism for the detection of Escherichia Coli (E.Coli), a harmful bacteria often found in contaminated water. ACEO produces counter-rotating vortices which pushes the bacteria from the electrode gap and assembles the microbes at predicted stagnation lines. This alters the electrode surfaces and produces unique impedance data which were correlated with

bacteria concentration in tap water and yielded enhanced sensitivity for point-of-care detection.

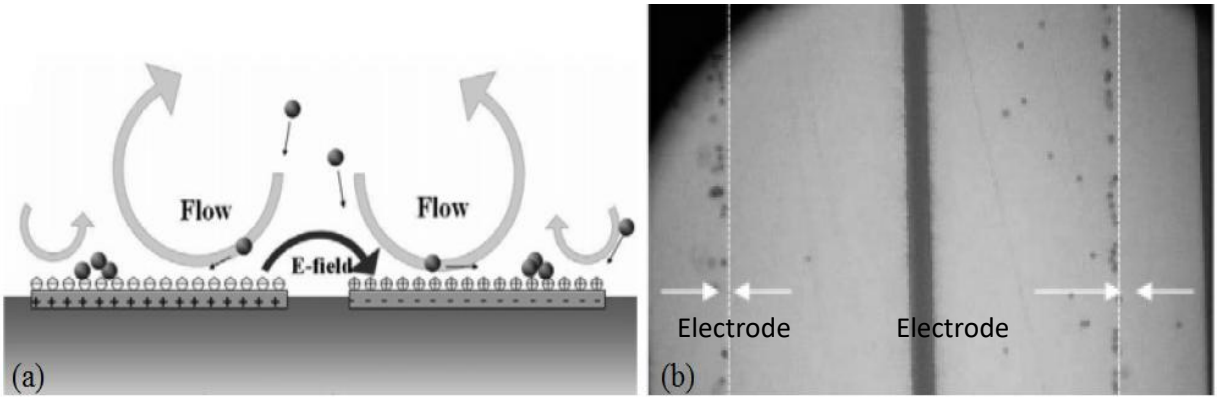

Figure 20 (a) counter-rotating vortices induced by ACEO using a pair of planar electrodes (b) assembly of E.Coli at the stagnation lines due to the flow motion of the counter-rotating vortices (Reprinted from reference [67] with permission from American Chemical Society).

Chiou et.al [68] reported an insulator-based (electrodeless) DEP microfluidic device for the low-level detection of arsenite, which is a toxic inorganic salt containing arsenic. This work is an interesting mix of microbiology and microfluidics coming together. Genetically modified E.Coli bacteria were used as biomarkers for the detection of arsenite. The modified bacterial biomarker was used as the expression level of the reporter proteins in the bacterial biomarker was dependent on the arsenite concentration in the surrounding media. By concentrating the bacteria in a designated zone of the device close to the electrochemical detection electrodes, the signal generated from the bacteria and subsequently, captured by the detection electrodes was amplified and very low levels of arsenite salts could be detected.

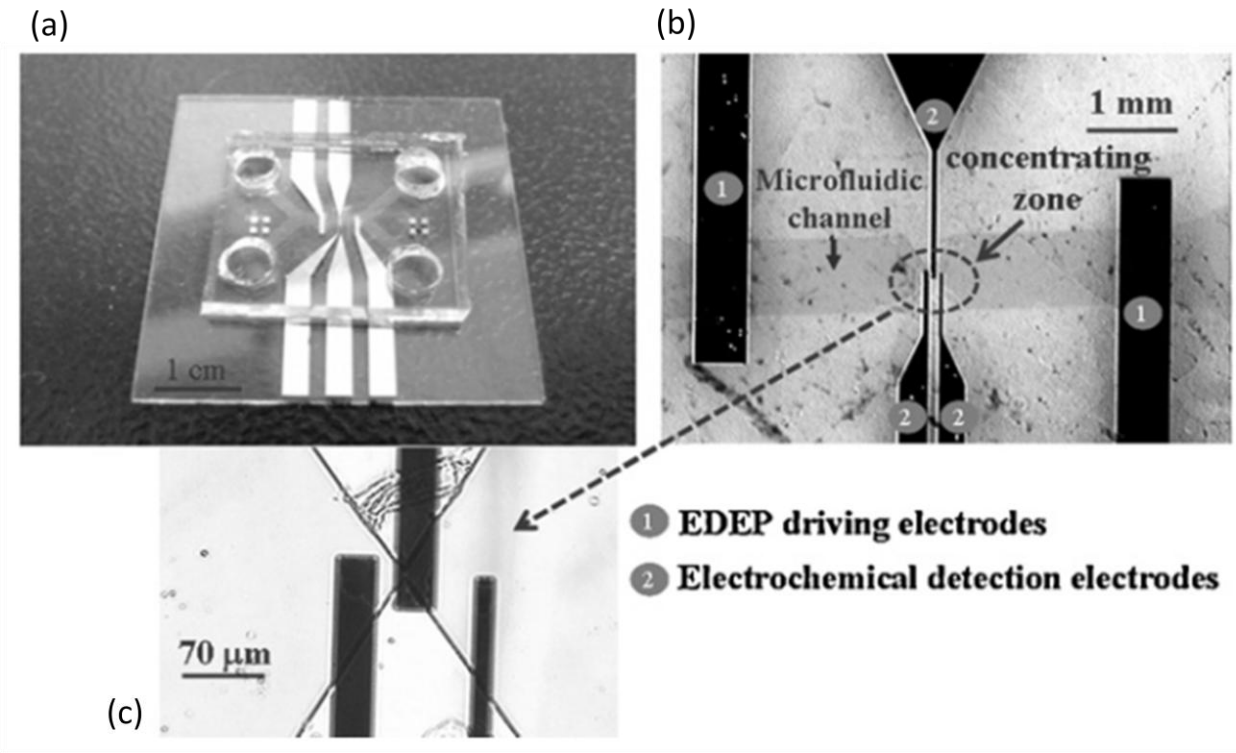

Figure 21 (a) Photograph of the microfluidic device (b) close-up of the concentrating zone, 1 and 2 represents driving electrodes and electrochemical detection electrodes, respectively (c) magnified view of the detection electrodes (Reprinted from reference [68] with permission from Elsevier).

DEP has particularly been attractive for the separation of cells and particles [69-71] of interest because the DEP force is generated by the electrodes itself and no moving components are necessary. However, within the context of our work; for the separation of ions and/or oil droplets from multiphase O/W emulsions; very little work has been published using microfluidic technologies so far. In 2014, Wang et. al [72] reported an acoustophoretic force based microfluidic device for the separation and detection of oil droplets from water. Two piezoelectric transducers (PZT) were used for the trapping and separation of oil droplets continuously. When the transducers were turned on, the oil

droplets moved towards the acoustic pressure anti-nodes of an acoustic standing wave which is near the sidewalls of the microfluidic channels. This occurs due to the negative acoustic contrast factor of the oil droplets as the density of the oil droplets is less than that of water. The PZTs were fixed at the bottom of the microchip containing the microfluidic channel.

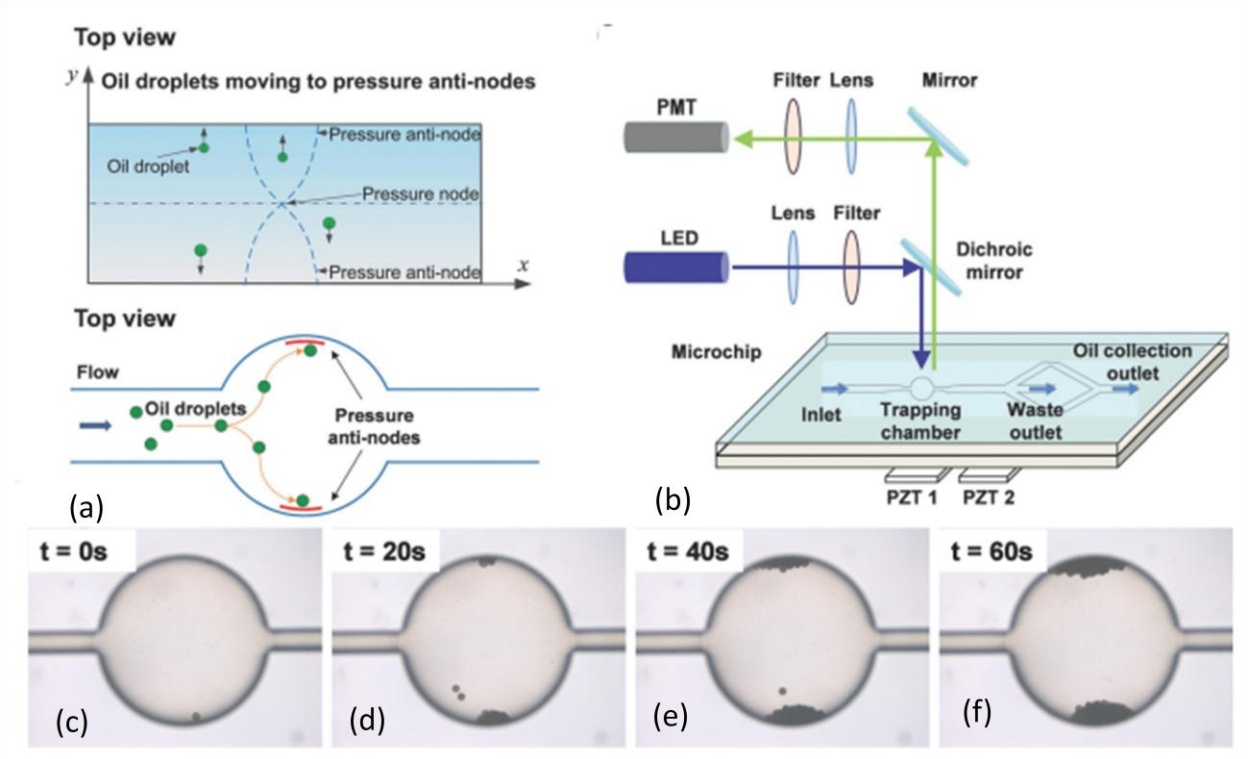

Figure 22 (a) Illustration of the oil droplets moving towards the pressure anti-nodes present in the circular chamber of the trapping chamber (b) oil droplet trapping and separation scheme aligned with the PZTs and with the fluorescent detection module (c) Experimental images showing the accumulation of oil droplets over time when the PZTs are turned on (Reprinted from reference [72] with permission from Royal Society of Chemistry).

2.8 Surface hydrophilization of PDMS/PDMS or PDMS/glass microchannels

In our work, we have focused on environmental monitoring applications for O/W emulsions which can be performed using microfluidic devices. However, polydimethylsiloxane (PDMS) which is the most widely used polymer for fabrication and prototyping of microfluidic chips is hydrophobic in nature. Hence, a surface modification step is performed prior to doing our experiments. Our protocol as employed in Chapters 4 and 5 was inspired by the publication of Bauer et.al [73] which reported a sequential layer-by-layer (LbL) deposition of polyelectrolytes yielding stable hydrophilic PDMS-based microfluidic channels. A syringe was used to draw into a tube alternate segments of poly(allylamine hydrochloride) (PAH) and poly(sodium 4-styrenesulfonate)(PSS) solutions (both 0.1% w/v in 0.5 M aqueous NaCl solutions) with aqueous NaCl washing solution (0.1M) segments in between.

Immediately, after plasma treatment (required for bonding PDMS/PDMS or PDMS/glass substrates), the surfaces of microchannels walls are rendered negatively charged. Thereafter, the channels are flushed with positively-charged PAH solution, followed by NaCl solution for expelling the loosely bound ions and subsequently, negatively charged PSS solution. This protocol was able to develop long-term stable hydrophilic coatings on the microchannel walls allowing for the production of monodisperse o/w droplets in the microfluidic devices even after 5 months of storage after the surface modification step. A schematic of the plug-based method is shown in Fig. 24(a). This LbL scheme works regardless of the fact that the base substrate is PDMS or glass and leads to a build-up of polyelectrolyte multilayers (PEM) at the channel walls [Fig. 24 (b)]. Fluorescence microscopy was also used to analyze the impact of the number of segments, n of the

polyelectrolytes on the resultant coating thickness in the microchannels. When PAH labeled with FITC fluorescent dye was used instead of pure PAH, it was observed that the fluorescent intensity rose with increasing number of segments, n [Fig. 24(c)]. This showed that the gradual build-up of PEMs is well controlled and highly reproducible.

Derzsi et.al[74]used these same polyelectrolytes, namely, PAH and PSS surface coatings for generation of O/W emulsions using poly-carbonated devices. Later, a solution of tin (II) chloride [75] was also used in place of polyelectrolytes rendering polycarbonate-based devices hydrophilic for the generation of O/W emulsions. Recently, in April 2016; another paper [76]was published which used branched polyethyleneimine (BPEI) and poly(ethylene-alt-maleic anhydride) (PEMA) as reagents for preparing stable hydrophilic polycarbonate microfluidic devices for producing O/W emulsions. Piccin et.al [77] used polyester-toner which has a partially hydrophilic surface for fabricating microfluidic devices for the generation of O/W emulsions. In this work, no surface treatment step was performed and only surfactants were used in the continuous phase. Park et.al [78] also reported a microfluidic flow focusing device for generating micron-sized oil droplets for their potential application as drug carriers. The PDMS devices, used in this study, were plasma treated for 5 minutes and used immediately.

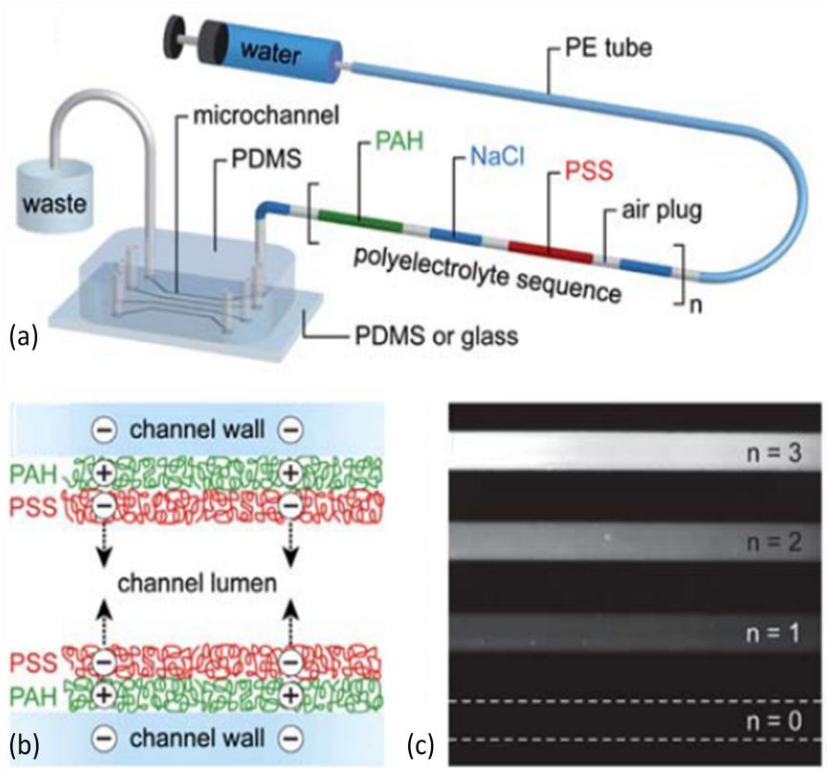

Figure 23 (a) Sequence of charged polyelectrolytes of a PDMS microchannel. Segments of NaCl, PAH and PSS solutions, separated by air plugs, are loaded into a piece of tubing and flushed through the channel at a constant flow rate. (b) PEM building up at the channel wall (c) Fluorescence micrograph of four microchannels modified with different solution sequences (n=0,1,2,3). The fluorescence intensity rises with increasing n (Reprinted from reference [73] with permission from Royal Society of Chemistry).

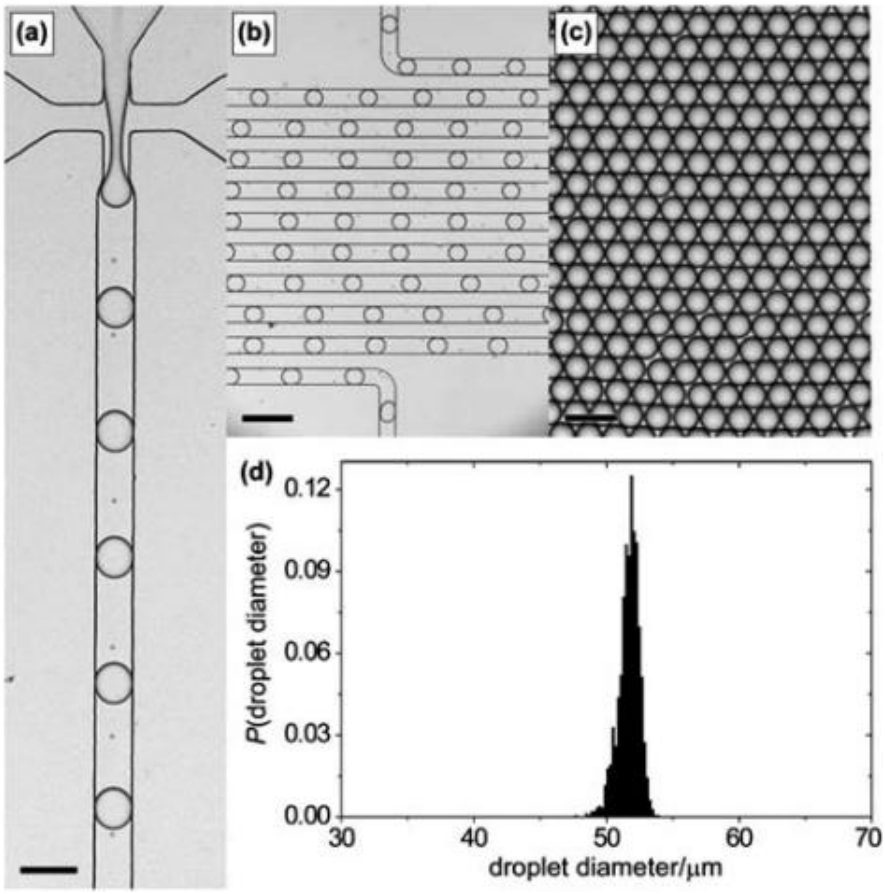

Figure 24 (a) formation of hexadecane-in-water droplets (b) the passage of droplets through the chip without any wetting defects (c) hexagonal close-packed monolayer of the droplets in a storage reservoir (d) diameter distribution reveals a very high level of droplet monodispersity. Scale bars denote (a) 100 μm, (b) 200 μm and (c) 50 μm (Reprinted from reference [73] with permission from Royal Society of Chemistry).

3. On-chip Droplet-based Liquid-Liquid Extraction (LLE) of Phenol from Silicone Oil on a PMMA platform

3.1 Introduction

Droplet-based microfluidic devices have already been used for a diverse list of applications in the past decade. It has been used for studying cell-based assays [79-81], enzymatic activity measurements [82-84] and enzymatic kinetics [85-88]. It has been used for screening applications of engineered proteins[89], protein crystallization[90] and reaction catalysts[91]. Here, we broaden the scope of droplet-based microfluidics further for performing solvent extraction techniques. Solvent extraction (SE) also known as liquid-liquid extraction (LLE) is a very important sample preparation method for quantifying the analytes in complex mixtures. Most analyses are carried out on samples containing complex mixtures of very small amounts of chemicals that need to be identified. However, real-time samples from the field such as oil spills and waste water are very complex and cannot be analyzed directly. Hence, elimination of unnecessary solvents is required via micro-scale extraction techniques. Along the same lines, Solvent Micro-Extraction (SME) is a fairly recent development and has been successfully complemented with most common analytical instrumentation equipments such as gas chromatography (GC), high-performance liquid chromatography (HPLC), capillary electrophoresis (CE) and atomic absorption spectroscopy (AAS). In this project, we have introduced a micro-device which can act as a precursor for separating out the water-soluble ions from complex donor solvent, namely silicone oil.

Several works have been published where batch reactors[8, 9] have been used for quantifying polyaromatic hydrocarbons (PAHs) in an aqueous medium using a pH gradient. However, these polycyclic aromatic hydrocarbons (PAH) are often linked to oil spills as these are lipophilic in nature and are one of the most widespread organic pollutants. Here, we aim to separate out the phenolate ions from the oil droplets in a droplet-based microfluidic extraction device. A droplet-based reactor offers the advantage of providing a higher interfacial area of contact between the two immiscible phases. Another advantage of using a microfluidic reactor is that continuous flow separation takes place, so high throughput screening is possible unlike a batch reactor. We use droplets as the donor phase which rejects the hydrophilic analytes onto the continuous phase and finally a fraction of the continuous phase is taken aside through a bifurcation channel at the outlet.

A PMMA chip is used instead of PDMS as PDMS swells in the presence of organic solvents like phenol due to cross-linking with the microchannel walls. This may cause alterations in the microchannel's width and height. Also, PMMA is moderately hydrophilic after plasma treatment and hence rapid prototyping is possible. Now, silicone oil is a synthetic liquid insulation which is a complex mixture of linear polymers with a distribution of molecular weights. It has excellent dielectric properties such as breakdown voltage, low losses factor, resistant to oxidation and has a high flash point. Hence, extraction of weak acids like phenol via diffusion by synthesizing a microfluidic emulsion of silicone oil droplets in an aqueous medium becomes a viable option. Silicone oil, also, has a very low biodegradability which makes it very vulnerable to the environment. A major motivation of the present work is that the idea can be

extended for monitoring the presence of other dangerous aromatic hydrocarbons such as naphthol, hydroxypyrene, etc [8] in oil spills which might have a complicated and unknown composition.

3.2 Experimental

3.2.1 Chip fabrication and device set-up

The PMMA acrylic sheet was cut to our specific dimensions using CO_2 laser (Universal M-300 Laser Platform, Universal Laser System Inc, Arizona, USA). The width of the microchannels is kept at 170 µm and the depth is 1 mm. This is followed by rinsing with 2-propanol and dried with nitrogen to remove the surface of all the dirt particles. The cut PMMA chips were then exposed to plasma treatment using a Harrick scientific plasma cleaner (PDC-32G) at a maximum power setting of 100 W for a 5 minutes for hydrophilization. The average value of contact angle of DI water on a freshly cut PMMA surface is 70^{o}- 75^{o} .This value reduces to 5^{o}-10^{o} after hydrophilization. The PMMA layers were then bonded together via hot embossing.

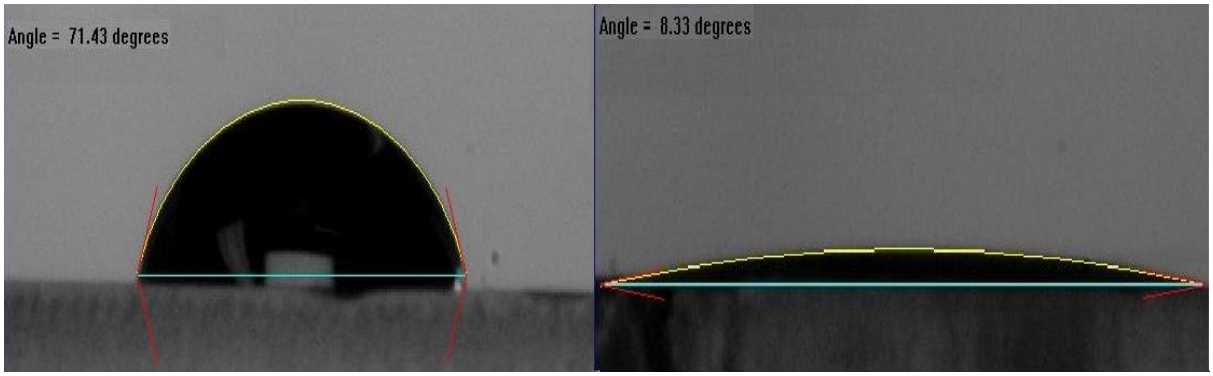

Figure 25: Contact angle measurement of DI water on PMMA before and after plasma treatment

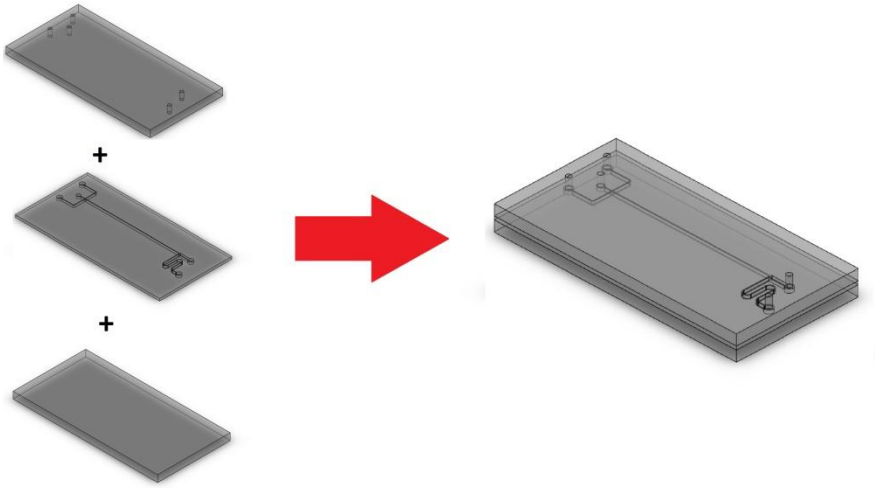

Figure 26: Assembly of the PMMA-based microchip after plasma treatment

After bonding the PMMA plates, 1/16” x 1.00mm tubes from PEEK were attached to the inlets using 5-Minute epoxy glue from Devcon and the fittings used, in the experiments, were obtained from Charlston. The chips were used immediately after fabrication and a new one was used for each extraction experiment.

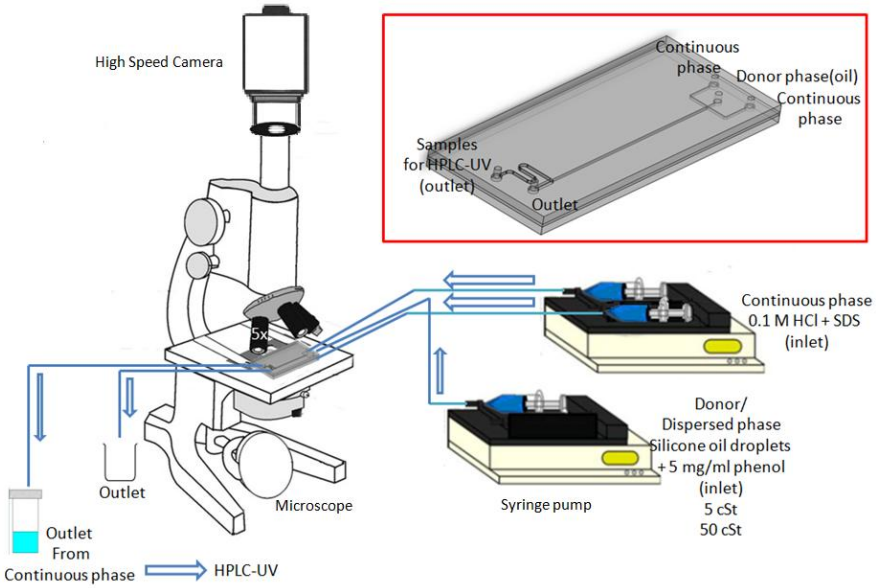

Figure 27: Schematic drawing of the experimental set-up. Inset drawing shows the inlets and outlets of the polymer device

3.2.2 Consumables and experimental set up

The dispersed phase is emulsified in an aqueous sodium dodecyl sulphate (SDS) solution at the CMC value. The concentration of the surfactant molecules is taken at CMC (critical micelle concentration) because upto the CMC, the surface tension reduces rapidly with increasing surfactant concentration. At CMC, the surfactant works at the lowest interfacial tension which is desirable as it increases the wettability of the microchannel walls and promotes hydrophilicity. Beyond CMC, the additional surfactant molecules will be used to form micelles. Increase in the number of micelles affects other parameters of the surfactant molecules in water such as solubilization, self-diffusion, etc [92]. Hence, to ensure repeatability of experiments; it is advisable to use the keep the concentration fixed at CMC. The dispersed phase is two samples of silicone oil with

viscosity as follows: 5 cSt and 50 cSt. To prepare 5 mg/ml phenol in silicone oil (donor phase), initially 0.05 gm of phenol is added in 10 ml of silicone oil and the resultant mixture was ultrasonicated overnight. Interfacial tension measurements between the continuous phase and silicone oil droplets and contact angle measurements of the continuous phase on the membrane were done using the goniometer (FTA 200).

The flow rates of the continuous and dispersed phase are controlled by two separate syringe pumps (Longer Pump Model: LSP02-1B). Droplet formation in the flow-focusing junction of the microchip was observed with a Carl Zeiss microscope Axiostar plus fitted with Zeiss lens CP-Achromat (5x/0.12). Droplet lengths were obtained using the Phantom Miro M310 digital high-speed camera. To determine static interfacial tension between the silicone oil and continuous phase interface, the less dense silicone oil droplet was formed upwards at the needle tip which is surrounded in the SDS solution [93]. Thereafter, pendant drop method was employed. The interfacial tension between 5 and 50 cSt silicone oil and the continuous phase is 10.89 ±0.8 and 22.08±0.8 mN/m, respectively. The samples, at the end of each experiment, were injected into HPLC-UV (Agilent 1100 series) for quantifying the microextraction of phenol at 218 nm. A reverse phase column, Zorbax PAH Eclipse Plus and a mobile phase of HPLC grade methanol: DI water is used in the gradient mode. After each run, the column is flushed with the methanol for an hour to ensure the longevity of the column.

3.3 Results and Discussion

3.3.1 Implementing a pH-gradient based scheme for liquid-liquid-liquid extraction from oil-in-water (O/W) emulsions on a microchip

In 2004, Marlow et.al [8] reported a three phase pH-gradient based extraction method where aromatic hydrocarbon molecules solubilized in an acidic donor solution would diffuse across a polypropylene membrane (loaded with octanol) onto the basic donor solution. This occurs because as soon as the hydrocarbon molecules such as phenol in the acidic donor phase dissociate, they get protonated. In order for the once ionized hydrocarbon molecules to stay in the dissociated state, they diffuse across the hydrophobic membrane to the basic acceptor solution at a higher pH >> pK_a so the phenol molecules become ionized in the basic solvent once more and stay trapped there in the ionized form after diffusing across the membrane. This process is very powerful as sample preparation technique and had a detection limit in the range of µg/ml. It was reported that phenol molecules had an extraction efficiency 31.1(± 5.1) %.

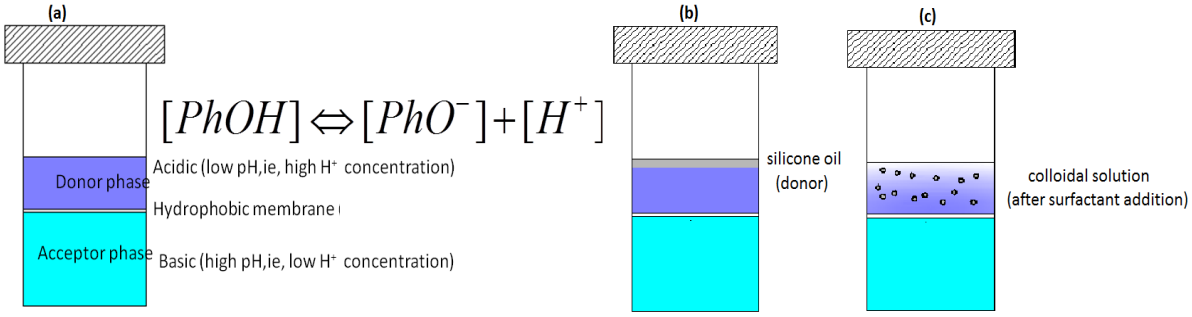

Figure 28: (a) Experimental set-up in a batch reactor as reported in literature[50] (b) batch reactor with silicone oil containing phenol in the acidic donor phase (c) colloidal suspension of silicone oil droplets in a surfactant solution in the donor phase which essentially replicates an oil-in-water (O/W) emulsion in the donor phase.

We tried to implement this process for the passive extraction of phenol molecules present in the form of a colloidal suspension in silicone oil, which in turn is suspended in an acidic solution. This process has real-time applications in the extraction of target analyte species present in oil droplets which are in the form of oil-in-water emulsions. The oil-in-water emulsion may be first centrifuged to separate out the water fraction so that some of the hydrocarbon molecules which ionize will get absorbed in the water fraction. This water fraction can then be acidified separately as per the scheme reported by Marlow et.al [8]. In the batch reactor having an O/W emulsion as shown in Figure 28 (b), we observe that silicone oil being lighter than surrounding acidic solution tends to float on the surface of the donor solution, so a surfactant was added to form a cloudy colloidal suspension of silicone oil droplets emulsified in the donor phase shown in Figure 28 (c). Moreover, as soon as the phenol molecules diffuse out from the silicone oil droplets to the surrounding acidic solution, they get protonated due to high pH as a result of which the phenolate ion being hydrophobic in nature enters back into the silicone oil. This prevented the phenol from reaching the bottom donor solution. So, a multi-tiered chip was fabricated to prevent this phenomenon. Once again, in a real-time scenario, the oil phase can be introduced in the form of droplets in surfactant solution (aqueous continuous phase) on a microfluidic chip. At this point, mass exchange of colloidal suspension will take place driven by a concentration gradient between the continuous and dispersed phase. The oil droplets can be separated at the outlet and a fraction of the continuous phase can be taken aside and acidified later. The surrounding continuous phase, after extracting the ionic impurities from oil droplets, may not necessarily be amenable to common analytical instrumentation equipments such as gas chromatography (GC), high-performance liquid

chromatography (HPLC), capillary electrophoresis (CE) and atomic absorption spectroscopy (AAS) as it may have a host of other colloidal impurities from the oil phase in the real-time scenario. Hence, we utilized a pH gradient[8, 50] based microextraction technique by virtue of which the phenoxide ions in the aqueous phase may be transported from the continuous phase onto a bottom receiver phase flowing underneath the layer containing the droplets across a polypropylene (hydrophobic) membrane was sandwiched between the two layers. The protonation step is only being carried out after the removal of the oil droplets because the presence of $[H^+]$ ions will otherwise hinder the diffusion of phenoxide ions from the silicone oil droplets to the continuous phase. Protonation of the continuous phase fraction having phenoxide ions leads to the formation of hydrophobic and neutral phenol molecules. Thereafter, the phenol molecules as they flow over the hydrophobic membrane, diffuse across it onto the bottom layer having dimethylformamide (DMF), a polar organic solvent (pH=9).Now, the mass transfer of the colloidal impurities in the oil to the surrounding continuous phase takes place in two stages which will be dealt with in the later part of the report. The top view of the proposed scheme of the microchip is shown below.

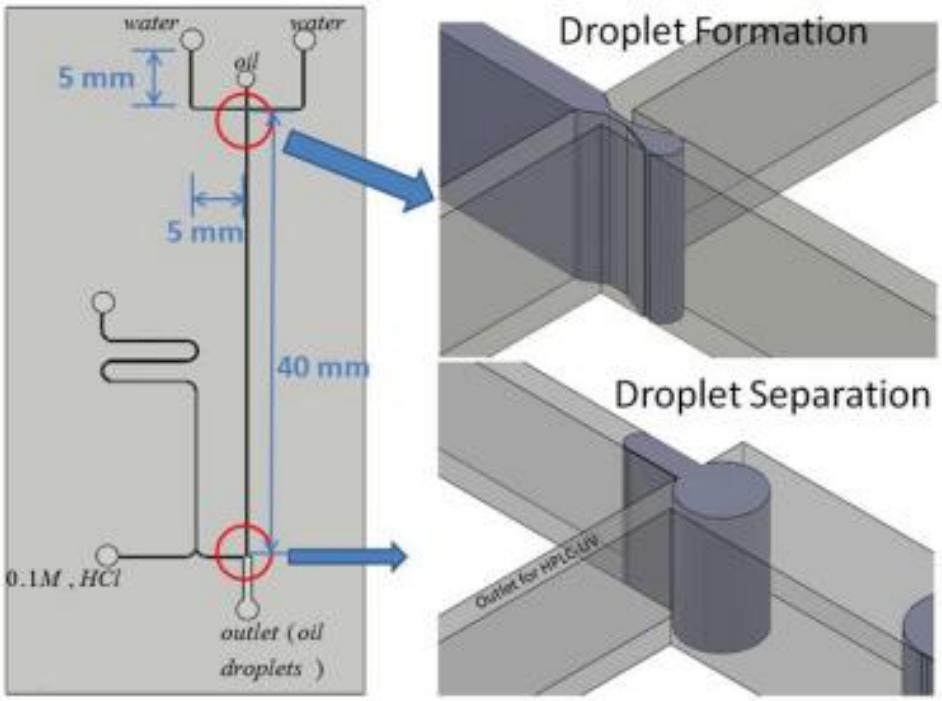

Figure 29: Proposed schematic of the microchip

It is to be noted that overall, it is a three-phase extraction process and the extraction equation[8] may be written as:

$$i_{o1} \underset{k_2}{\overset{k_1}{\Longleftrightarrow}} i_{a1} \underset{k_4}{\overset{k_3}{\Longleftrightarrow}} i_{o2}$$

where the subscript $\boldsymbol{i_{o1}}$ denotes the organic donor phase (silicone oil droplets), $\boldsymbol{i_{a1}}$ denotes the aqueous continuous phase (SDS solution + HCl) and $\boldsymbol{i_{o2}}$ denotes the organic receiver phase (DMF, bottom layer). The constants; k_1, k_2, k_3, k_4 are first-order extraction rate constants.

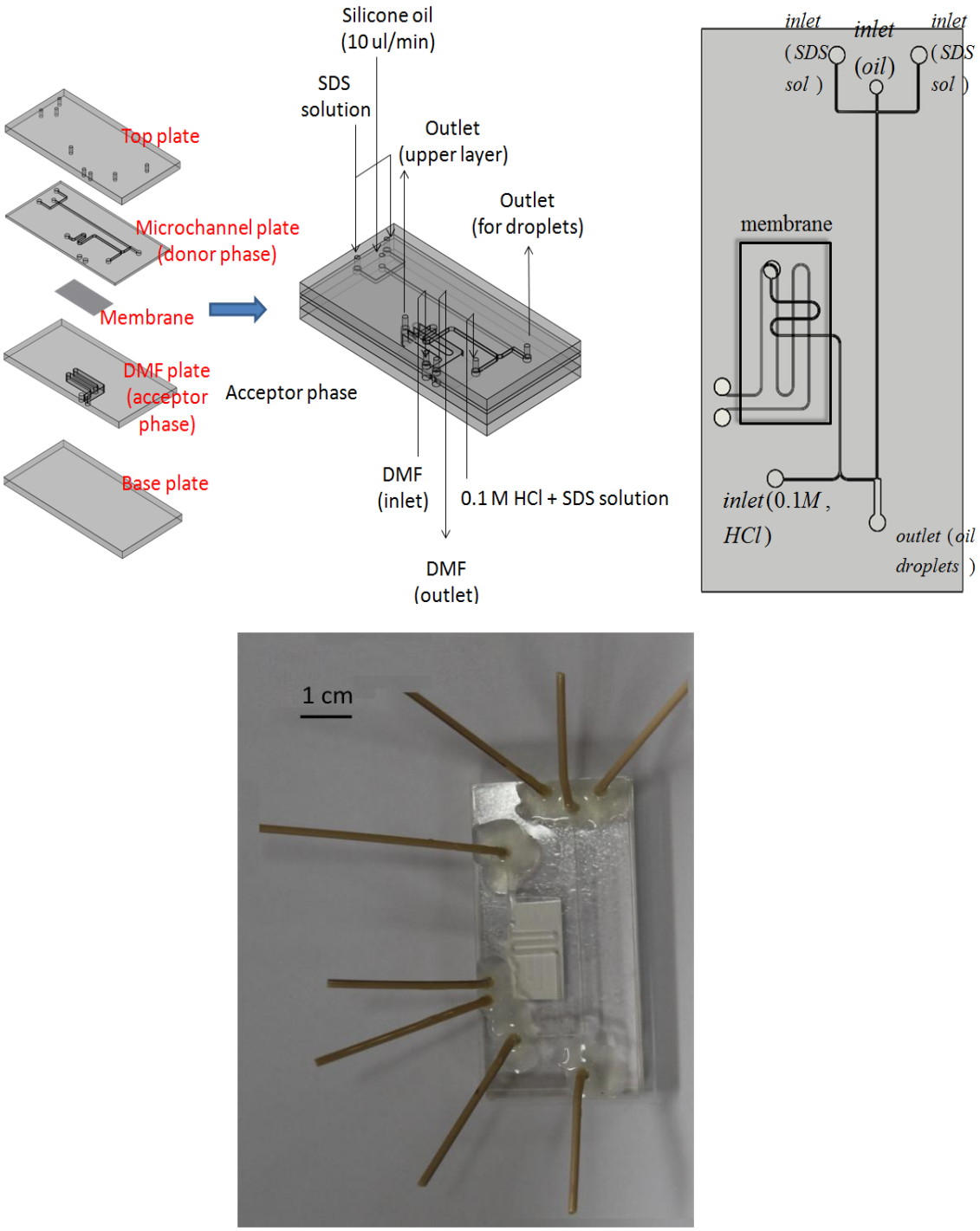

Figure 30: Schematic of the assembly of membrane-based multi-tiered microchip and photograph of the actual microfluidic device.

3.3.2 Droplet generation cycle at the cross-flow junction and droplet separation in the outlet bifurcation (experimental observations)

The emulsification of the dispersed oil phase into droplets depends on the relative effect of viscous forces versus surface tension acting across an interface between two immiscible phases. These are the two main competing forces which will act on the oil-water interface. The critical capillary number considers the conditions necessary for the breakup of the dispersed phase into the discrete droplets by these two forces. It has been reported[94] that the critical capillary number depends only viscosity ratio, i.e, the viscosity of the dispersed phase to that of the continuous phase. When this ratio is greater than 4 which holds good in our case (for 5 cSt and 50 cSt silicone oil droplets in DI water), the confinement exerts an additional shear stress on the interface and promotes the breakup process. In our study, the overall oil droplet formation cycle at the cross flow junction may be divided or broken down into three identifiable stages: the filling stage, the necking stage and the lag stage as shown in Figure 31. The mechanism is similar to that of a T-junction[95]. Initially, the oil phase stations itself at the junction which may be referred to as the start-up point. It is to be noted that as the velocity of the oil stream increases, the start-up point progressively shifts downwards into the main channel. Thereafter, the filling period begins wherein the oil phase extends into the main channel upto beyond the pinch off point. The distance that the oil stream traverses beyond the pinch-off point determines the length, L of the droplet. The filling period continues as long as the oil stream grows until the shear stress is exceeded by the interfacial tension acting at the oil-water interface, after which the dispersed phase snaps in the form of discrete droplets. This may be regarded as the necking stage followed by the lag stage where the oil stream retracts back to its original position, the start-up point. Again, the

entire cycle is repeated. From the perspective of analyte extraction between the continuous and dispersed phase, the filling period is associated with the shear enhanced via axial diffusion which has been discussed later.

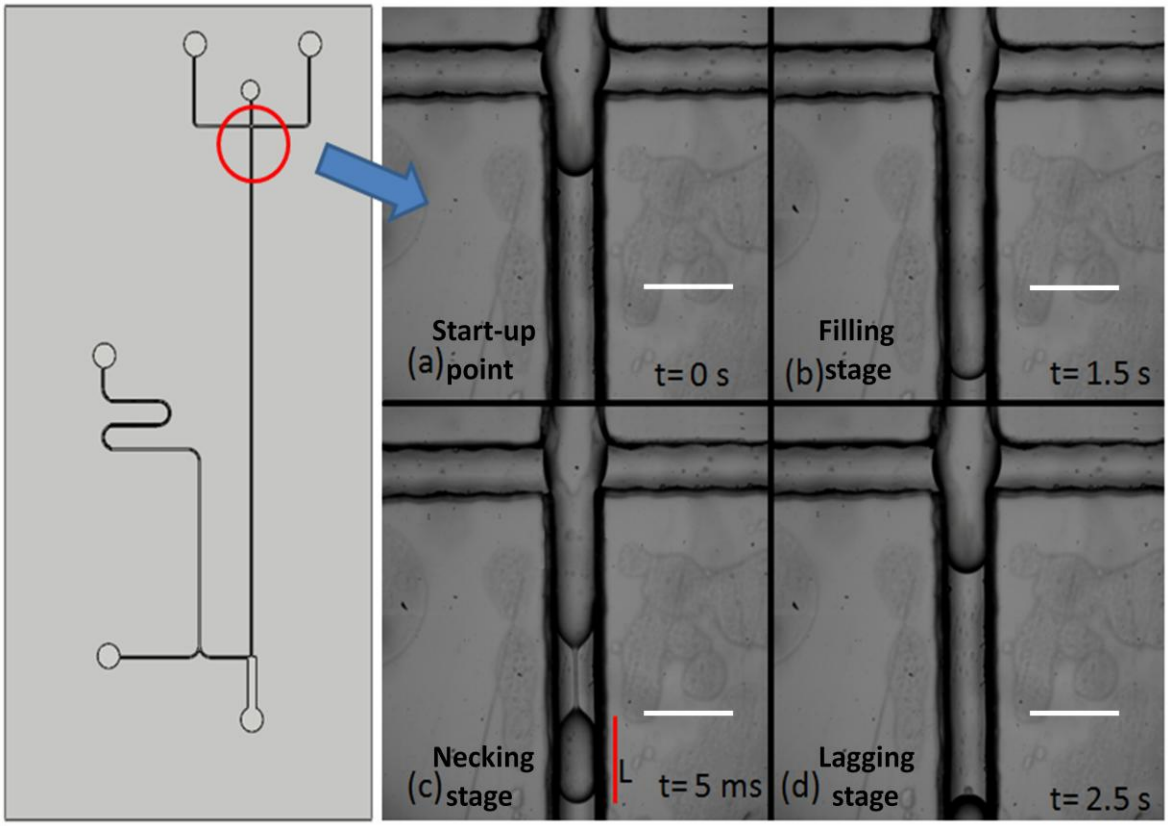

(e)

Figure 31 : Sequence of images showing the different stages of the droplet formation cycle with the duration taken by each of the stages. (a) shows the start-up point ;(b) shows the filling stage, the greater, the volume of oil dispensed in the filling period, the

longer is the length of the droplet ;(c) shows necking stage where the pinch-off and the subsequent droplet formation takes place. L denotes the droplet length; (d) shows lagging stage where the retraction of oil stream back to the start-up point takes place. (e) SEM image of the PMMA-based cross flow junction. Scale bars denote 400 μm.

The Phantom Camera Control (PCC 2.14b) software was used to analyze the videos so as to determine the fraction of time duration occupied by the three stages. The results are displayed in Figure 32 for the 5 cSt silicone oil. It was observed that as the velocity of the continuous phase was increased, keeping the dispersed (oil) phase velocity constant, the fraction of time occupied by the filling stage progressively decreases whereas that occupied by the lagging stage increases. Now, the droplet formation regime in immiscible fluids occurs because of the competition between viscous shear and interfacial tension forces at the oil-water interface. This progressive increased and decreased duration of filling and lagging stage as shown in the Figure 32, respectively, can be explained from the fact that as the continuous phase velocity is increased, the viscous shear becomes more dominant as compared to the interfacial tension forces. In other words, the increased shear forces at the interface, eases the pinching of the oil stream. The necking stage, which involves the pinch-off of the oil stream, is of the order of a few milliseconds. Hence is not visible in the Figure 32.

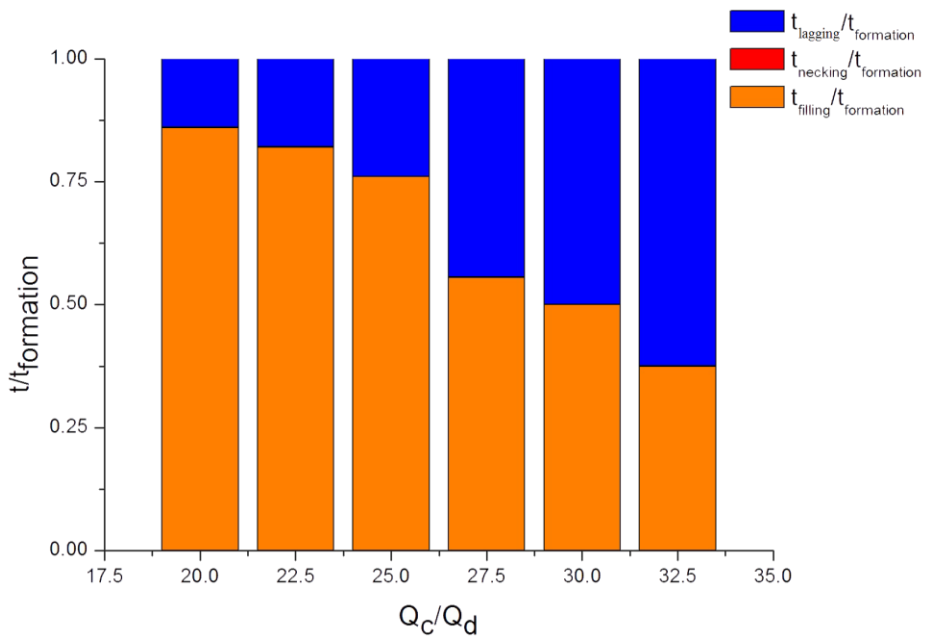

Figure 32: shows the effect of flow rate ratio on the ratio of the individual droplet formation stages to the overall duration of droplet generation of the 5 cSt silicone oil.

At the outlet, a bifurcation is provided which imparts a sudden expansion from 170 µm to 750 µm. Considering that flow rate is analogous to resistance along the arms[96], we calculated the pressure drop using the expression[38], it was calculated that the ratio of the pressure drop along the two arms is Q_x:Q_y=12:1. Also, due to the increase in the channel width, the net Laplace pressure drop along the droplet interface y-axis is greater then along the x-axis. These two factors ensure that all the droplets flow into the arm along the x-axis only.

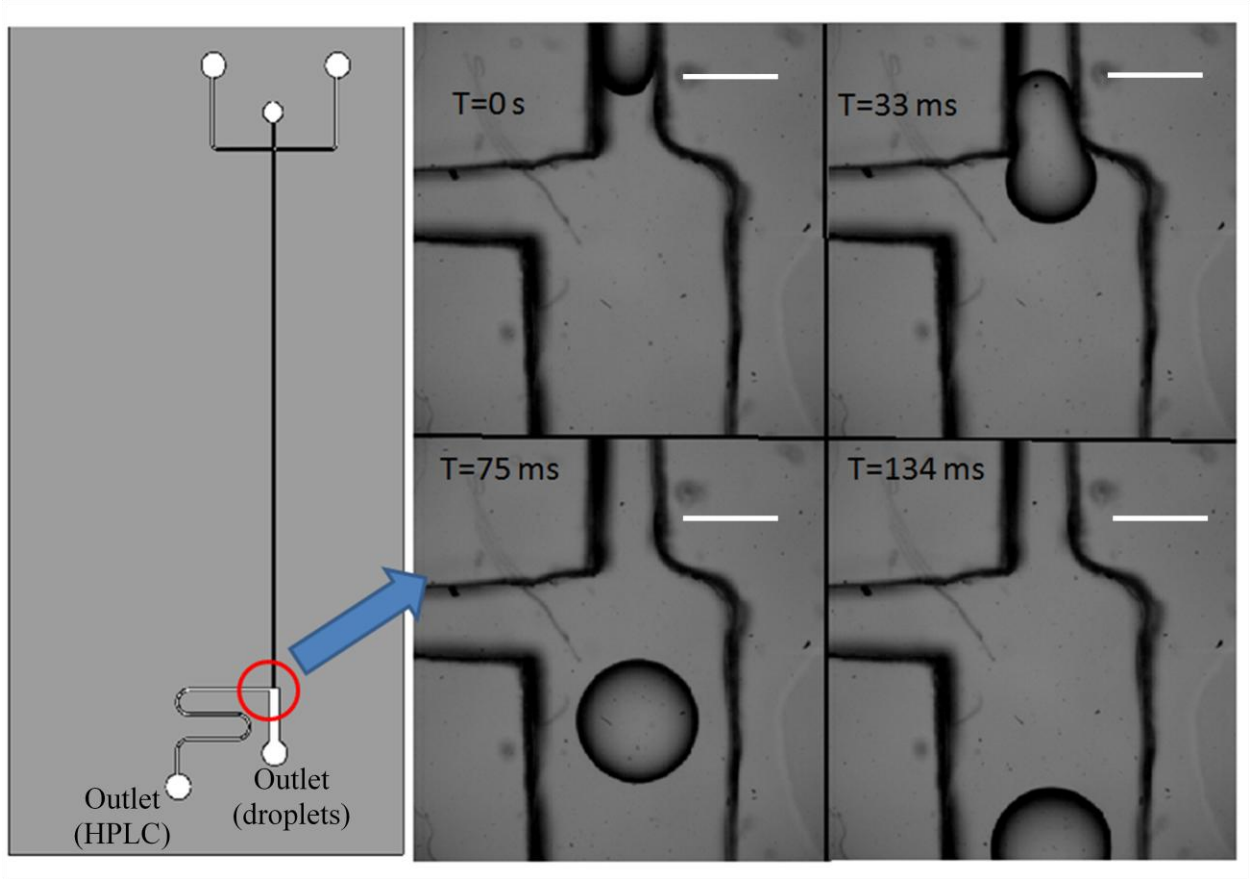

Figure 33: Sequence of images showing the position of the droplet that exits the microchip at the outlet junction via the microchannel along the x-axis. Scale bars denote 400 µm.

3.3.3 Effect of flow-rate ratio on the droplet length

In our experiments, the rate of the liquid-liquid extraction reaction is investigated by varying the flow rates of the continuous phase, Q_c from 200 to 325 µl/min while keeping the dispersed phase velocity, Q_d fixed at 10 µl/min. This is repeated with two different viscosities of silicone oil droplets, 5 and 50 cSt and observations are made on the rate of the extraction efficiency patterns. We observed that as we increased the velocity of the continuous phase, the shear stress component of the capillary number increases. This

increases the shear force exerted by continuous phase which gives us smaller sized oil droplets. Fig.34 shows that ratio to silicone oil droplet length to microchannel width is inversely proportional to the flow-rate ratio [97]. Also, the higher viscous oils give longer droplets as the interfacial tension between the continuous and dispersed phase is higher which lowers the penetrating power of the continuous phase.

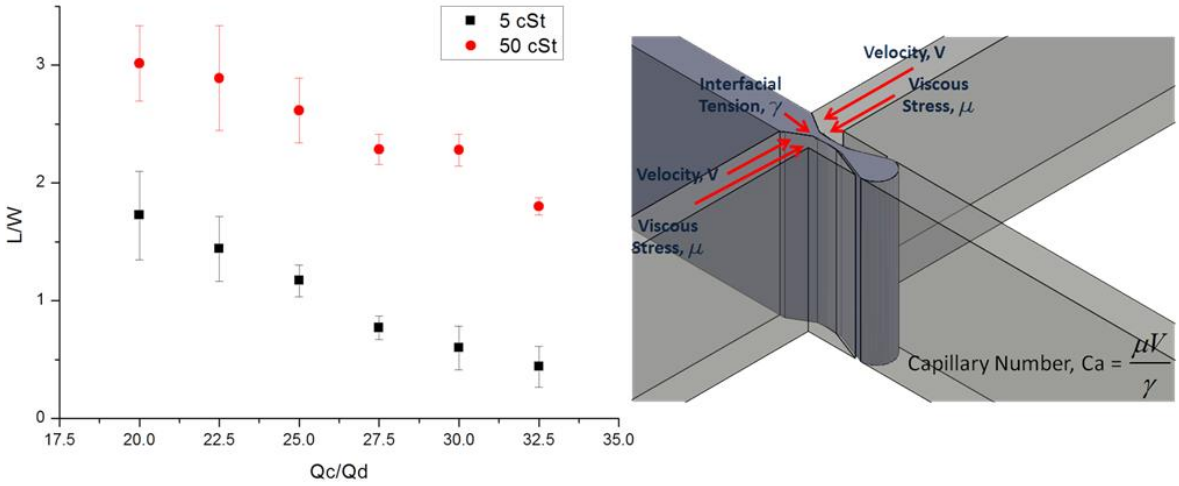

Figure 34: Ratio of droplet length (L) to channel width(W=170 µm) as a function of water-to-oil flow rate ratio with oil flow rate(Qd) = 10 µl/min.

3.3.4 Diffusion mode between continuous and dispersed phase

Although, it is a three phase extraction process; first the relationship between the extraction efficiency of phenol from dispersed to the continuous phase and the flow rate ratio of the two immiscible phases needs to be studied for optimising the overall process. The relationship between the oil- water interfacial area and the moles of ions transferred per unit time may be represented by a mass transfer equation, as per Fick's law, given below:

$$J = \frac{A_I}{\tau}\frac{[KC_{int} - C_{ext}(\tau)]}{\delta}$$

where J is the number of moles transferred, A_i is the interfacial area of contact between the two phases and is actually the surface area of the droplets here, $\mathcal{T}$ is the residence time of the droplets in the microreactor, **δ** is the thickness of the oil-water interface which acts as a membrane; K is the partition coefficient of the molecules, C_{int} and C_{ext} denote the concentration of molecules in the interior and outside the droplet, respectively.

To increase the extraction efficiency of phenol from oil droplets to water, we increase the flow rate of the continuous phase to obtain smaller sized droplets[21] thereby increasing the interfacial area of contact per unit volume between the dispersed and the continuous phase which will, in turn, increase the mass transfer rate between the two immiscible phases as per Fick's law. Hence, increasing the flow rate ratio should increase the mass transfer rate between the two phases as per the transient mass transfer equation. But it is not so, i.e; the extraction efficiency reduces with increase in the flow rate ratio as there are two different diffusion regimes: during the droplet formation stage and after the formation of discrete oil droplets; and the duration of a droplet formation (filling) stage plays a more critical role than the size of the droplets in the microreactor. Because in the droplet formation (filling) stage; as the flow rate, Q_d of the emerging oil phase is much slower than that of the continuous phase, achieving convective mass transfer equilibrium takes longer. But, after the formation of discrete oil droplets, these droplet travels through the channel at approximately the same velocity of the continuous phase[21] which makes the molecular diffusion rate much faster. So, the size of the droplets obtained at high flow rate ratios become irrelevant. In other words, because mass balance equilibrium is

achieved much slower in the droplet formation stage; the longer duration of this stage is important. The duration of this droplet formation (filling stage) however reduces with the increase of the flow rate ratio of continuous to dispersed phase as shown in Figure 32. So, to increase the duration of the droplet formation stage, low flow rate ratio should be preferred.

During the filling stage of the droplet formation cycle, the oil stream flows down the microchannel after going past the cross flow junction [Fig. 31]. For colloidal suspensions, it has been reported that dispersion of solutes occur along the axial direction[98]. In this stage, the colloidal particles in the oil which has points of contact along the microchannel wall has zero velocity and there is maximum velocity along the axis. Hence, the flow is streamlined in the shape of a parabola (pressure-driven flow) as the fluid velocity is laminar. This stage exists as long as the oil stream is in the filling stage; and with increasing flow rate ratio, the duration of this stage decreases [Fig. 32]. In this stage, the analyte species encapsulated within the dispersed phase penetrate mostly across the elongated tip of the dispersed phase along the axis before the Rayleigh-Plateau instability cause it to break into droplets[31]. This happens at the oil tip as the shearing impact of the microchannel walls is minimum at the central z-axis as a result of which the axial dispersion is at its maximum. The shearing impact by the micro-channel walls accounts for a cross-streamline diffusivity because of the shearing effect by the microchannel walls, in the oil phase given as[98]:

$$D_r = D_{phenol,oil} + a^2|\dot{\gamma}|$$

where $D_{phenol,oil}$ is the diffusion coefficient obtained from the Wilke-Chang equation[32] and a is the particle radius. The second term,

$$\dot{\gamma} = \frac{\partial u(r)}{\partial r} = \frac{\partial [2u\left\{1 - \left(\frac{r}{R}\right)^2\right\}]}{\partial r} = -4ur/R^2$$

$|\dot{\gamma}|$is the shearing rate(no slip) because of the microchannel wall. The lower the shearing rate, by the microchannel walls, higher is the diffusion rate. The closer the streamlines in the oil tip, get to the microchannel walls, the shearing rate increases which cause the analyte species to migrate towards the central z-axis and hence, the diffusion in the axial direction decreases. It is because of this reason that the analyte species mostly penetrate across the elongated tip of the dispersed phase.

With regards to the discrete oil droplets after the droplet formation stage, it is squeezed between the microchannel channel walls and unless the droplet length exceeds 1000 µm (height of the microchannel), it retains a spherical disk shape in the upright position if viewed from the side ways. After droplet formation, streamline pattern within the droplets takes the formation of the Hill's spherical vortex[31]. The velocity streamline function as shown in the inset of the figure below is given in literature[99] where r is the droplet radius and z is the microchannel width.

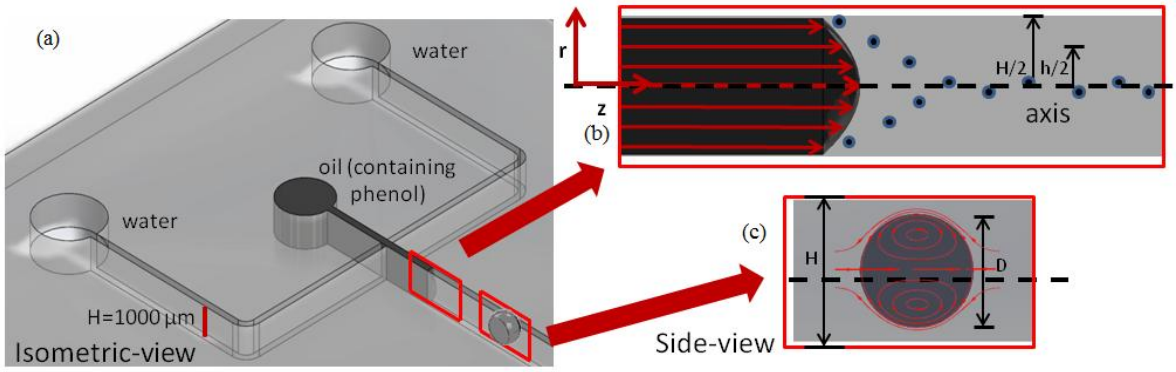

Figure 35: (a) Illustration showing the isometric view of the microfluidic cross-flow junction; (b) Side view of the droplet formation stage with the velocity profle with the elongated oil phase in the filling stage of the droplet generation cycle; (c) Side view of an oil droplet along the channel height showing the streamline pattern which takes the formation of the Hill's spherical vortex. H is the channel height, D is the droplet diameter.

Following this, comes the diffusion regime from individual oil droplets as the droplets move down the microchannel. Different from freely suspended droplets, which are spherical[100]; due to geometric confinement in the microchannels, uniaxial stretching of the droplets takes place resulting in a flattened disk-like shape[21] of droplets. As we have adopted an aspect ratio of W<H, the oil droplets become circular from the sideways as long as the height (H) of the channel exceeds the diameter (*D*) of the circular disk-shaped droplet and the streamline pattern within the oil droplets takes the formation of the Hill's spherical vortex[99] [Fig.35(c)].

3.3.5 Effect of flow rate ratio of continuous to dispersed phase on the mass transfer rate of phenol from the droplets to the surrounding water phase

We made a comparison of the diffusion rates between the two stages for the same inlet concentration, of 5 mg/ml phenol in 5 cSt silicone oil with an assumption of an equal surface area of the oil domain. A two dimensional scheme is implemented using a finite element method (FEM) model in Comsol Multiphysics 4.3b. First, the velocity field of the outer continuous phase is obtained from the steady-state Navier-Stokes equation in an Eulerian frame of reference. Using this, the time-dependent convection-diffusion

equation is applied in the oil and water domain for quantifying the diffusion of phenol from dispersed to continuous phase considering slip velocity boundary conditions at the immiscible oil-water interface. We did not take into account the normal stresses due to interfacial tension which will restrict the diffusion of ions between the two immiscible phases and displacement of the oil phase with time.

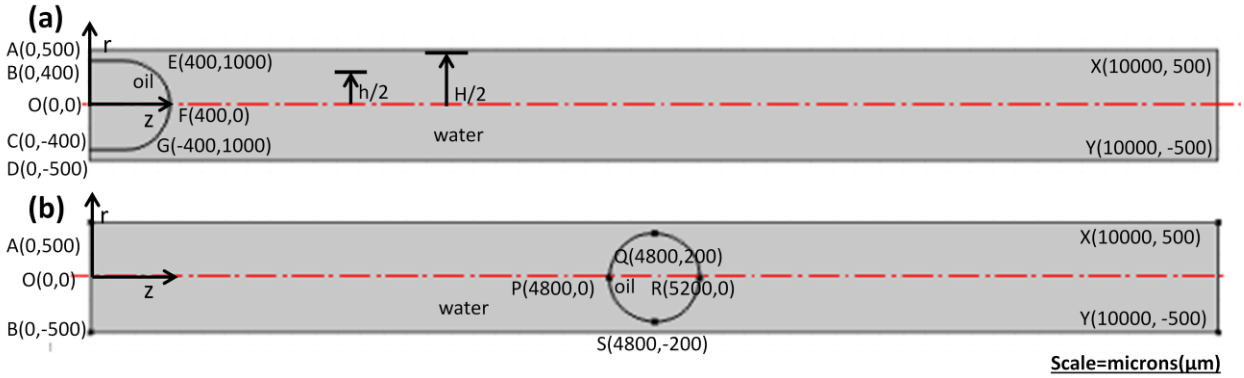

Figure 36: Snapshots showing the geometrical description of the two stages of diffusion during (a) the droplet formation (filling stage) and (b) the droplet formation stage as applied in Comsol Multiphysics 4.3b in a two dimensional (2D) scheme.

Governing equations:

Steady state velocity field for continuous phase:

$$\rho(u.\nabla u) = -\nabla p + \mu\nabla^2 u$$

Initial values:

Case (a) Axial inlet velocity, u at AB and CD= Q_c/(WH) [m/s]= 0.0196 m/s

Case (b) Axial inlet velocity,u at AB = Q_c/(WH) [m/s]= 0.0196 m/s

Case (a and b) Outlet pressure at XY= 0 Pa.s

Where Q_c =200 ul/min is the flow rate of the continuous phase injected by the syringe pump and W = 170 um, H = 1000um.

Transient convection-diffusion equation between continuous and dispersed phase:

$$\frac{\partial C}{\partial t} + \nabla.(-\mathrm{D}\nabla\mathrm{C}) + \mathrm{u}.\nabla\mathrm{C} = 0$$

There are two separate domains to be considered: the oil and the water domain.

Initial values:

Initial concentration in Oil domain, C_i=5mg/ml=53.129 mol/m^3.

Initial concentration in Water domain, C_i=0 mol/m^3.

In the oil domain, case (a) u_r = 0 m/s, u_z=u_{oil}/2 and case (b)

$$u_r = \frac{3}{2}u\frac{zr}{droplet\_radius^2}, u_z = \frac{3}{2}u(1 - \frac{2r^2 + z^2}{droplet\_radius^2})$$

The velocity profile in the droplets as given above is obtained from Hill's spherical vortex[99].

Droplet radius, droplet_radius = 400 um

The velocity field in the continuous phase, is to be obtained from the solution of the Navier-Stokes equation.

Diffusion coefficient, D_w = $D_{phenol,water}$ in the water phase and D_o = $D_{phenol,\ oil}$+$a^2|\dot{\gamma}|$ in the oil phase for both case (a) and (b) where $D_{phenol,water}$ and D = $D_{phenol,\ oil}$ are obtained from Wilke-Change equation[32] which is given below:

$$D_{phenol/solvent} = \frac{7.4 * 10^{-8} * (\emptyset_{solvent} * M_{solvent})^{0.5} * T}{\mu_{solvent} * V_{phenol}^{0.6}}$$

Φ=association factor=2.6(water),1(silicone oil); T=room temperature (298 K), V_{phenol}=molar volume of phenol= 8.79*$10^{(-5)}$ m^3/mol.

$M_{solvent}$=Molecular weight=18 for water, 236 for silicone oil, assuming n=1 in $CH_3SiO-[Si(CH_3)_2O]_n- Si(CH_3)_3$

We take n=1 in the general molecular formula for Silicone oil as we are only making a comparison between two cases: (a) and (b).

In oil domain, the second term, $a^2|\dot{\gamma}|$ denotes cross-streamline diffusivity because of shear enhanced diffusion .

Boundary conditions:

No flux (-n.N=0) at AX and DY.

Outlet (-n.D∇C=0) at AB, CD and XY.

Constants:

H=1000 um, W=170 um

Continuous phase flow rate, Qc =200 ul/min

(Linear) continuous phase flow rate in z-axis, u = uc=200*10^(-9) /(H*W)=0.0196 m/s.

Dispersed phase velocity, Qd=10 ul/min

(Linear, filling stage) dispersed phase velocity in z-axis, uoil = 9.8 *10^(-4) m/s

Droplet radius, droplet_radius = 400 um

Viscosity of SDS solution in DI water at CMC,μ= 8.15 *10^(-4) Pa.s

Density of continuous phase, ρ_{water}= 1000 kg/m^3

Density of dispersed phase, ρ_{oil}= 900 kg/m^3

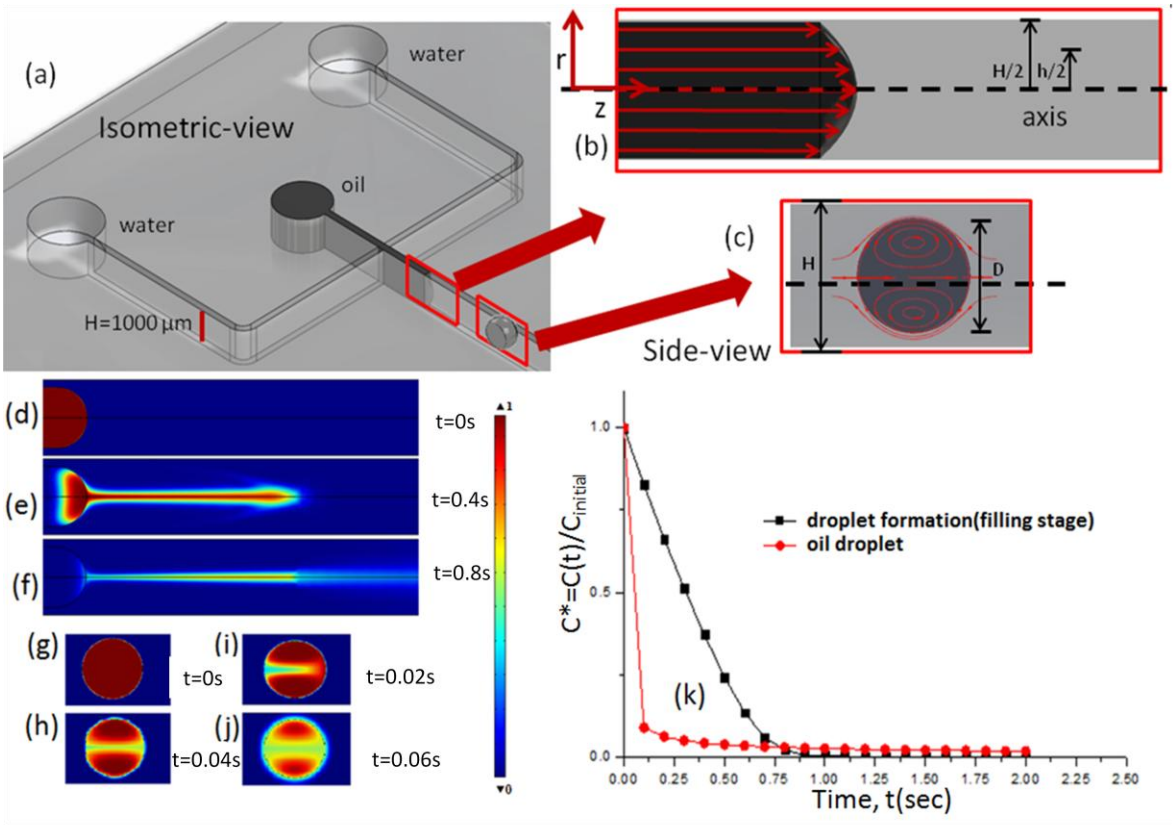

31

Figure 37: Numerical simulation results (a),(b),(c) and (d),(e),(f),(g) showing the diffusion of phenol from oil phase in the filling stage and after the formation of individual droplets, respectively at different times with continuous phase flow rate at 200 µl/min and dispersed phase at 10 µl/m; (h) Normalized surface area averaged concentration in the oil phase both in filling stage and after the formation of droplet versus time.

The results of the numerical simulation are given in Figure.37. From Fig.37(a-c), in the droplet formation case, we observe that ion concentration present in the elongated oil tip diffuses much slower to the water initially because emerging oil tip moves much slower than the continuous phase. But it empties itself completely over time as the streamlines in the oil tip directly intersect the oil-water interface. Experimentally, we have observed that

the concentration of phenol in the water phase never reached equal to that within the oil phase as the volume of the water exceeds the volume of oil which is proportional to the flow rate ratios. Another factor is that only the phenol molecules which break down into hydrophilic phenoxide ions diffuse to water. The diffusion coefficient obtained from Wilke-Chang equation [16] does not take into account the acid dissociation constant of phenol molecules. The ions in the discrete oil droplets diffuse faster to the water initially as the droplets move at approximately the same velocity of the continuous phase [17] while they move down the microchannel. But the ion concentration does not drop to zero as the streamlines does not directly intersect the interface. Nevertheless, for optimizing droplet-based liquid-liquid extraction; we can conclude that longer duration of the droplet formation stage is preferable as the ion concentration in the oil phase falls gradually over time.

Experiments are also performed for investigating the liquid-liquid extraction efficiency of phenol from dispersed to continuous phase as a function of flow rate between the two phases. The mass transfer rate of phenolate ions from oil phase to the water phase may be represented by the extraction efficiency (I/Io) which is the ratio of I, the absorption peak intensity of phenolate ions per unit volume in the DI water (continuous phase) present in the 0.5 ml of the outlet of the microreactor [Fig.33] for all the flow rate ratios and Io is the absorption peak intensity of phenolate ions per unit volume in the DI water assuming there is 100% mass transfer while collecting 0.5 ml from the same outlet. Io is obtained taking into consideration the dilution factor as the phenolate ions are transferred from oil phase to the water phase which is proportional to the flow rate ratios set by us in the syringe pumps. This occurs because we have increased the continuous phase flow rate,

keeping the dispersed phase flow rate constant in our study which reduces the concentration of the ions accordingly as there is an expansion of volume. For instance, if the dispersed phase flow rate is 10 ul/min and continuous phase flow rate is 200 ul/min, the concentration of ions in the oil phase gets diluted 20 times as the ions diffuse from oil to water. So, we prepare samples containing (5/20) mg/ml concentration of phenol in DI water to get Io for all the flow rate ratios. Now, the residence time of droplets of microreactor used at Q_c = 325 µl/min (Qc/Qd=32.5) is ~1.32 seconds whereas the residence of droplets at Q_c = 200 µl/min (Qc/Qd=20) is ~2.142 seconds. Hence, we constructed a series of microreactors with longer microchannels (Fig.33) so as to keep the residence time the same for all the flow rate ratios.

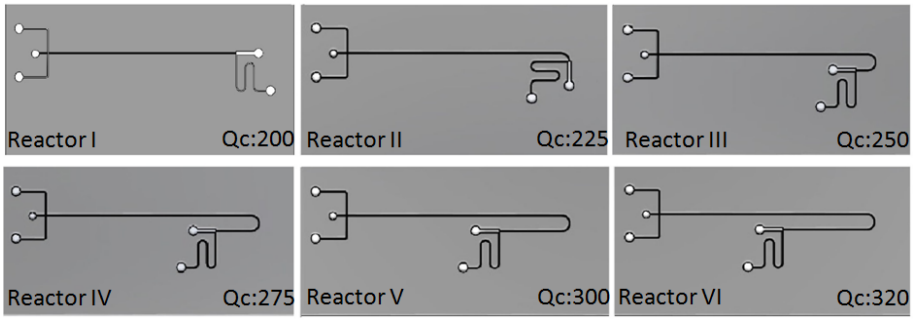

Figure 38: shows the top schematic view of the microchips with gradually increasing microchannels length for equal residence time(τ) of the oil droplets as the velocity, Q_c of the continuous phase (µl/min) increases .

We observed that even with longer microchannels for equal residence time for all the flow rate ratios and smaller sized droplets at higher flow rate ratios, higher extraction efficiency is obtained at lower flow rate ratio as can be seen from Fig. 34. . This implies that lower flow rate ratio (Qc/Qd) for higher extraction efficiency which provides for

longer droplets bearing higher filling stage regime during droplet formation. This correlates well with our numerical results as we observed that the diffusion rate of phenol from oil phase to water is slower in the droplet formation as shown in Figure. 37(h) and so, enhanced duration of the droplet formation stage is necessary for improving the overall extraction efficiency of phenol from the dispersed phase to the continuous phase.

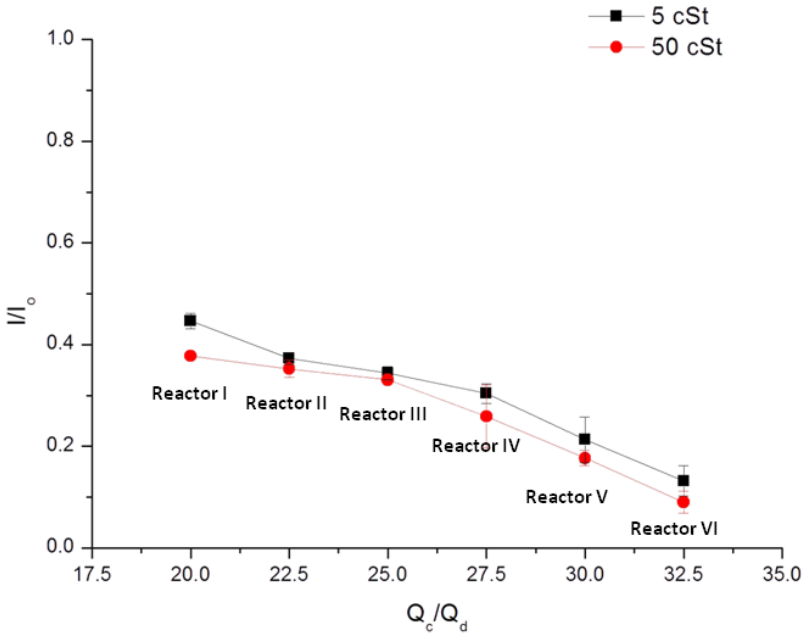

Figure 39: Plots of observed HPLC chromatogram peak of phenolate ions in the outlet of the microchips (with respective microchannel lengths as shown in the Fig.26 at varying flow rates of the continuous phase from 200 µl/min to 325 µl/min with dispersed phase constant at 10 µl/min.

3.3.6 Interpretation of extraction efficiency as a function of Capillary number

In order to make the results more meaningful, the extraction efficiency may also be plotted as a function of the capillary number and we observed that our experimental results agreed with the physical interpretation of the capillary number. The capillary

number (Ca) represents the relative effect of viscous forces versus surface tension acting across an interface between two immiscible phases. As the shearing mechanism of droplet formation is a rate-of-flow controlled break-up process[21]; hence, extraction rate can further be correlated with the capillary number, Ca. In our experiments, Ca<1 for all flow rate ratios. As the flow rate is reduced further, the interfacial tension forces which resist the pinching of the droplets become more dominant. From a practical point of view, our study provides guidelines that for obtaining maximum extraction efficiency, the lower capillary number must be preferred as the interfacial tension forces are more dominant which eases the effusion of the analyte species from the dispersed phase.

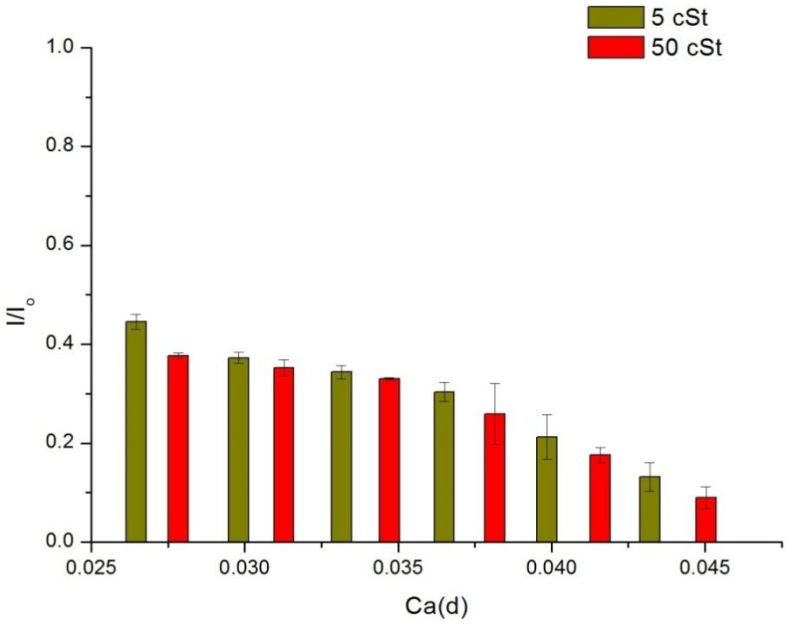

Figure 40: Extraction (mAU) of the previous figure plotted as a function of capillary number, Ca(d). Here Ca(d) represents the capillary number, Ca, of the dispersed phase such that Ca(d)= μ(d)*V/γ where μ(d) is the viscosity of the dispersed phase and V is the superficial velocity (m/s) of the droplets.

3.3.7 Other miscellaneous factors affecting the extraction of phenol from silicone oil droplets to the continuous phase

The extractability of a weak acids such as phenol from silicone oil droplets onto a immiscible aqueous phase depends on the pH of the surrounding aqueous phase, ionization constant of phenol in the two phases and partition coefficient of ionized phenol between the two phases [101]. In order to extract the analyte species from the silicone oil droplets (dispersed phase), the phenol molecules must be dissociated into phenoxide ions first. Only, the phenol molecules (HA) in its deprotonated form (A^-) having a negligibly small oil-water partition coefficient will be extracted to the aqueous phase as the negative formal charge on phenoxide ion provides for stronger attractions to (and hence more solubility in) polar solvents for phenoxide ion thereby making it hydrophilic. In the receiver phase the phenol molecules stay trapped there in the ionized form after diffusing across the oil-water interface. Although SDS micelles present a favorable environment for the oil solubilize[102] , aromatic hydrocarbons like phenol molecules are almost insoluble in water at ordinary room temperatures. It is assumed that there is no mass transport of phenol molecules between the silicone oil droplets via micellar mediation because all the droplets have the same composition which provides zero concentration gradient.

3.3.8 Multilayered membrane-based device for liquid-liquid-liquid extraction (LLLE) of phenol molecules from silicone oil droplets onto the bottom phase via continuous phase

Finally, experiments were conducted using the membrane-based microchannel device as shown in Fig.30 for further refining the process. A multi-layered PMMA device with polypropylene (hydrophobic) membrane was fabricated for this purpose.

From our previous experiments, we observed that higher extraction rates were obtained at lower flow rate ratios of continuous to dispersed phase. Hence, using a continuous flow rate velocity at 200µl/min and dispersed flow rate velocity at 10 µl/min (the lowest flow rate ratio used for our experiments); liquid-liquid-liquid extraction (LLLE) can be successfully conducted. The bottom acceptor phase consisting of DMF and the surfactant solution with 0.1 M HCl (which is introduced after the removal of oil droplets) are both given a flow rate of 10 µl/min. Finally the bottom phase collected at the outlet is analyzed using HPLC for quantifying the concentration of phenol. The HPLC chromatogram of the bottom phase as given below in Fig. 41 shows the two peaks; one observed for DMF and the other for phenol. The mass transfer of phenol is first from 5 cSt silicone oil (donor phase) to the surrounding continuous phase; and thereafter from continuous phase to the bottom phase (LLLE) via the membrane.

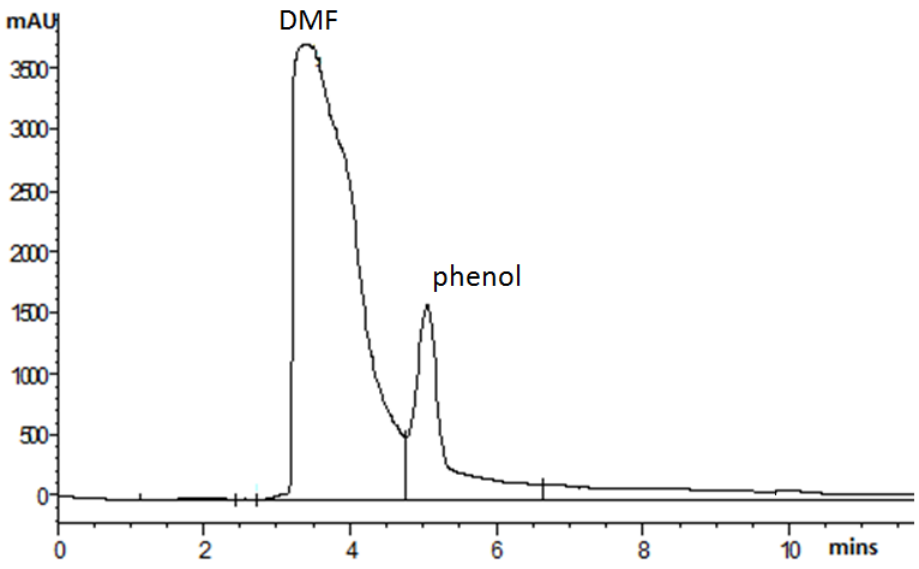

Figure 41: HPLC chromatogram of the DMF outlet from the acceptor phase underneath the hydrophobic membrane containing phenol molecules.

The extraction efficiency (=I/I_o*100) of phenol molecules from 5 cSt silicone oil is ~ **18 ± 5 %** with a continuous and dispersed flow rate of 200 and 10 µl/min, respectively. Here, I_o is chromatogram peak obtained by taking the phenol concentration at (5/20) mg/ml in DI water and I is the signal obtained from the sample outlet taken from the bottom plate.

3.4 Summary

A PMMA-based microreactor was designed which could extract phenol molecules from silicone oil droplets, a very complex donor phase solvent. This experimental study provides an insight for extraction of impurities from oil-in-water emulsions on a microfluidic platform. It has been demonstrated that for best extraction of analytes from a highly viscous donor phase such as silicone oil droplets onto a less viscous fluid, the longer duration of droplet formation plays a major role and mass transport of most of the

phenol molecules occurred via the shear-enhanced diffusion regime in the initial stages. Thereafter, only mass diffusion via Fick's law takes place after the droplet generation process is complete. Hence, lower flow rate ratio of continuous to dispersed phase or in other words lower capillary number is preferred as it enhances the filling stage of the droplet formation process. We did not use continuous phase velocities lower that 200 µl/min as parallel flow pattern is observed for 50 the cSt oil under such conditions and as such the separation of droplets at the outlet bifurcation would not be possible. For better efficiency further downstream, an etched PMMA plate containing thousands of microreactors with longer microchannels working in parallel may be implemented. Using a reflux for the microchannel which goes over the membrane as well as having multiple cross-flow junctions will also further improve the process.

3.5 Declaration

Part of the work presented in this chapter has been published in *Separation Science and Technology*.

Das D, Duraiswamy S, Yi Z, Chan V, Yang C. Continuous Droplet-based Liquid-Liquid Extraction of Phenol from Oil. Separation Science and Technology 15 Jan, 2015; 50(7): 7.

4. Continuous Detection of Trace Level Concentration of Oil Droplets in Water using Microfluidic AC Electroosmosis (ACEO)

4.1 Introduction

Isolation and detection of micron-sized oil droplets in water is of great importance to environmental oil spillage monitoring applications. Disasters such as the Deepwater Horizon[1] (DWH) oil spill following an explosion in April, 2010 in the Gulf of Mexico remind us about the vulnerability of our ecosystem. It is necessary to break down the floating oil slicks because the marine mammals and seabirds require routine contact with the sea surface[103] and as such oiling of furs and feathers can cause hypothermia, ingestion of toxic hydrocarbons, etc. Thus in the aftermath of such disasters, usually surfactants such as Corexit EC9500A[4] are used to break down the oil slicks which eventually reduce to oil droplets of sizes less than or equal to 70 microns. Oil spill at or near the water surface is also subjected to many physico-chemical processes[104], one of which is the mechanical spreading due to interfacial tension forces, gravity, etc. causing oil slicks on the water surface. The turbulence caused by waves, wind and water currents further break the oil slicks into stable oil-in-water (O/W) emulsions. Owing to a widespread use of such chemicals and external mechanical forces, the micron-sized droplets travel a distance which is very hard to determine accurately via satellites because a substantial portion of the oil is carried by underwater plumes. It was observed after the DWH disaster[1] that more than 212 kilometers of Gulf coastline was moderately to heavily oily by late August, 2010. Currently, fluorescence-based oil detectors [10-12]

with detection sensitivity below 1 ppm (parts-per-million) are being used extensively to quantify oil concentration in water. But the major drawback of these detectors is that they are not reliable as the fluorescent signal generated by the instrument does not truly reflect the actual concentration of oil in water[10]. Since the instrument is calibrated using specific oils, the concentration yield which is represented by the fluorescent signal is relative to those specific oils only. Another major disadvantage is that these instruments are bulky, and thus on-field analysis is challenging. Recently, trapping and separation of oil droplets in water was reported by utilizing acoustophoretic force in microfluidic channels etched in silicon wafer [72]. A fluorescent module was incorporated for the optical detection of trapped oil droplets.

In this chapter, we present a microfluidic module for the trapping and detection of oil droplets in water by using an alternating current (AC) electric field. When an external AC electric field is applied to an electrolyte contained in microchannels with charged walls, it leads to the formation of an electric double layer (EDL)[105] at the electrolyte-channel wall interface. The EDL can be divided into an inner compact layer and an outer mobile layer[106]. Under the influence of an electric field, the net migration of ions in the outer mobile layer is transmitted to the bulk fluid by viscous forces and regarded as electroosmotic (EO) flow. This kind of fluidic motion has been used to direct electrolytes[106, 107] and referred to as ACEO micropumps. This ACEO phenomenon has also been conveniently used for trapping or concentrating bio-particles around the electrodes[67, 108-110]. In this paper, we use this ACEO phenomenon to trap the oil droplets around the electrode edges. The electroosmotic flow velocity is given by $U_{eo}=(\varepsilon\varepsilon_0\zeta/\eta).E_t$, where ε is dielectric constant, ε_0 is the permittivity of vacuum, ζ is the

surface zeta potential at the electrolyte-charged microchannel wall interface, η is the viscosity of the medium and E_t is the tangential component of the electric field. In other words, U_{eo} is in direct proportion to the amplitude of the applied AC electric field and the strength of the EDL characteristics such as the ζ- potential. But for ACEO, the ζ-potential is not constant as it depends on the applied frequency which determines the rate of polarization of the microchannel and electrolyte interface. It has been reported[111] that at low frequencies, the counterions completely saturates the EDL thereby shielding the EDL from the bulk solution, thus the net flow of the bulk fluid goes to zero. At high frequencies, the counterions do not have enough time to migrate to the rapidly changing charge applied to the electrode surface which affects the formation of the EDL.

In addition to ACEO, applying a non-uniform AC electric field also generates a dielectrophoretic (DEP) force[112, 113] on the bio-particles on account of the difference in polarizability between the particles such as oil droplets and the surrounding aqueous fluid such as water. The time-averaged DEP force[71] is given by

$$\langle \vec{F}_{DEP} \rangle = 2\pi\varepsilon_m a^3 Re[K(\omega)]\nabla\left|\vec{E}_{rms}\right|^2$$

where ⟨ ⟩ represents the time average, ε_m is the permittivity of the medium, *a* is the size of the particle. It is to be noted that the strength of the DEP force increases with increasing size of the particles. $\vec{E}_{rms}$ is gradient of the square of the applied electric field, $\nabla\left|\vec{E}_{rms}\right|$ is the root-mean square electric field, Re[K(**ω**)]=Re[($\underline{\varepsilon}_p$-$\underline{\varepsilon}_m$)/($\underline{\varepsilon}_p$+2$\underline{\varepsilon}_m$)] is the real part of the Clausius-Mossotti(CM) or polarization factor ranging from -0.5 to 1, $\underline{\varepsilon}$=ε-i (σ/ω) is the complex permittivity with σ as electrical conductivity, $i = \sqrt{-1}$, ω=2**p**f is the frequency of the applied electric field. $\underline{\varepsilon}_p$ is the permittivity of the particle, $\underline{\varepsilon}_m$ is the

permittivity of the medium. Depending on whether the bio-particles are more or less polarizable than the surrounding fluid, they tend to move towards or away from the high intensity electric field zone and henceforth, the DEP force is classified as positive, p-DEP(such that $Re[K(\boldsymbol{\omega})]>0$) or negative, n-DEP(such that $Re[K(\boldsymbol{\omega})]<0$), respectively. The present study utilizes the fact that as oil droplets are less conductive than water, it will be repelled by the high electric field zones. Several n-DEP force-based traps[114] have been reported for concentrating generic particles like latex[115] and polystyrene[116] beads, cells like escherichia coli[117], yeast[118] and so forth.

Due to hydrophobic nature of PDMS, oil droplets usually stick to native PDMS walls and eventually clog the microchannels. Hence, a surface treatment step[73] is incorporated. Thereafter, experiments are performed to study the effect of frequency on electroosmosis via its trapping efficiency. In our experiments, we also observe the fusion of oil droplets to attain a larger size in the entrapment zone and that there is an increase in the linear velocity for the larger sized droplets as they exit the entrapment zone. This confirms the presence of a size dependent DEP force which implies that the entrapment efficiency would be enhanced for larger sized droplets.

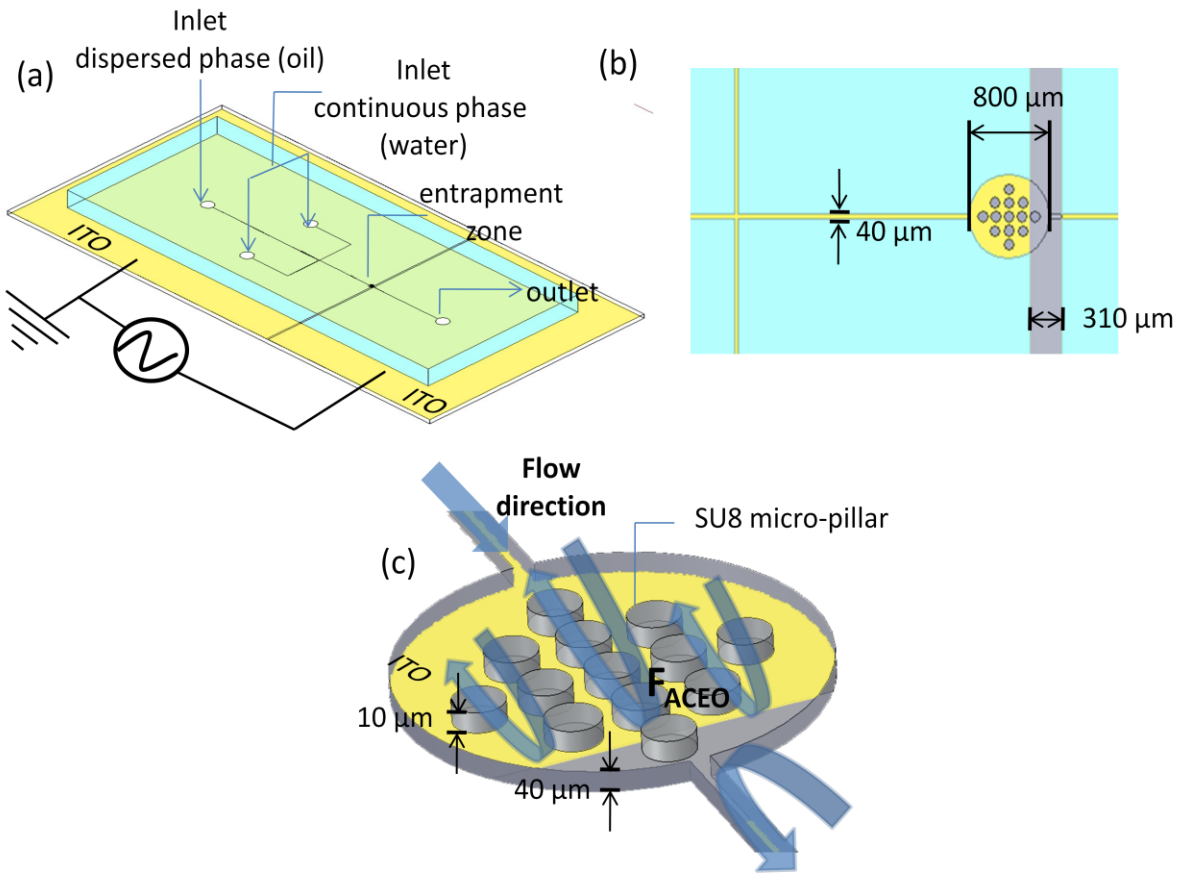
(a)
Inlet
dispersed phase (oil)
Inlet
continuous phase
(water)
entrapment
zone
outlet
ITO
ITO
(b)
800 µm
40 µm
310 µm
(c)
Flow
direction
SU8 micro-pillar
ITO
10 µm
F_{ACEO}
40 µm
(d)
1 cm
entrapment
zone

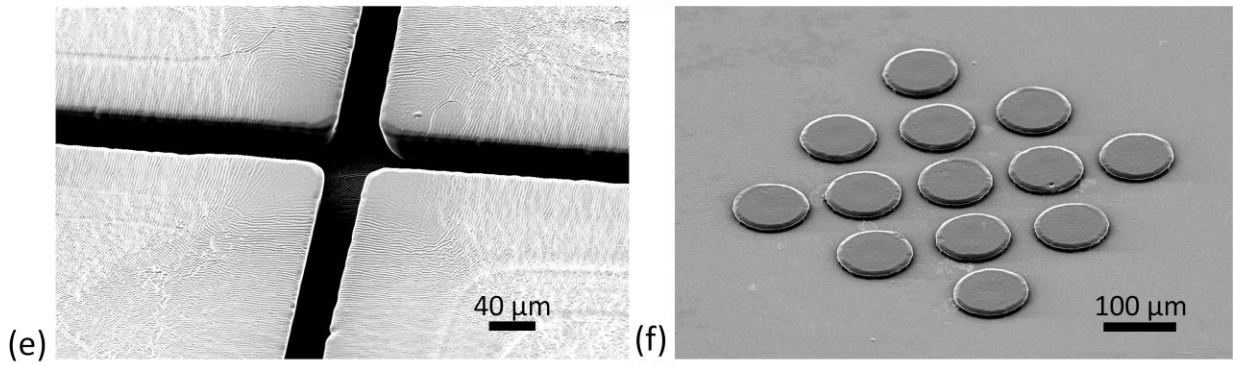

Figure 42 (a) Schematic illustration of the microchip showing the inlets for dispersed phase, oil and continuous phase, water; the entrapment zone and the ITO electrodes over the base glass substrate (b)Dimensions of the microchannels(both width and height is 40 µm), entrapment zone(800 µm) and the electrode gap(310 µm) (c) Droplet entrapment zone with the counter-rotating vortices emerging from the parallel ITO electrodes and the SU8 micro-pillar array of height 10 µm and diameter 100 µm each (not drawn according to scale) (d) Photograph of the actual microfluidic device. (e) and (f) are SEM images of the cross-flow junction of the PDMS block used for the generation of oil droplets and SU8 micro-pillars on the glass substrate, respectively.

4.2 Experimental

4.2.1 Microchip fabrication

A schematic of the microfluidic device is shown in Fig. 42(a). First, a 0.7-mm thick glass coated with a conductive indium tin oxide (ITO) (Optoelectron Technologies, Singapore) film was taken as the base plate of the microfluidic device. ITO was chosen as it is optically transparent and enables us to visualize the droplets through the electrodes as the droplets are trapped over the electrodes due to the ACEO flow field. The ITO patterns on glass were obtained by using AZ photoresist followed by acid etching in HCl: H2O:

HNO3 (4:2:1 by volume) solution to obtain an electrode gap of 310 microns. Thereafter, SU8 micro-pillars of 10 microns height, was obtained by spincoating followed by UV exposure over the ITO patterned glass substrate. PDMS blocks were then placed over the micro-pillars on the ITO etched base glass plate after plasma treatment. We used a 310 micron electrode gap size as it is the smallest gap that we could obtain after etching ITO coated glass. A schematic of the protocol is shown in the figure below.

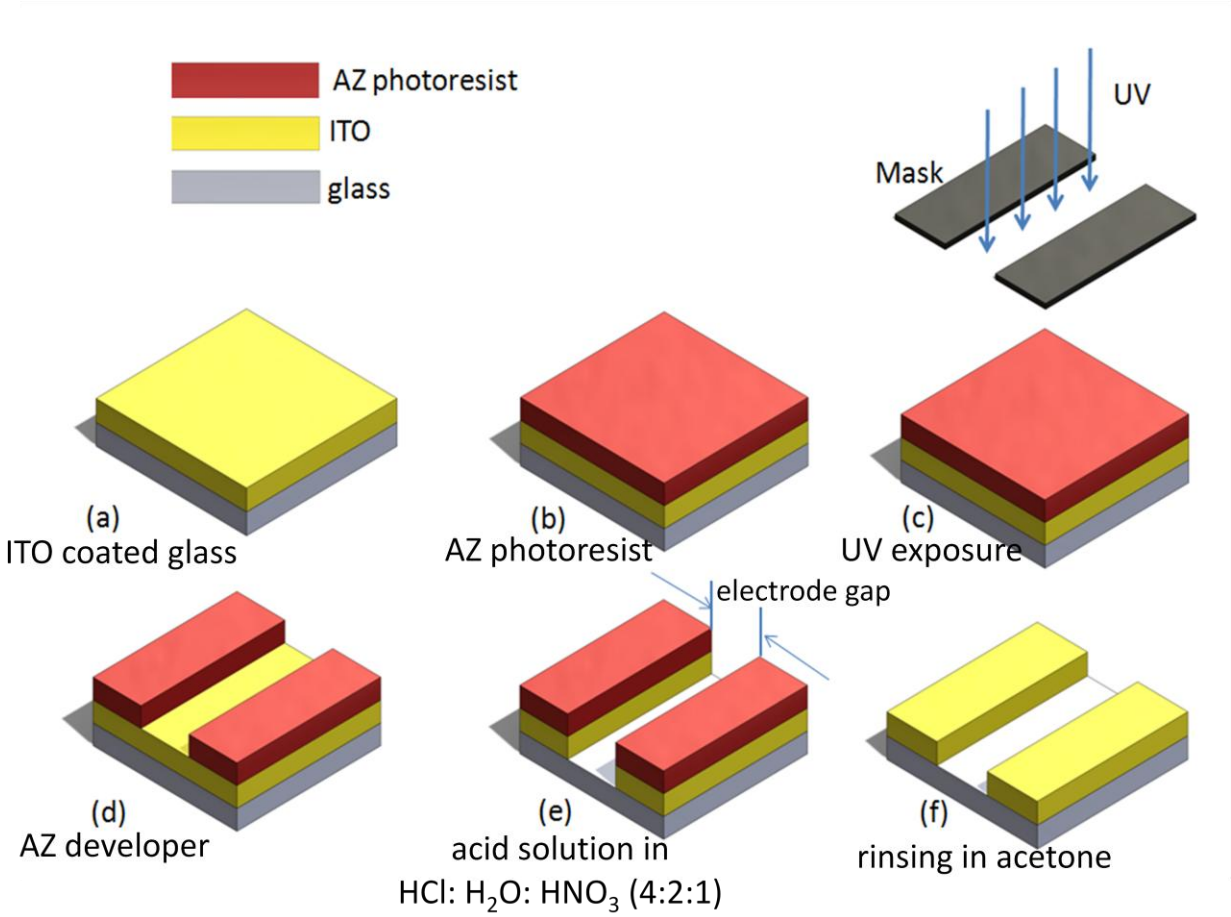

Figure 43 (a) ITO coated glass (b) thin layer of AZ photoresist after spin-coating (c) controlled UV exposure using an optical mask (d) after immerging in AZ developer (e) ITO etching in an acid solution which is HCl: H_2O: HNO_3 (4:2:1 by volume) (f) after rinsing with acetone to remove the remaining AZ photoresist.

The width and height of the microchannels is 40 microns whereas the diameter of the circular shaped oil droplet entrapment zone is 800 microns as shown in Fig. 41(b). Then hydrophilization of the PDMS-glass substrate microchannels was through (LbL) deposition scheme of alternately charged polyelectrolyte solutions poly(allylamine hydrochloride) (PAH) (Sigma, Singapore) and negatively charged poly(sodium 4-styrenesulfonte) (PSS) (Sigma, Singapore) by flushing it in the sequence PAH-PSS-PAH-PSS[73] immediately after plasma treatment because plasma oxidation induces a negative change of the microchannel surfaces. NaCl solution is also used in between the charged polyelectrolytes so as to flush out the loosely bonded ions. The flushing is done using a syringe pump at 0.4 ml/hr for 30 minutes each. A detailed sequence of the steps is shown in Fig. 44. The final step#8 [as shown in Fig. 44] of flushing by PSS renders the microchannel surface negatively charged which is then followed by flushing the microchannels with Triton X-100 at critical micelle concentration (CMC) in order to remove the loosely attached ions from the microchannel walls and make the same slippery. It is observed that the flushed and hydrophilized microchannel walls show great durability even upto 5 hours of continuous usage and no wetting of the PDMS-PDMS as well as PDMS-glass microchannel walls by the oil droplets takes place.

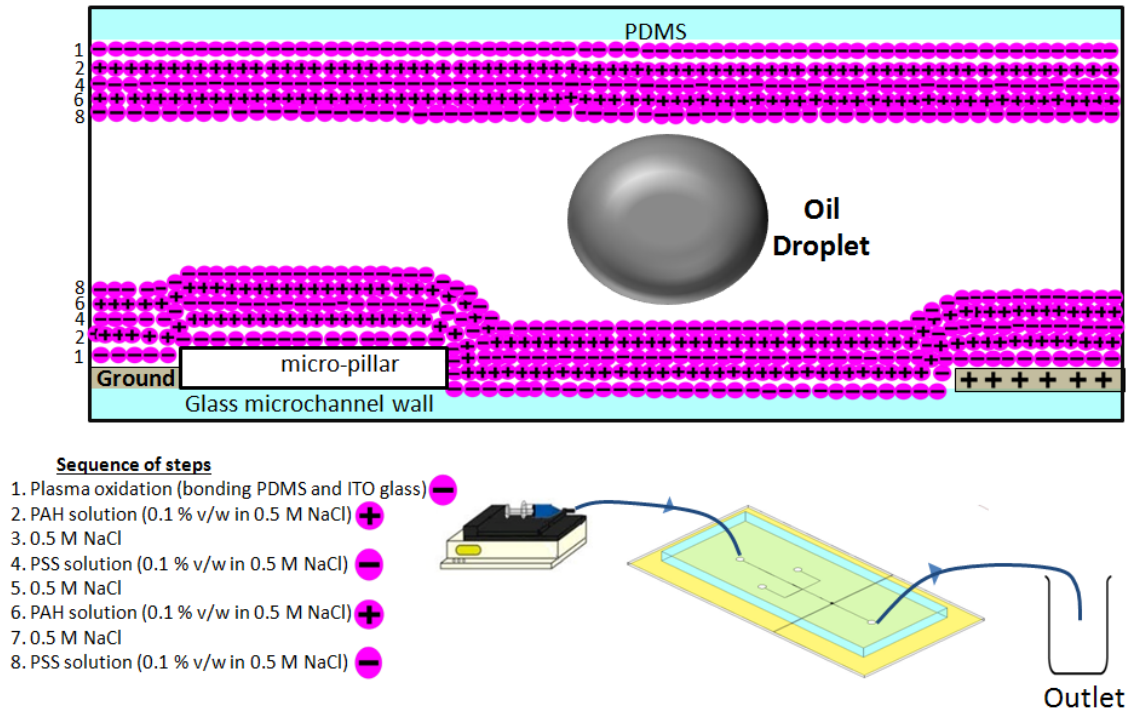

Figure 44 Schematic illustration of step-by-step sequence for the hydrophilization of PDMS-glass based microfluidic device.

4.2.2 Consumables and experimental set-up

Silicone oil (Sigma, Singapore) of viscosity 50 cSt was used as the dispersed phase. The oil phase was then emulsified into discrete droplets in an aqueous and immiscible non-ionic surfactant Triton X-100 (Bio-Rad Laboratories, Singapore) solution at the critical micelle concentration value, which makes up the continuous and immiscible aqueous phase. We used a cross flow junction for the emulsification of dispersed phase consisting of silicone oil (50 cSt, density=960 kg/m3) into individual droplets as shown in Fig.46 (a). We did not use ionic surfactants because they might lead to rapid oxidation, darkening and degradation of the ITO electrodes and gas formation at both electrodes at high voltages due to their higher conductivity. The dispersed oil phase was sheared off by the continuous water phase. The initial size of the oil droplets was slightly bigger before the flow was fully stabilized. Gradually over time, the size of the droplets became more

consistent. In our experiments, we kept the dispersed oil phase flow rate at 0.01 ml/hr and continuous phase water flow rate at 0.04 ml/hr to have a consistent droplet size.

Two syringe pumps (KD Scientific) with 0.5 ml Hamilton glass syringes are used for pushing the two immiscible fluids: dispersed phase, oil and the continuous phase, water. The droplet trapping at the circular zone of the microchip is observed with a Carl Zeiss microscope fitted with a Zeiss lens (CP-Achromat 5x/0.12) and a Phantom Miro M310 digital high-speed camera at 200 frames per second. A function generator (Agilent 33250A) is connected with an amplifier (AVC 790 Series Power Amplifier) by a BNC cable to produce AC voltages of desired frequencies which is imposed on the ITO electrodes.

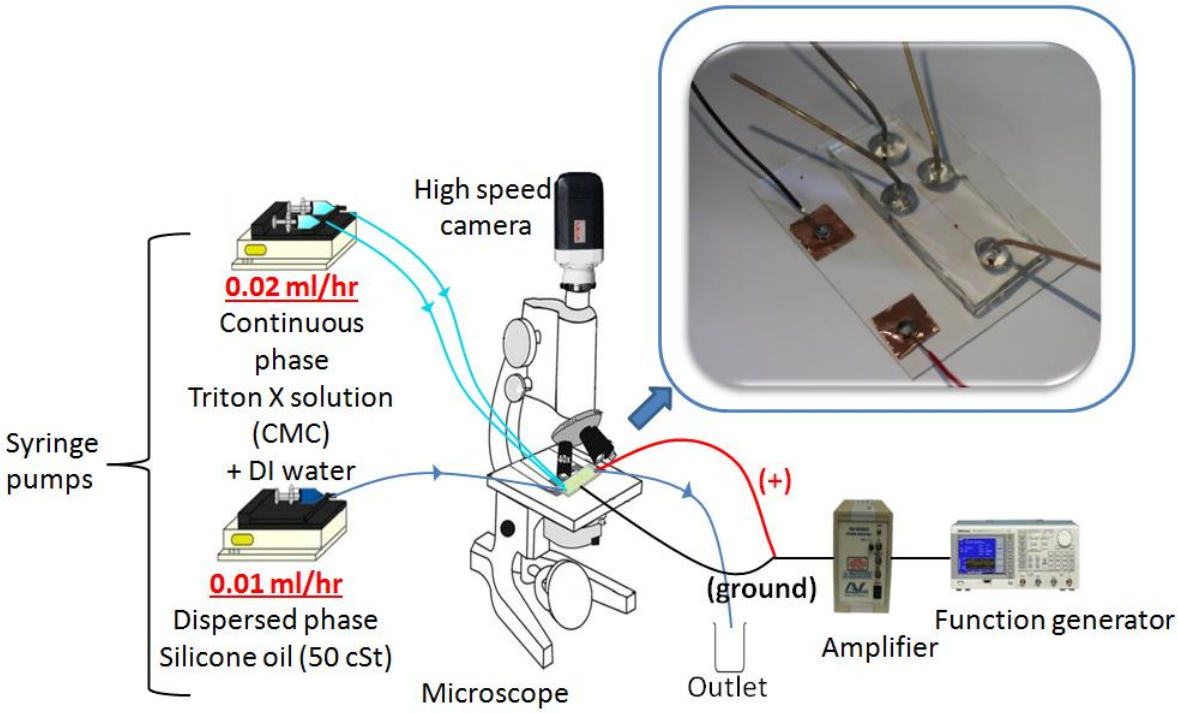

Figure 45 Schematic drawing of the experimental set-up. Inset drawing a photograph of the microfluidic device.

4.3 Results and discussions

4.3.1 Micro-pillar array and oil droplet trapping

Trapping of oil droplets is achieved in a circular shaped oil droplet enrichment zone which contains the micro-pillar array. Initially, the gap between the micro-pillars was filled with droplets. These droplets become immobilized and together with micro-pillars offer the hydrodynamic resistance which is necessary to slow down the incoming oil droplets. Finally, equilibrium is achieved such that a finite volume of oil droplets is maintained in the circular oil enrichment zone as the rate of the incoming droplets is equal to the rate of droplets exiting the enrichment zone. Fig. 46 (b) and (c) shows two images of oil droplets as one enters the entrapment zone, another exits the same. The trajectory of the oil droplets is shown in Fig. 46(d) which indicates that the oil droplets make its way around the micro- pillars.

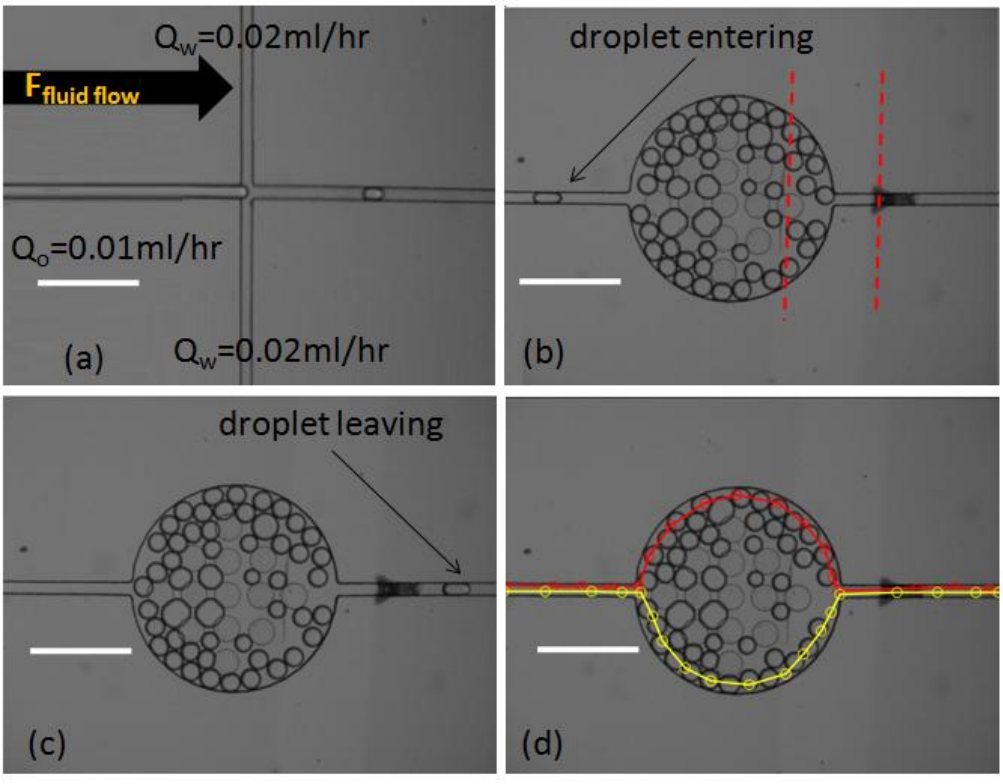

Figure 46 (a) Cross-flow junction for generation of oil droplets where Q_o and Q_w are the volumetric flow rates of oil and water, respectively. (b) a droplet entering the trapping structure and the highlighted red lines are electrode edges towards the outlet. (c) a droplet exiting the trapping structure. (d) trajectory of the droplets around the SU8 micropillar array. Scale bars denote 400 μm.

To prevent the escaping of droplets from the enrichment zone, an electric field is imposed. Two ITO electrodes are positioned in such a way that the escaping droplets will have to go over the electrode gap at the outlet from the circular shaped entrapment chamber. We chose this electrode design because it is motivated by the ACEO flow field experiments[67, 108] around the planar electrodes where the particles are pushed away from the electrode gap. Hence, our device is designed in such a way that the droplets would have to go over the electrode gap to escape from the entrapment zone.

Calculation of the electric field [V/m]at the outlet of the oil entrapment zone is done in Comsol Multiphysics 4.4.

Governing equations:

The electric field potential, V, satisfies the Poisson's equation and is given by

$$-\nabla.(\varepsilon_o \varepsilon_r \nabla V) = \rho$$

where ε_o is the permittivity of free space, ε_r is the relative permittivity of DI water, applied electric potential, V=Vp-2-p/$\sqrt{2}$=200/$\sqrt{2}$=141.42 V; ρ is the space charge

density. The electric field and the displacement are obtained from the gradient of V and given by

$$E = -\nabla V$$

$$D = \varepsilon_o \varepsilon_r \mathrm{E}$$

Normalized electric field and its squared scalar magnitude is given by

$$|E| = \sqrt{E_x^2 + E_y^2 + E_z^2}$$

Boundary conditions:

Applying zero surface charge at the boundary, we take n.D=0. Thereafter, the model is drawn in Comsol and the results obtained in Fig. 47 shown below.

Due to the constriction of the circular shaped entrapment shape, a non-uniform electric field is generated and the strength of the normalized electric field (V/m) is highest at the outlet where the droplets are trapped [Fig.47(b)].

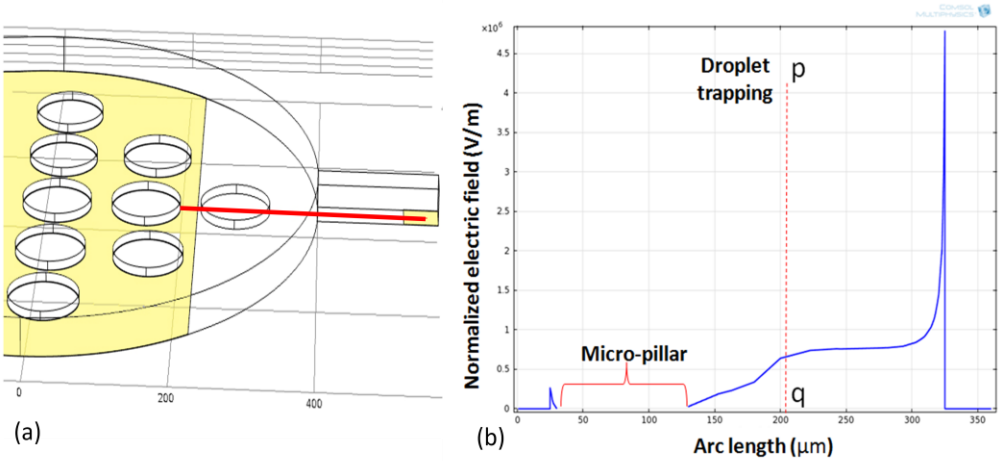

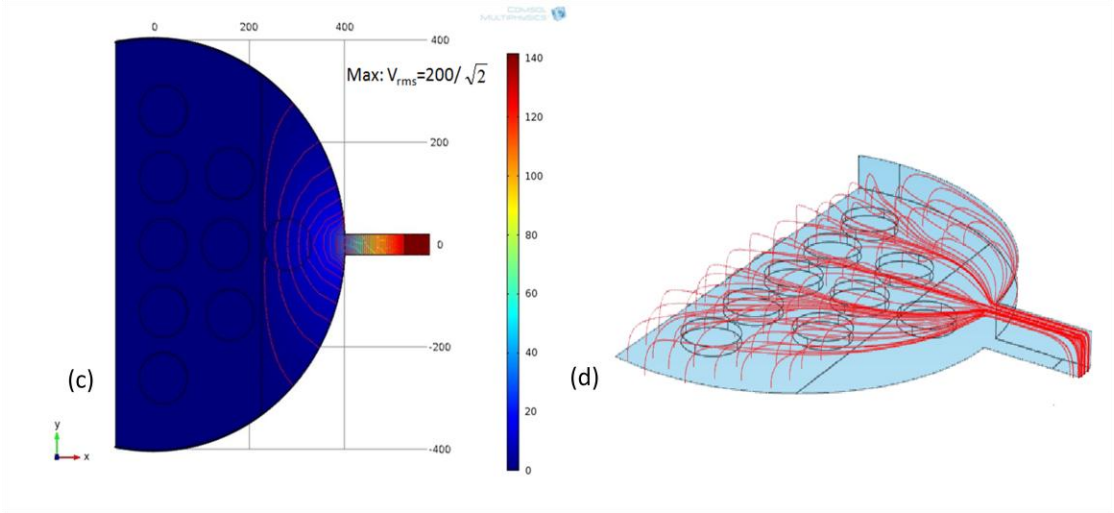

Figure 47 (a) cut-line is red is shown at the outlet of the microfluidic device. (b) Normalized electric field strength (V/m) along the cut-line at an applied AC voltage of 200 Vp-2-p at the bottom of the microchannel. pq shows the increase electric field strength where the droplets are trapped. (c) Electric potential (V) at the same applied AC voltage (d) constriction of the electric field lines at the outlet; (b)-(d) obtained from Comsol Multiphysics 4.4.

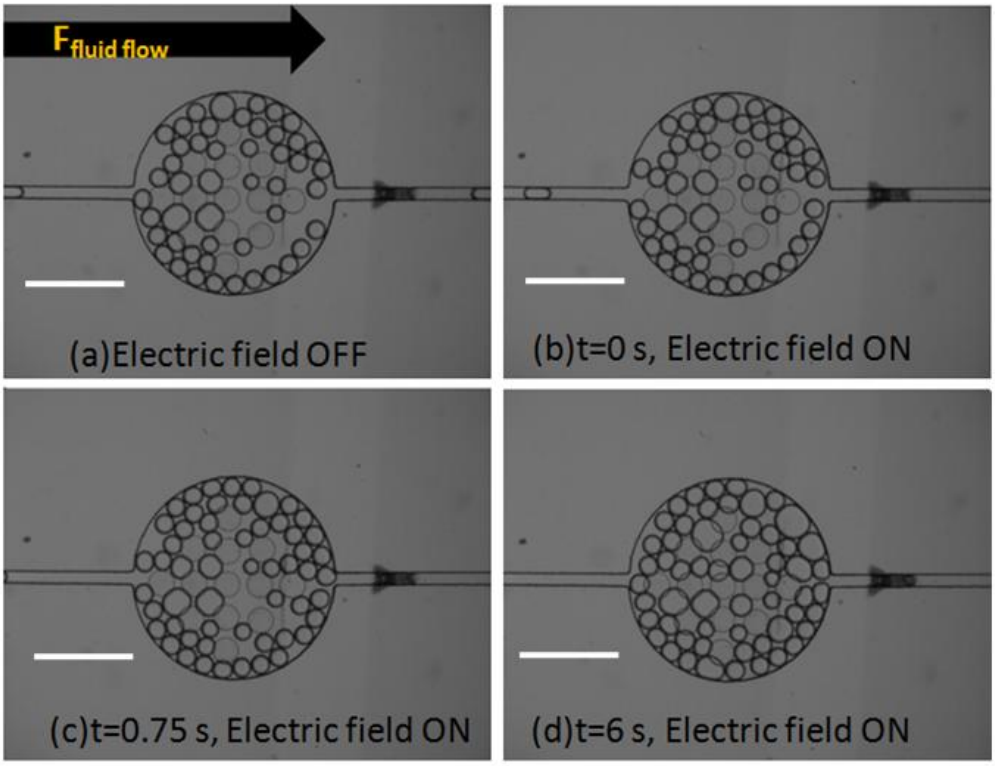

Figure 48 (a), (b), (c), (d) the trapping of the oil droplets over time under an AC electric field of 200 V and 100 Hz is applied. Scale bars denote 400 μm.

When the applied AC signal was 200 V and 100 Hz, the trapping efficiency in the entrapment zone was increased by up to 47.6% [Fig.48], which finally became saturated and caused oil droplets to leak after the oil concentration exceeded the threshold limit.

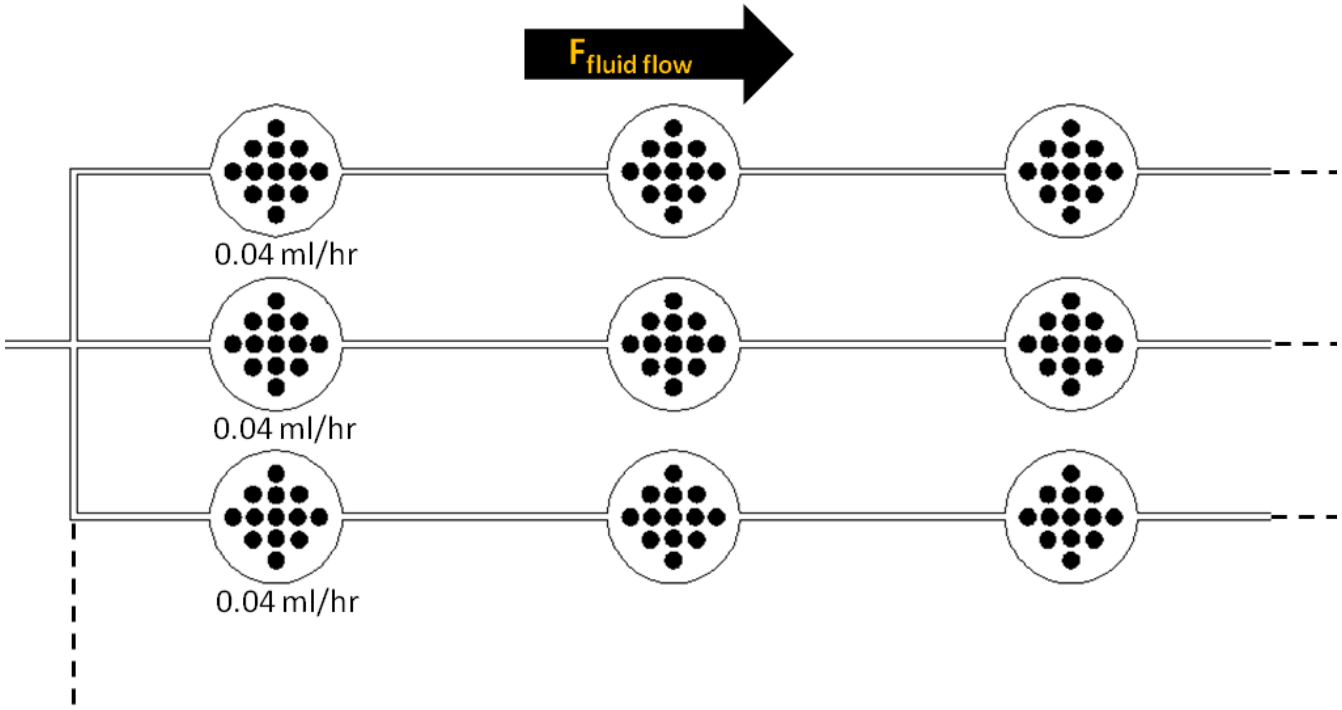

Figure 49 Schematic for oil droplet trapping at higher throughput rates using multiple entrapment zones simultaneously.

Considering that the smallest oil droplets trapped has 40 microns in diameter and a density of 960 kg/m3 for 50 cSt silicone oil (Sigma, Singapore), we can calculate the weight of the oil droplet as

$$40\mu m, diameter \Rightarrow V_{oil} = \frac{4}{3}\pi(\frac{40}{2})^3 = 33510.4\mu m^3$$

$$W_{oil} = density * volume = (\frac{960}{10^{18}\mu m^3}) * 33510.4\mu m^3 = 3.2 * 10^{-11} kg = 3.22 * 10^{-5} mg$$

In our experiments, Q_{oil}= 0.01 ml/hr and Q_{water}=0.04 ml/hr.

So, volume of fluid pumped and the detection limit (ppm) for the microfluidic device in 15 minutes is given as

$$V_{fluid} = 0.04\frac{ml}{hr} * \frac{1}{4} hr = 0.01ml = 10^{-5} L$$

$$ppm = \frac{[mg]}{[L]} = \frac{3.22 * 10^{-5}}{10^{-5}} = 3.22$$

For obtaining a higher throughput of droplet trapping and detection, we can also consider several such droplet entrapment zones in series and in parallel as shown in the Fig. 49. This detection limit can be further improved by increasing the size of the circular entrapment zone and also by reducing the gaps between the micro-pillar arrays for trapping smaller sized droplets.

4.3.2 Dielectrophoretic (DEP) force for oil droplets entrapment

Two ITO electrodes are positioned in such a way that the escaping droplets will have to go over the electrode gap at the outlet from the circular shaped entrapment chamber. Due to the constriction of the microchannel geometry at the outlet, a non-uniform electric field is applied. Since the dielectric permittivity of oil (ε_{oil} = 2.5) is much lower than that of water (ε_{water} = 80)[119], a negative DEP force will repel the oil droplets from the high electric field zone at the outlet. Hence, the oil droplets would be trapped. It was reported that silicone oil has a virtually constant electrical conductivity ~10^{-13} Sm^{-1} [120]

regardless of the electrical field applied. Taking the electrical conductivity of DI water as 5.5 mS/m , we obtained the values of the real part of the CM factor using the expression[121]

$$\mathrm{Re}[K(\omega)] = \frac{\omega^2(\varepsilon_p - \varepsilon_m)(\varepsilon_p + 2\varepsilon_m) + (\sigma_p - \sigma_m)(\sigma_p + 2\sigma_m)}{\omega^2(\varepsilon_p + 2\varepsilon_m)^2 + (\sigma_p + 2\sigma_m)^2}$$

and obtained that Re[K(**ω**)] stays constant at approximately at -0.47 from 0 to 100 kHz. Here, ε_p and ε_m implies the dielectric permittivity of oil droplets and DI water, respectively. Hence, changes in the frequency for the applied AC electric field does not impact the strength of the DEP force, provided the size of the droplets remain the same. However, we observed fusion of droplets as they were trapped between the micro-pillars as they were pushed forward by the fluidic motion from behind and push back by the combined n-DEP and ACEO flow field, simultaneously upon activation of the electric field. In Fig. 50(a, b), we present the linear velocity of the droplets as the rear end of the droplets goes over the electrode edge at the outlet to confirm the presence of n-DEP force as it acts both towards and away from the electrode edge. The Phantom Camera Control (PCC 2.14b) software was used to analyze the videos in order to determine the exact velocity of the droplets. The different sizes of droplets are obtained from the fusion of the smaller droplets around the micro-pillars in the circular shaped entrapment zone. Droplets of length 90 to 100 microns are obtained using dispersed oil phase flow rate at 0.01 ml/hr and continuous phase water flow rate at 0.04 ml/hr whereas fusion of two droplets gives a droplet length varying between 180 to 190 microns. Similarly, three droplets fuse together to give a droplet length varying between 310 to 320 microns. The fusion of the droplets is shown in Fig. 50 (a). It can be concluded that as the size of the droplets increases, the velocity of the droplets as it goes past the electrode edge also increases

accordingly as shown in Fig. 50 (d) which confirms the presence of the size dependent n-DEP force. This may have profound effect on the entrapment efficiency of the microfluidic reactor if it is used to trap larger sized droplets as the strength of the n-DEP force would be enhanced.

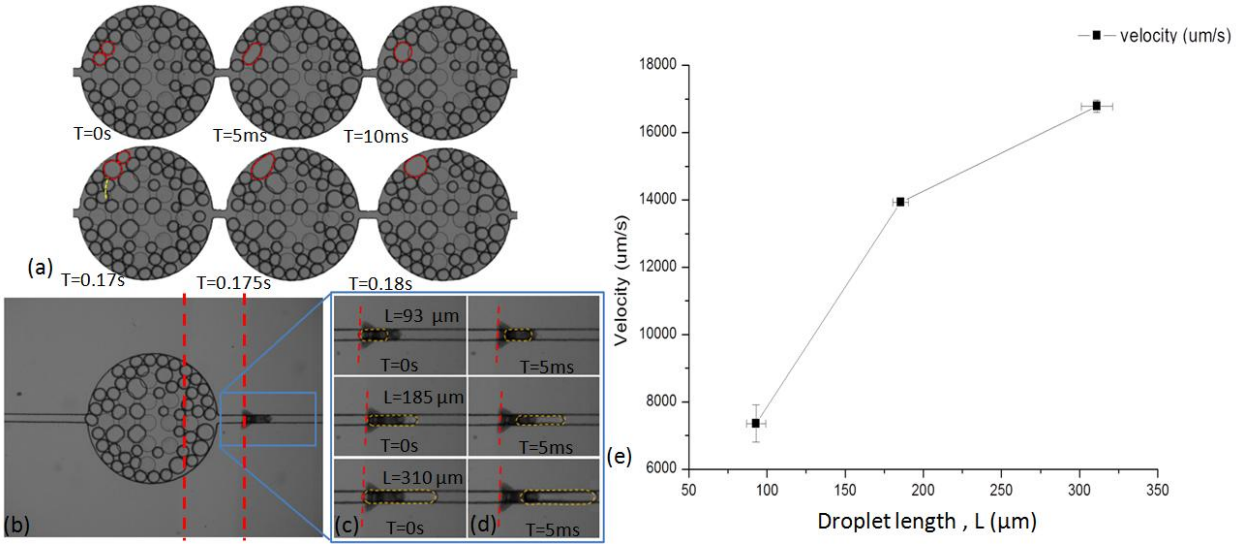

Figure 50 (a) fusion of three oil droplets over time. The droplets which fuse are highlighted in red. The first two droplets fuse at t= 0.005 s. At t= 0.17s, we have shown the trajectory of the droplets in yellow, thereafter which it fuses again at t=0.175 s;(b) exit channel from the entrapment zone and (c) shows inset figure of the same for three different droplet lengths, L=93 µm (obtained from the cross-flow junction used for droplet generation), 185 µm (obtained from the fusion of two droplets) and 310 µm (obtained from the fusion of three droplets) as the rear-end of the droplet over the electrode edge shown in dashed red line after it has exited the entrapment zone, (d) the position of the same three droplet after 0.005 s ;(e) shows the effect of the droplet length, L on the velocity of the same as it goes past the electrode edge obtained from the images as shown in (d).

4.3.3 ACEO flow field and entrapment efficiency for the oil droplets entrapment

A 200 Vp-p is applied for a range of frequencies to observe the impact of the rate of polarization of the EDL and the consequent ACEO flow field on the entrapment efficiency. ImageJ (National Institutes of Health, USA) , an open-source image processing software was used for estimating the enrichment efficiency. A similar image processing scheme was used by Conn, Ma, Hirasaki and Biswal, 2014[122] for quantifying oil displacement mechanism in microfluidic device. First, 8-bit images of the circular entrapment were taken using the high-speed camera when the electric field is off and after the electric field is turned on. This is shown in Fig.51 (a) and (b). The above images (a) and (b) were obtained when the applied AC signal is 200 V and 100 Hz. After obtaining the raw images, thresholding (c) of the images was determined in ImageJ for increasing the contrast and for accentuating the finer details in the image. This was followed by selection (d) of the oil droplets and counting the pixels within the selected oil droplets. Finally, the enrichment efficiency was determined by

$$\frac{[P(t) - P_o]}{P_o} * 100$$

where P(t) is the pixel count at time,t seconds and P_o is the pixel count before the electric field is applied and the pixel counting is done within the oil phase only. In the images shown in Fig. 51, P_o = 9438 and P(t=6s)=13931, so the enrichment efficiency obtained using the above equation is 47.6%.

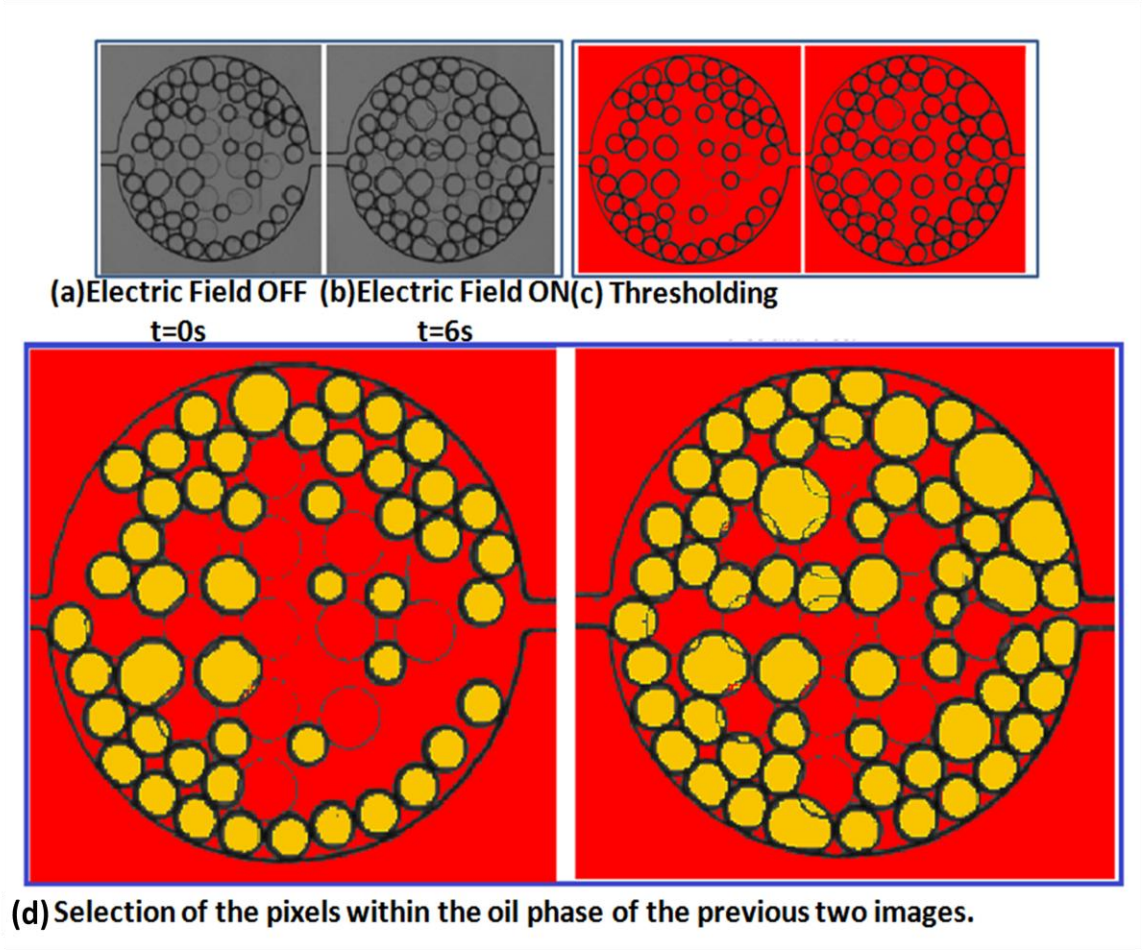

Figure 51 Image processing based protocol for estimating the entrapment efficiency is shown.

It was observed that reversing the direction of the electric field makes no difference to the entrapment efficiency as the ACEO flow field, induced by the counter rotating vortices, is independent of the applied voltage. The vibration of the droplets at large distances from the electrode gap also confirms the presence of a strong ACEO flow field. Since the electroosmotic force is not size dependent, this design can be used to trap oil droplet for a wide range of sizes. For all frequencies from 10^0 to 10^4 Hz, we noticed that the droplets immediately get trapped as soon as the applied electrode field is turned on. At

low frequencies, the droplets are only trapped for first half the cycle when the AC field is positive and gradually as the electric field changes sign in the next negative half of the AC cycle, the ions generated from the electrochemical reactions gets consumed by the reverse reactions which reduces the net ACEO flow and causes the droplets to get released due to the incoming hydrodynamic drag force of the bulk electrolyte solution from behind. The results of our experimental observations are plotted in Fig. 52. The lowest entrapment efficiency is observed at 1 Hz. At 10 Hz, the entrapment efficiency increases significantly which is further improved by the 100 Hz flow field where the maximum entrapment efficiency of 47% is observed. Beyond 100 Hz, the entrapment efficiency gets reduced as the rate of polarization of the electrode is too fast for the formation of EDL in the dielectric medium which is DI water as a result of which the generated ACEO flow field gets weakened. Hence, we conclude from the experimental results that an applied voltage at 100 Hz provides the optimum oscillation frequency as it is comparable to the charge relaxation time scale of the EDL obtained from our hydrophilization coating schemes.

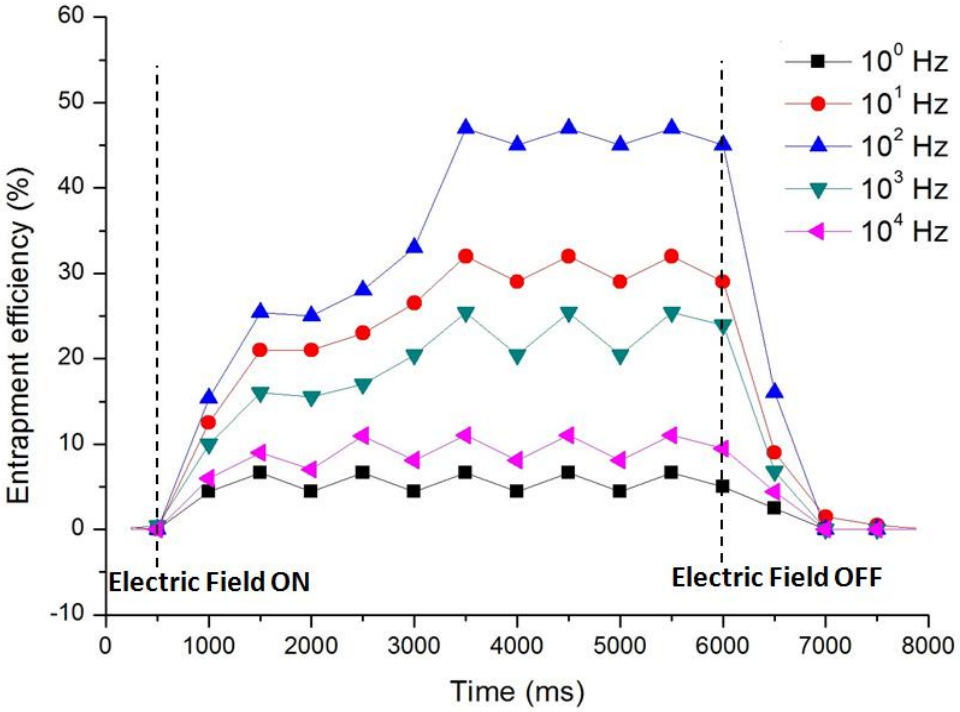

Figure 52 Entrapment efficiency of the device obtained as a function of frequency at 200 V_{p-p}. The electric field is turned on at 500 ms and turned off at 6000 ms.

From the experiments, we also observe that it is imperative to flush the microchannels with a non-ion surfactant for about 45 minutes prior to switching on the electric field because the presence of loosely attached polyelectrolyte ions can result in a large current density passing through the electrolyte. This causes rapid degradation of the ITO film in high electric field regions as the oxides in ITO gets reduced, i.e, In_2O_3 and SnO_2 gets reduced to form Indium, In and Tin, Sn and the evolved oxygen gives rise to bubbles[123]. The evolved metal ions of In and Sn then migrate under the influence of electric field and causes darkening of the electrodes.

Initially, videos were obtained to capture the passage of oil droplets through the enrichment zone using a digital high-speed camera, Phantom Miro M310 at a rate of 200

frames per second. Thereafter, snapshots were taken at a specific time intervals. In the absence of electric field, there is a balance between the rate of incoming droplets and the rate of outgoing droplets in the enrichment zone and thus the total volume of droplets stays the same. This is reflected in Fig. [46(b) and (c)] where the total pixel count within the droplets stays constant versus time as long as no applied electric field . When the electric field is turned on, the number of droplets trapped in the enrichment zone increases as seen in Fig. 48 until the hydrodynamic drag force in the entrapment zone is able to overcome the n-DEP force and ACEO flow field. This is reflected in the increase of pixel count within the droplets, when the electric field is turned on, which eventually becomes stable. We used the ratio of total number of pixels within the oil droplets before and after the electric field was applied to

quantify the effect of the applied electric field on the entrapment efficiency.

4.4 Summary

This work reported a new microfluidic reactor for the continuous detection of oil droplets in water. A PDMS and ITO glass based microreactor was developed to continuously trap oil droplets from DI water by AC electroosmosis. The micro-pillars were used to slow down the hydrodynamic drag force of the incoming oil droplets. Since PDMS is inherently hydrophobic, we demonstrated the LbL surface modification technique which renders the PDMS and glass negatively charged hydrophilic also contributes to a strong ACEO flow field for oil droplet trapping. We also demonstrated an appropriate frequency range for obtaining the highest entrapment efficiency in our microfluidic device as well as confirmed the presence of a DEP force as the droplets go over the electrode edge. The trapped oil droplets can also be released by switching off the electric field.

4.5 Declaration

Part of the work presented in this chapter has been published in *RSC Advances*.

Das D, Yan Z, Menon NV, Kang Y, Chan V, Yang C. Continuous detection of trace level concentration of oil droplets in water using microfluidic AC electroosmosis (ACEO). RSC Advances 2015; 5(86): 70197-203.

5. A Multi-Module Microfluidic Platform for Continuous Pre-Concentration of Water-Soluble Ions and Separation of Oil Droplets from Oil-in-Water (O/W) Emulsions using a Positive DC-biased AC Electrokinetic Technique

5.1 Introduction

Separation of water-soluble ions from oil-in-water emulsions (O/W) is of great importance for environmental monitoring applications with regard to oil spills. Water soluble ions such as polycyclic aromatic hydrocarbons (PAHs)[1] are present in crude oil which are extremely dangerous to the environment. In the aftermath of an oil spill from oil tankers, surfactants are used to disperse the oil which breaks down the oil slicks on the surface into small oil droplets of sizes less than or equal to 70 microns[4] resulting in the formation of stable O/W emulsions. These smaller crude oil droplets with enhanced surface area can readily release PAHs to the surrounding vicinity. Hence, the detection of these water soluble ions such as PAHs in O/W emulsions is extremely important. But, these O/W emulsion samples cannot be directly injected into standard analytical instrumentation equipments such as gas chromatography (GC), high-performance liquid chromatography (HPLC), capillary electrophoresis (CE) and atomic absorption spectroscopy (AAS) for the detection of PAHs as the presence of oil in these multiphase O/W emulsions will give inaccurate results. So, novel designs are necessary for the detection and pre-concentration of these ions in the O/W emulsions.

Environmental monitoring[2, 124, 125] and detection[126] of target analyte species using microfluidic devices is a growing area of research as it has presented significant advantages over traditional batch reactors such as portability for on-field analyses, development of fully automated and multi-functionality designs for continuous extraction and concentration at low sample volume consumptions, low risk of contamination by eliminating the need for transportation of samples etc. To simulate the complexity of the real time O/W emulsions containing PAH ions in the water phase in our work, we used an emulsion of silicone oil droplets in an external deionized (DI) and solubilized fluorescein sodium salt in the DI water. It is to be noted that both phenolate ions and fluorescein ions are negatively charged when solubilized in water. In this project, we have introduced a novel micro-fluidic device design with two modules: module I and II.

In module I, we have introduced a nanoporous Nafion membrane for pre-concentrating the ions present in the water phase of O/W emulsion in a designated zone. This is done by using an electric field by using an ion concentration polarization (ICP)-based trapping scheme. This pre-concentration step may have future application as a method of identification of trace quantities of ions in O/W emulsions. This is because formation of enriched ion concentration zones can amplify the detection sensitivity of PAH ions in terms of stronger UV absorbance using online fluorescence based detection techniques[127]. In the second module II, we have incorporated an electrokinetic valve for separation of micron sized oil droplets from water. For this, we have incorporated a Y-junction with two outlets. By activating the electric field, we can block the passing of oil droplets in one of the two outlets. This may be useful for the separation of water-

soluble ions from O/W emulsions by shutting off the oil droplet flow in one of the two outlets.

A schematic of the two modules and that of the overall device is shown in Fig. 53. The device has five electrodes: two of which are connected to the positive terminal, V of the power supply. The remaining three electrodes: G1, G2 and G3, are connected to the ground. For inducing concentration polarization effect in module I, electrodes V and G1 needs to be turned on. As a result, ion enrichment zones are observed in the regions between AA` and the nafion membrane as well as between BB` and nafion membrane. Module II has two electrodes connected to the ground, G2 and G3. When electrodes, V and G2, are turned on; the droplets can no longer escape from outlet 1 due to the oil entrapment zone along outlet 1. Similarly, when electrodes, V and G3, are turned on; the droplets can no longer escape from outlet 2 due to the oil entrapment zone along outlet 2. As long as the electrodes V and G1 are turned on, it is observed that the ions enrichment zones are formed in module I regardless of whether or not ground electrodes G2 and G3 are connected to the power supply.

Ion concentration polarization[13] (ICP) is a transport phenomenon which is observed when an electric potential is applied near the microfluidic and nanofluidic interface. The electric field is generated across a nanoporous membrane sized pores which is connected to two larger sets of microfluidic channels: one connected to a higher voltage potential, the other to the ground. The pores within the membrane act as nanochannels. For the nanoporous membrane, we used an ion-selective membrane, nafion which is a negatively charged material with sulfonic groups. When an electric field is applied, positively

charged electric double layers (EDL) are generated within the negatively charged nanopores. As both nanopores and EDL are of the same order, overlapping[13] of the EDL takes place under an applied electric field. This leads to the accumulation of cations in the EDL and influences the ion fluxes at the junction where the nafion is connected to the larger channel. Once the ICP process is stabilized, ion enrichment zones are induced in those regions. This behaviour has been utilized for a wide range of application such as separation, concentration[13, 60, 128, 129], desalination[58, 130], mixing[131], etc of target analyte species. Traditionally, single phase solutions and a direct current (DC) power supply source have been used for ICP. Due to the presence of oil droplets in water in this work, we observed that a DC voltage exerted a strong electroosmotic force on the droplets from the anode up to the nafion which is connected to the ground. Hence, we did not observe any ion enrichment zone near the nafion as those regions were already saturated with oil droplets. When we applied a positive DC-bias to an alternating current (AC)[132] field, an ion enrichment zone was successfully generated near the nafion at the Y junction. We also observe an increase in the axial velocity of droplets as the droplets were going past the Nafion membrane at along both the arms of the Y junction. The ion enrichment zone occurs because the net positive DC bias maintains a steady electrophoretic (EP) force on the ions to migrate the anion depleted Nafion membrane. As the cation concentration is greater within the nanopores; to maintain electroneutrality in the region, we observe the gradual build up of fluorescein anions. This leads to formation of the ion enrichment zone. Adding the AC component to the DC field also generates an electrokinetic vortex due to the ion concentration gradient directed from the ground towards the anode[133]. The oil droplets are also influenced by the formation of the ion enrichment zone even though the droplets are several orders bigger than

dimensions of the nanopores and the pre-concentrated ions. This is because the accumulation of ions at the Nafion edge generates a strong electric field as the ion concentration rapidly decreases with distance from the membrane. This exerts a strong dielectrophoretic (DEP) force on the non-polar oil droplets. Hence, we observed the faster axial velocity of the oil droplets near the Nafion region. We also integrated this module with a Y junction for trapping the oil droplets in one of the two outlets and selectively releasing the same from the other. This is because the same planar electrodes which we used for ion pre-concentration could also be used for simultaneous trapping and separation of the oil droplets in one of the two outlets The trapping design presented here is the same as that of our previous work[134]. However, we used a positive DC bias AC field and still succeeded in trapping the droplets at 100 Hz. The motive behind using the same electric field for both modules has been to operate both modules simultaneously.

Prior to the generation of oil droplets at the cross flow junction [Fig. 53(c)], a surface treatment step [73, 134] is performed for hydrophilizing the polydimethylsiloxane (PDMS) microchannels as native PDMS is hydrophobic in nature. The protocol is the same as has been explained in the previous chapter. In the absence of a surface treatment step, oil droplets will stick to native PDMS walls and eventually clog the microfluidic device.

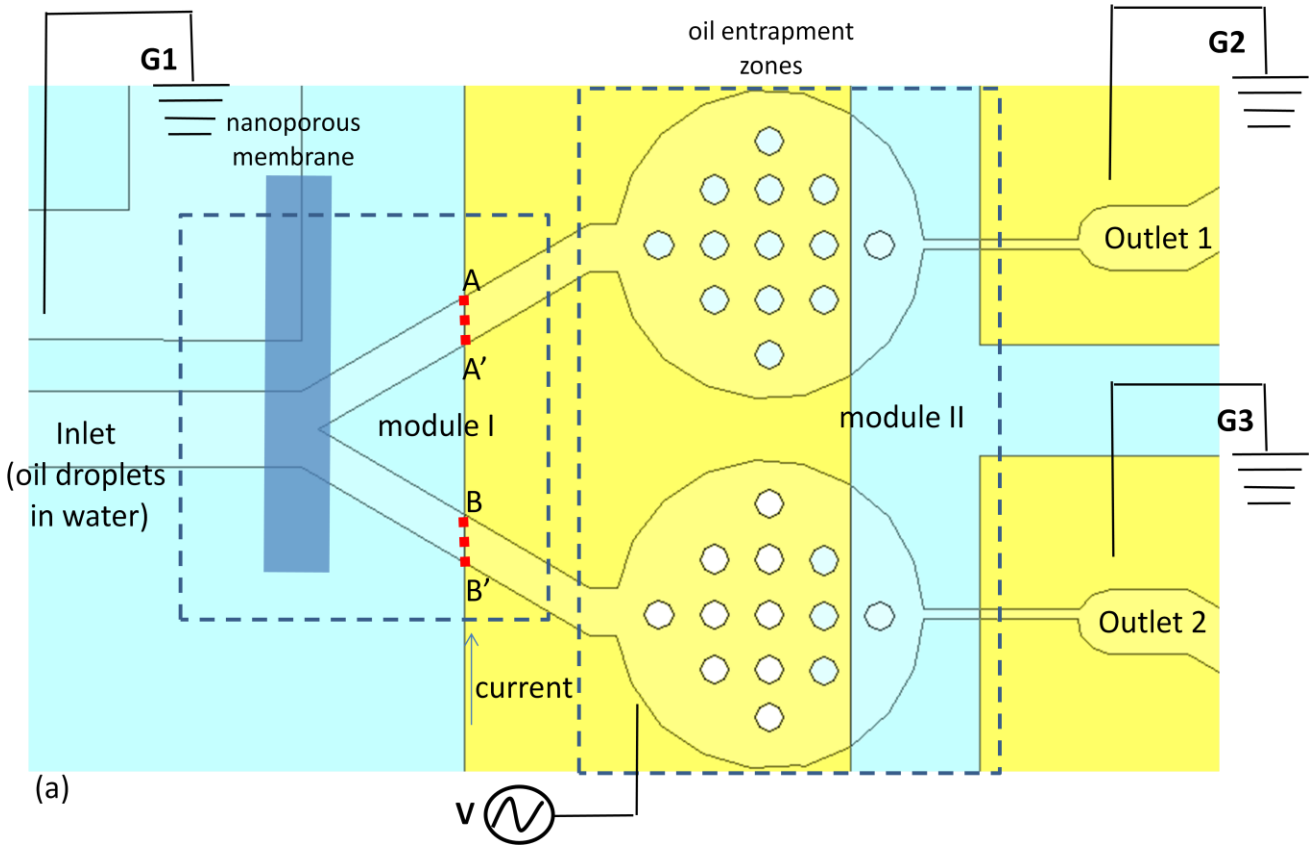
G1
nanoporous
membrane
oil entrapment
zones
G2
Outlet 1
A
A'
module I
module II
G3
Inlet
(oil droplets
in water)
B
B'
Outlet 2
current
(a)
V

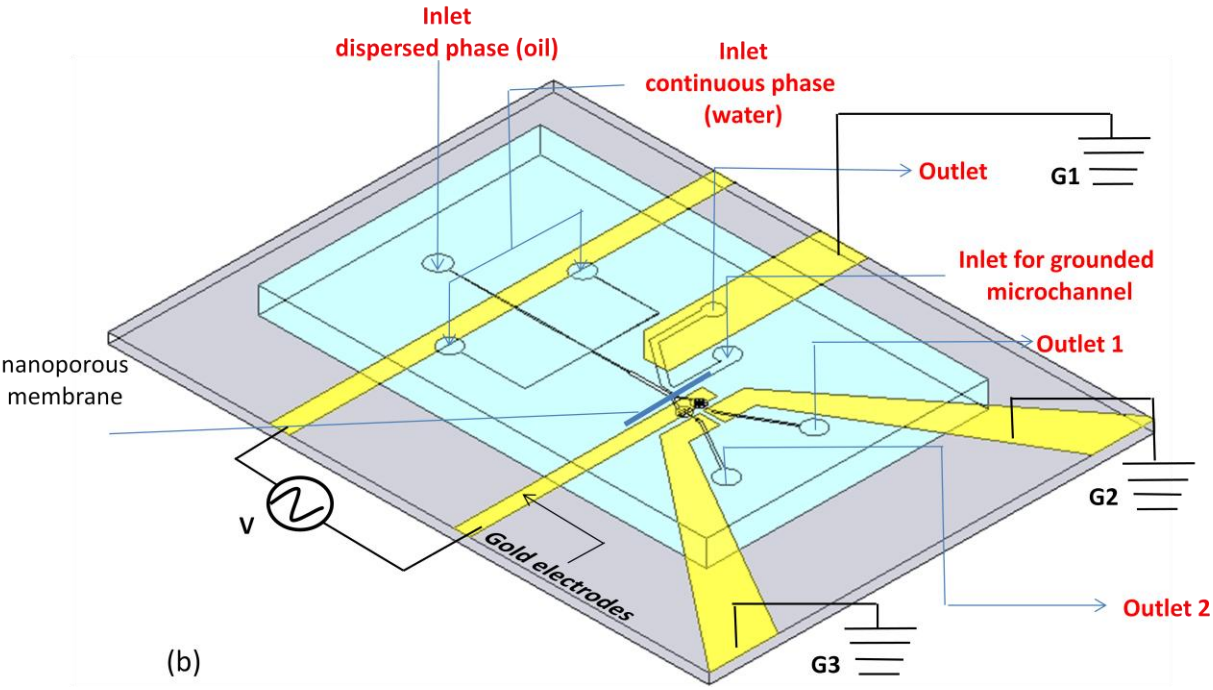
Inlet
dispersed phase (oil)
Inlet
continuous phase
(water)
Outlet
G1
Inlet for grounded
microchannel
Outlet 1
nanoporous
membrane
G2
V
Gold electrodes
Outlet 2
G3
(b)

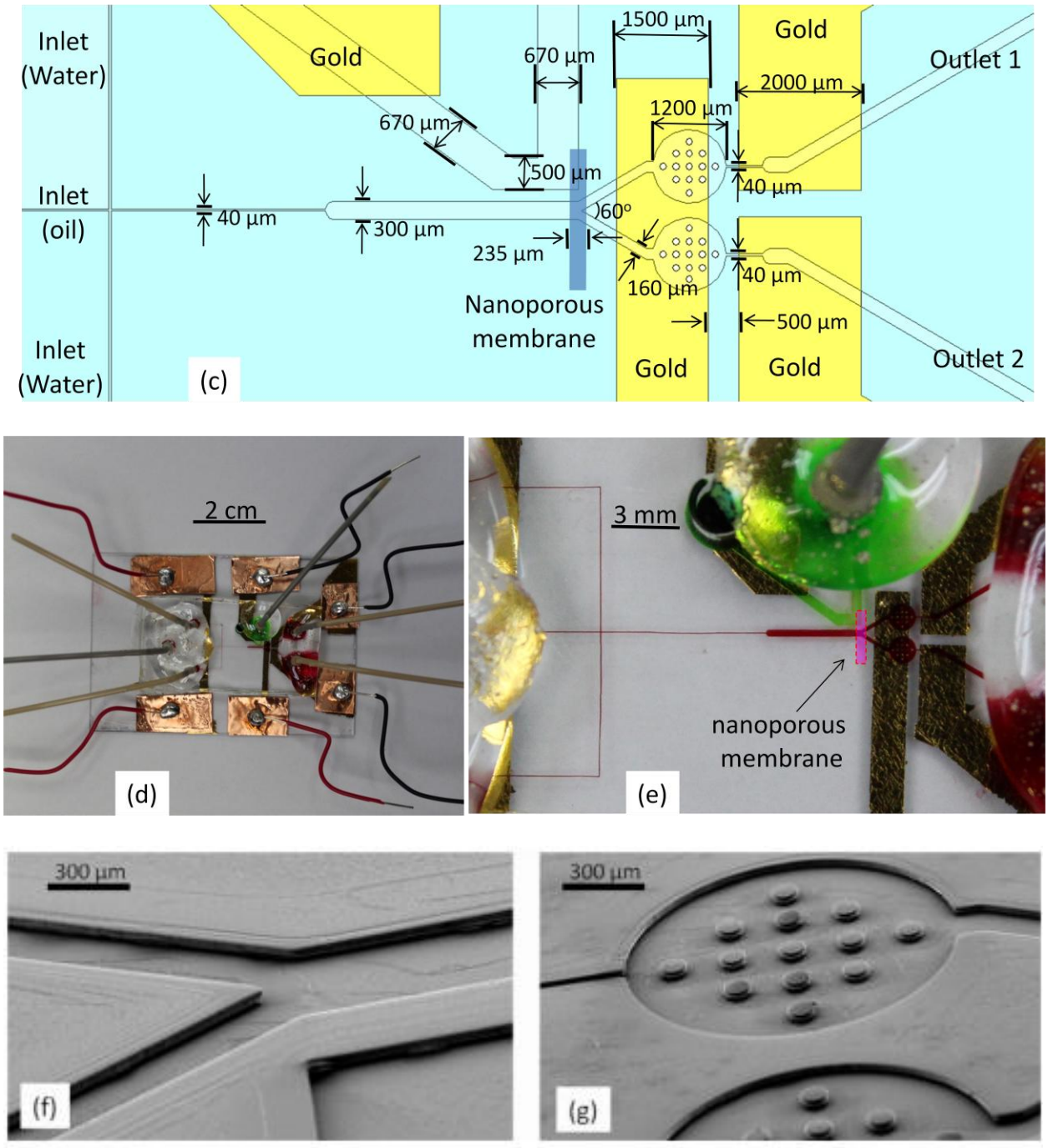

Figure 53 (a) Module I for ion preconcentration in the zone between AA` and Nafion as well as between BB` and Nafion; Module II with the two trapping zones for oil droplets either along outlet I or outlet II. Electrodes designated as V are connected to the positive terminal of the power supply source and electrodes; G1, G2 and G3 are connected to the ground. (b) Schematic illustration of the microchip showing the inlets for dispersed

phase, oil and continuous phase, water; nanoporous Nafion membrane and the gold electrodes over the PDMS-coated glass substrate. (c) Detailed dimensions of the microchannels and electrode gaps. Height of the microchannel and micro-pillars is 40 microns and diameter of the micro-pillars in the two circular oil droplet entrapment zones is 110 microns (d),(e) Photographs of the actual microfluidic device. (f),(g) SEM images of the PDMS block showing module I and II, respectively.

5.2. Experimental

5.2.1 Microchip fabrication

The microfabrication process for the nafion integrated gold electrode substrate is shown in Fig. 54. It should be noted that the etching of gold in the final step involves the use of both acetone as well as scotch tape and requires a lot of practice. First, a glass slide is taken which is spincoated at 500 rpm with a 1:1 weight fraction of PDMS prepolymer(Dow Corning, Slygard 184, Singapore) and hexane[135](Fisher Scientific, Singapore) mixture. The PDMS prepolymer itself is first prepared by mixing PDMS curing agent with the PDMS base monomer in the 1:10 weight fraction. Nafion membrane (NR-212, DuPont Co.) is then placed carefully over the top of the spincoated surface[60]. We place the substrate at room temperature so the polymers can reflow over the membrane. The substrate is again spincoated at 500 rpm with another layer of 1:1 weight fraction of PDMS prepolymer and hexane to form a completely flat surface. Thereafter, the substrate is cured at 80 ^{o}C for 2 hours. This step of integration of Nafion membrane is followed by fabrication of gold microelectrodes on the substrate. First, microelectrode patterns are formed over the substrate by using AZ 9260 photoresist followed by UV exposure. Then, an adhesion layer of chromium (~20 nm) followed by gold (~ 250 nm) is sputtered over the substrate. A lift-off process is then performed by

acetone and scotch tape to finally form the gold microelectrodes. The gap of 500 microns between the gold electrodes in module II has been etched manually using the tip of the BD insulin ultrafine needles (outer diameter of 336 microns). A PDMS block is then placed over the base substrate after plasma treatment. The height of the microchannels is 40 microns. Finally, hydrophilization of the PDMS microchannels is done by (LbL) deposition scheme of alternately charged polyelectrolyte solutions poly(allylamine hydrochloride) (PAH) (Sigma, Singapore) and negatively charged poly(sodium 4-styrenesulfonte) (PSS) by flushing it in the sequence PAH-PSS-PAH-PSS[73] immediately after plasma treatment. The protocol is the same as has been explained in the previous chapter.

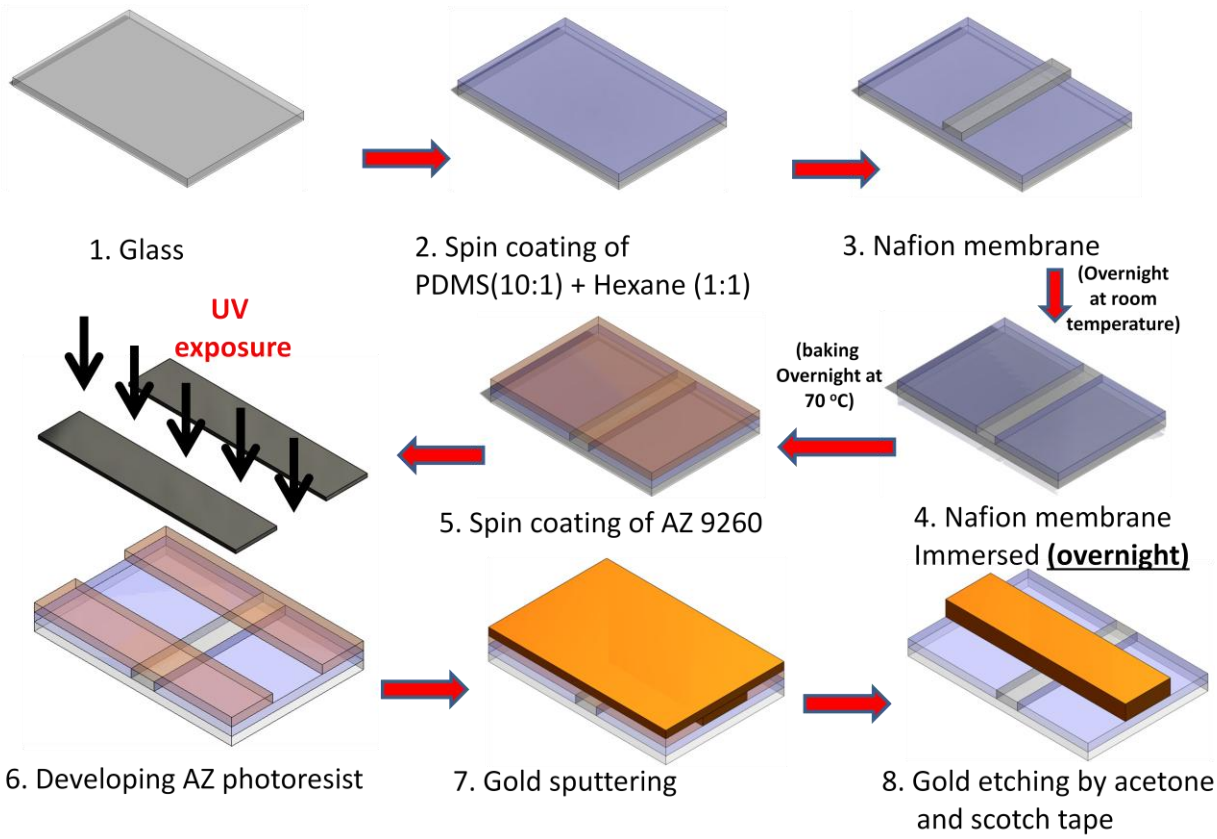

Figure 54 Schematic for the integration of the nafion membrane into the base substrate and the photolithographic deposition and etching of gold electrodes on the same.

5.2.2 Experimental set up

Silicone oil (Sigma, Singapore) of viscosity 50 cSt was used as our dispersed phase. The oil phase was then emulsified into discrete droplets in an aqueous and immiscible non-ionic surfactant Triton X-100 (Bio-Rad Laboratories, Singapore) solution at the critical micelle concentration (CMC) value, which makes up our continuous and immiscible aqueous phase. The continuous phase also contains sodium fluorescent salt (Sigma, Singapore) at 10 μM concentration. We used a cross flow junction for the emulsification of dispersed phase consisting of silicone oil (50 cSt, density=960 kg/m3) into individual droplets[134].

Two syringe pumps (Longer) with 0.5 ml Hamilton glass syringes are used for pushing the two immiscible fluids: dispersed phase, oil and the continuous phase, water at 0.02 ml/hr and 0.1 ml/hr, respectively. A syringe pump (Longer) is also used at the two outlets,1 and 2, in the withdrawal mode at 0.4 ml/hr. The fluorescent imaging and the oil droplets separation at the bifurcation zone of the microchip is observed with a Carl Zeiss microscope fitted with a mercury lamp. The microscope is also fitted with a Zeiss lens (CP-Achromat 5x/0.12) and high-speed CMOS camera (Phantom Miro ex4). The fluorescent images are obtained at an exposure time of 99000 microseconds. A DC power supply (Model PS 350, Stanford Research systems, Inc.) is used to provide the DC field whereas a function generator (Agilent 33250A) connected with an amplifier (AVC 790 Series Power Amplifier) by a BNC cable is used to produce DC-biased AC field on the gold electrodes. The DC-bias AC signal is monitored by an oscilloscope (CombiScope, HM 1008-2). In the next section, we will report our experimental observations for module I and II.

5.3 Results and discussion

5.3.1 Module I: Ion concentration enrichment

5.3.1a DC voltage

In this module, we pre-concentrated the ions present in the water phase of the oil-in-water emulsions using a positive DC-biased AC electric field. The generation of droplets at the cross-flow junction[134] is done using an external water phase flow rate at 0.1 ml/hr and oil flow rate at 0.2 ml/hr. Prior to using positive DC-biased AC electric field, a conventional DC field was tried to achieve this as DC has been the popular choice for

ICP so far. The experimental observations are shown in the Fig. 55. When a pure DC field of 120 V is applied, three competing forces are exerted on the O/W emulsion system: hydrodynamic force due to the incoming fluid flow, electroosmotic force (EOF) and the electrophoretic force (EP). Strong Faradaic reactions[133, 136] occur at the surface of the electrode giving rise to additional ions into the electrolyte and due to this, a strong EOF is exerted on the droplets as well as the ions. This repels the oil droplets from the anode. Also, an electrophoretic force (EP) is generated on the charged fluorescein ions in the water phase. As the region between the anode and the nafion is completely saturated with oil droplets [Fig. 55(b)], no ion concentrated zones are seen adjacent to the Nafion membrane [Fig. 55(d)]. Similar observations were also made at lower DC voltages.

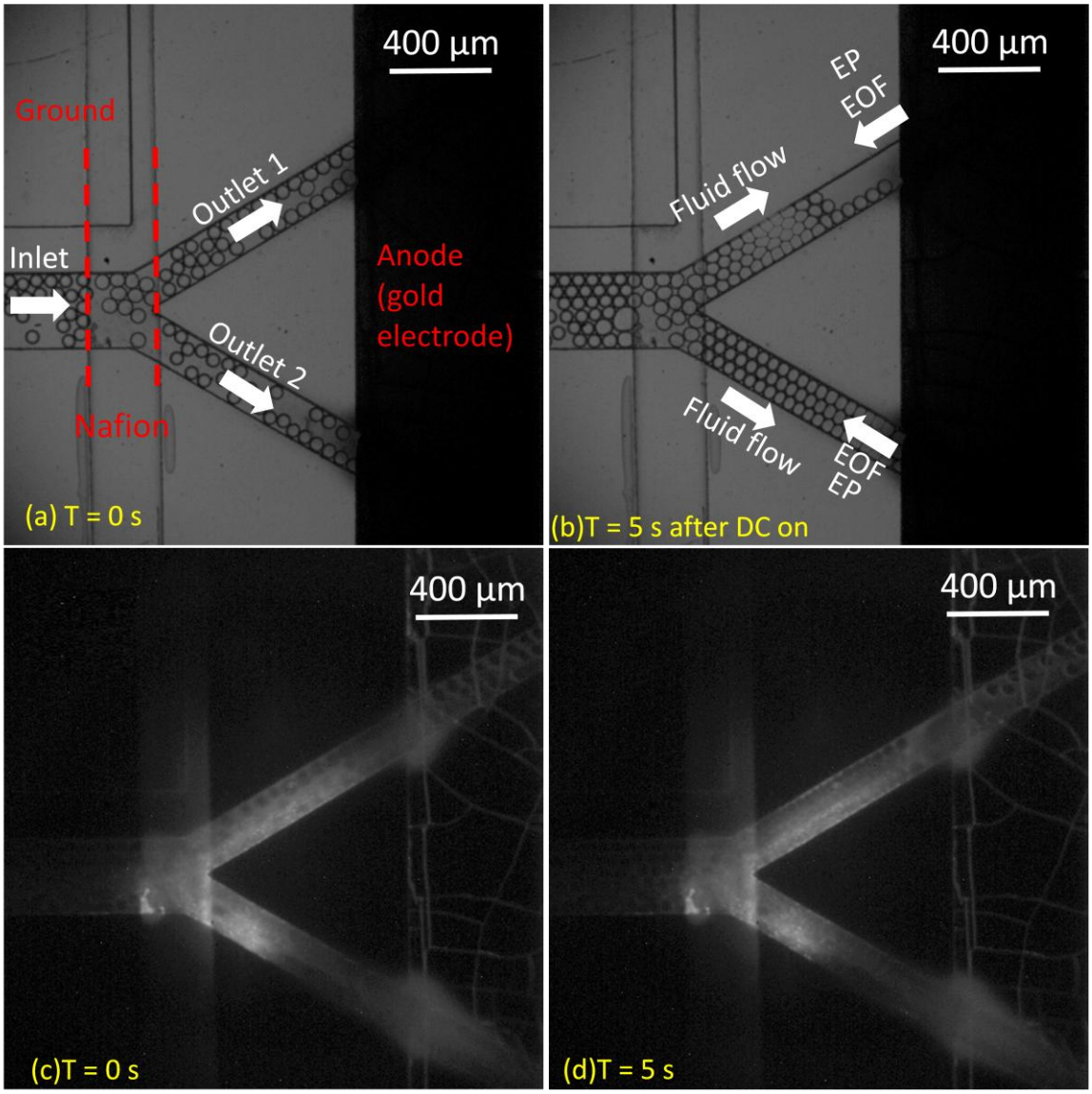

Figure 55 (a) the exit of oil droplets from the Y junction via outlet 1 and 2 ;(b) strong repulsion of droplets from the anode due to the EOF generated when DC field of 120 V is applied(c) fluorescein ions present in the water phase become visible when normal light is turned off and the mercury lamp is turned on, respectively. No DC is applied; (d) no concentrated zone of fluorescein ions observed when DC field of 120 V is turned on.

5.3.1b DC-biased AC voltage

When a positive DC biased AC field is applied, an electrokinetic flow is generated in form of a single rotating vortex[133]. The direction of the vortex is from the ground towards the anode. The EOF competes with this force which is being exerted on the fluorescein ions from the anode towards the ground. As we have used a Nafion which is a cation selective membrane, there will be a net accumulation of cations due to the overlap of the EDL within the nanopores of the membrane. To maintain the electroneutrality in the region, there will be a strong electrophoretic (EP) force exerted on the negatively charged fluorescein ions towards the cation saturated nafion membrane. This will be further strengthened by the EOF force. This results in a net accumulation of anions near the nafion membrane against the hydrodynamic force. This force is also strong enough to overcompensate the opposing DC biased AC electrokinetic flow vortex. This is because the electrokinetic response created by the anion depleted zone at the nafion membrane creates an amplified electrophoretic force and is often accompanied by an overlimiting current[137]. This phenomenon is observed at the interface of microfluidic and nanofluidic channels and to be precise, often at the edges of the nanoporous membrane only. Subsequently, we see the gradual build up of anions at the edge of the nafion membrane over time until the concentration polarization is stabilized. An illustration of the forces is shown Fig. 56 (b). Our experimental observations using a positive DC biased AC electric field is shown in Fig. 57. Fig. 58 shows the increase in the axial linear velocity of the oil droplets due to the presence of the DC biased AC electrokinetic flow vortex. The velocity is calculated by measuring the relative displacement of the droplets between the consecutive frames at 100 frames per second using the high speed CMOS camera. A dielectrophoretic (DEP) force is also exerted on the oil droplets due to high

concentration of ions near the nafion membrane which decreases with increasing distance from the membrane. As a result, the axial velocity of the droplets enhances along both outlets, from nafion to AA` and from nafion to BB`. However, DEP is a very short range force[67]. So, the primary force exerted on the oil droplets away from the nafion edge is the electrokinetic flow vortex [Fig.56 (b)]. However, the velocity of the droplets decreases near the anode edges due to the strong EOF force which is being exerted both from AA` and BB' towards the Nafion connected to the ground. Fig. 59 shows the fluorescence intensity profile before and t= 6 seconds after the electric field is applied. Before the electric field is turned on, the lack of smoothness in the grey scale value of the fluorescence intensity profile in Fig. 59 is because of the background noise[73] due to the presence of the multiple polyelectrolyte layers at the PDMS microchannel walls which was necessary for the hydrophilization effect. In the region where we obtain the enriched ion concentration; if we take the average grey scale value of the fluorescent intensity profile as 90 before the electric field is turned on and the grey scale of 122 after the electric field is turned on, we obtain a 35.6% amplification in the fluorescent signal for the ions in the water phase of the O/W emulsion.

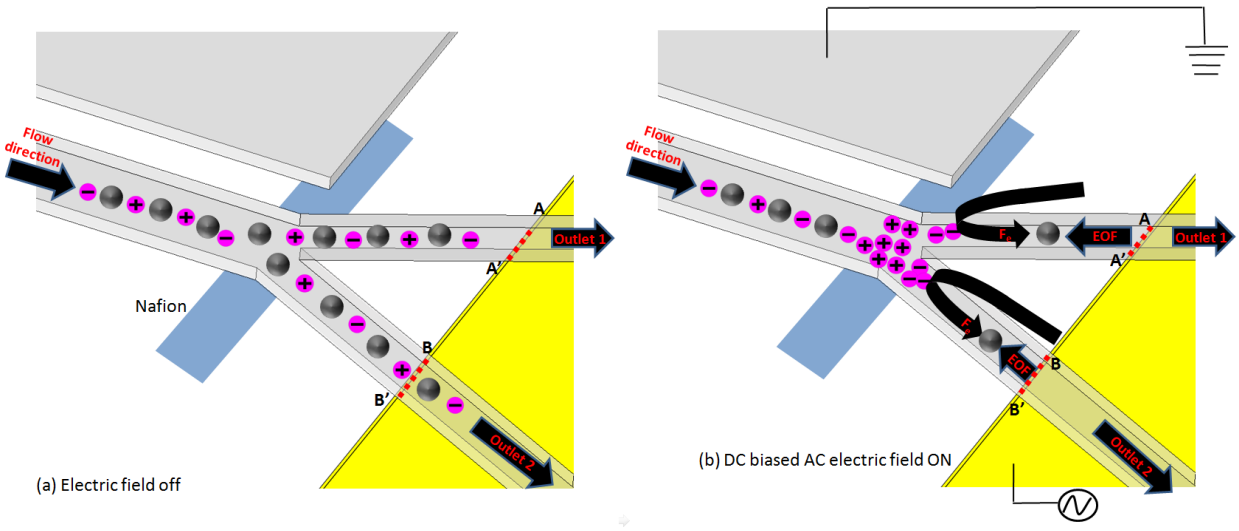

Figure 56 Schematic illustration of the forces on the O/W emulsion with ions in the water phase when the electric field is (a)off and (b)on. F_e denotes the DC-biased AC electrokinetics flow vortex.

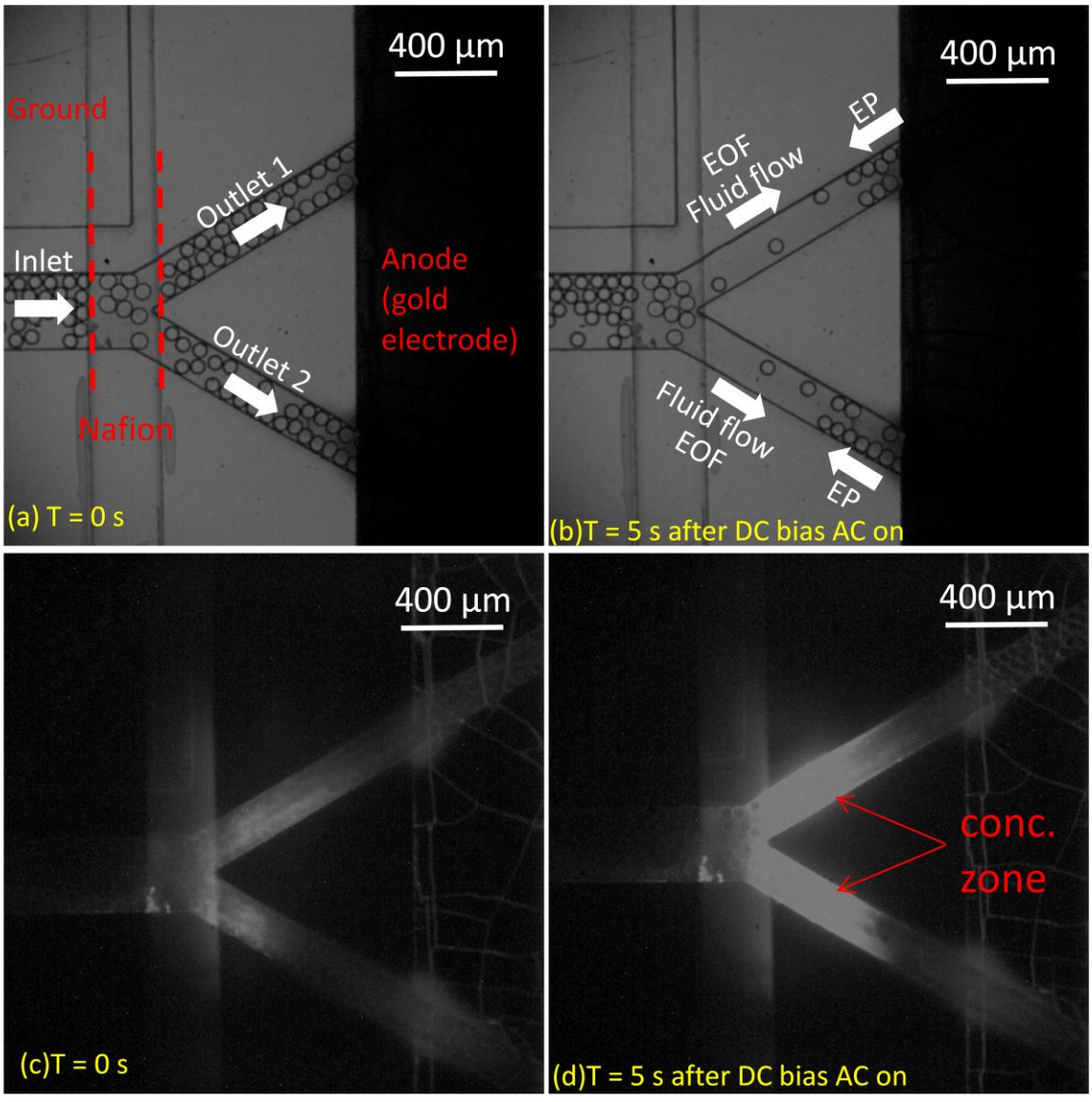

Figure 57 (a) Exit of oil droplets from the Y junction via outlet 1 and 2 ;(b) strong repulsion of droplets from the anode due to the EOF generated when positive DC biased AC field of DC offset= 78 V and V_{p2p} =173 V at 100 Hz is applied(c) fluorescein ions

present in the water phase become visible when normal light is turned off and the mercury lamp is turned on, respectively. No electric field is applied; (d) concentrated zone of fluorescein ions observed when electric field is turned on 5 sec.

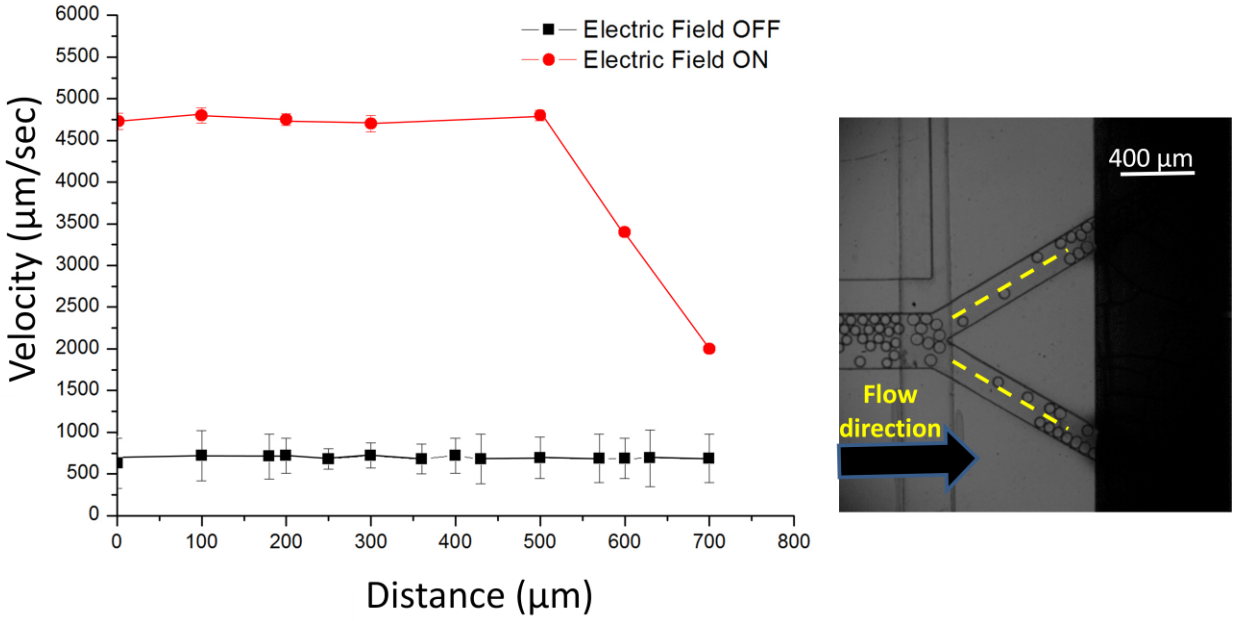

Figure 58 Average axial velocity of the droplets along the dashed yellow line (inset figure) before and after electric field is applied.

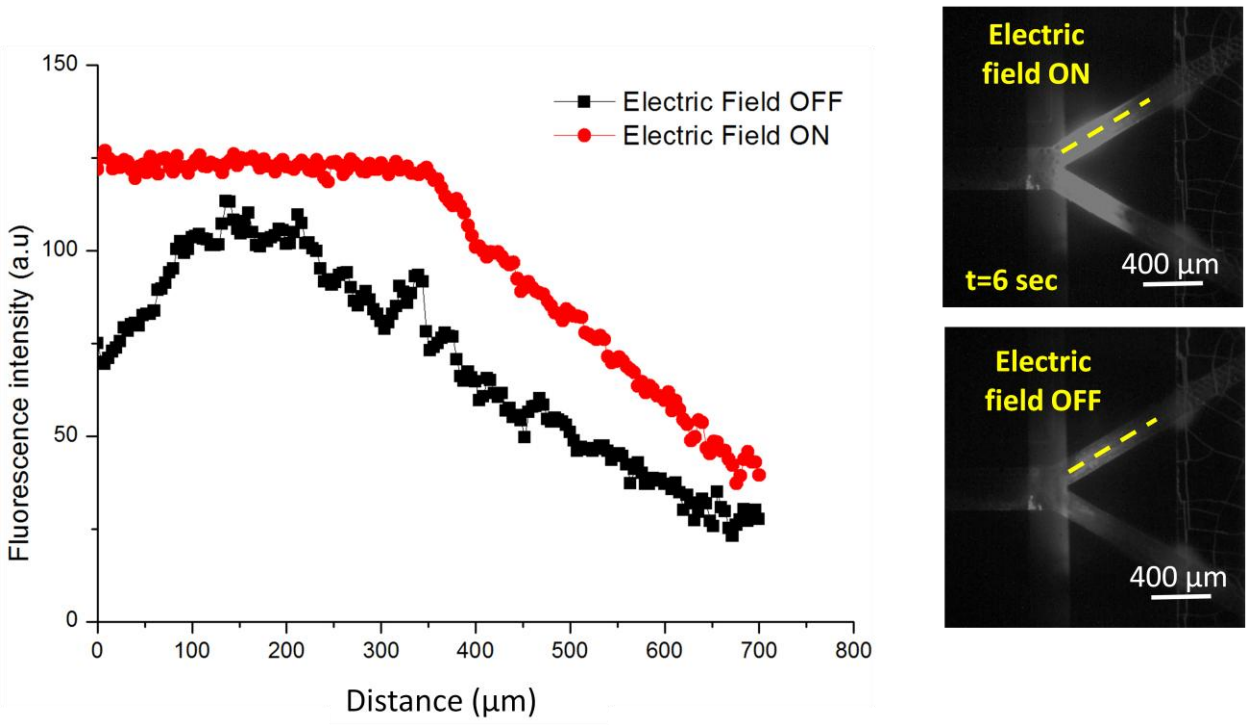

Figure 59 Fluorescence intensity along the dashed yellow line (inset figure) before and t= 6 seconds after positive DC-biased AC electric field is applied.

5.3.1c Expansion of the ion enrichment zone

We explain in detail the different stages of the gradual build up of fluorescein ion concentration at the nafion edge. These stages are shown in Fig. 60. We applied an electric field of 78V +173sin(2π(100 Hz)). This computes to a total voltage of 200V (calculated from the RMS value of V_{ac} plus the DC offset). The fluorescein ions face two different EOF forces: one from AA` to the Nafion membrane and the other from BB` to the Nafion membrane. However, the strength of the EOF force is greater along BB` than the other as it is closer to the voltage power source. Because current always follows along the path of least resistance, there is a higher voltage at BB'. This results in the faster building up of fluorescein ions at the Nafion edge towards BB` initially upto 0.4 seconds.

Then onwards, ion concentration trapped in the region between the nafion edge and BB` exerts a repulsive force to the incoming ions. So, an increase in the ions concentration is seen upto 2.8 seconds after which a balance is attained between the hydrodynamic force and the EOF force (between BB` and the nafion). Thereafter, 2.8 seconds onwards due to the repulsive force due to the higher ion concentration along outlet 1 to the incoming ions and EOF forces along both outlets, the ion concentration along outlet 2 increases. Finally 5.2 seconds onwards, a balance is attained along both outlets and a steady ion concentration is maintained. Fig. 60(c) shows the increase in the ion concentration area along both outlet 1 and 2 over time.

(a)

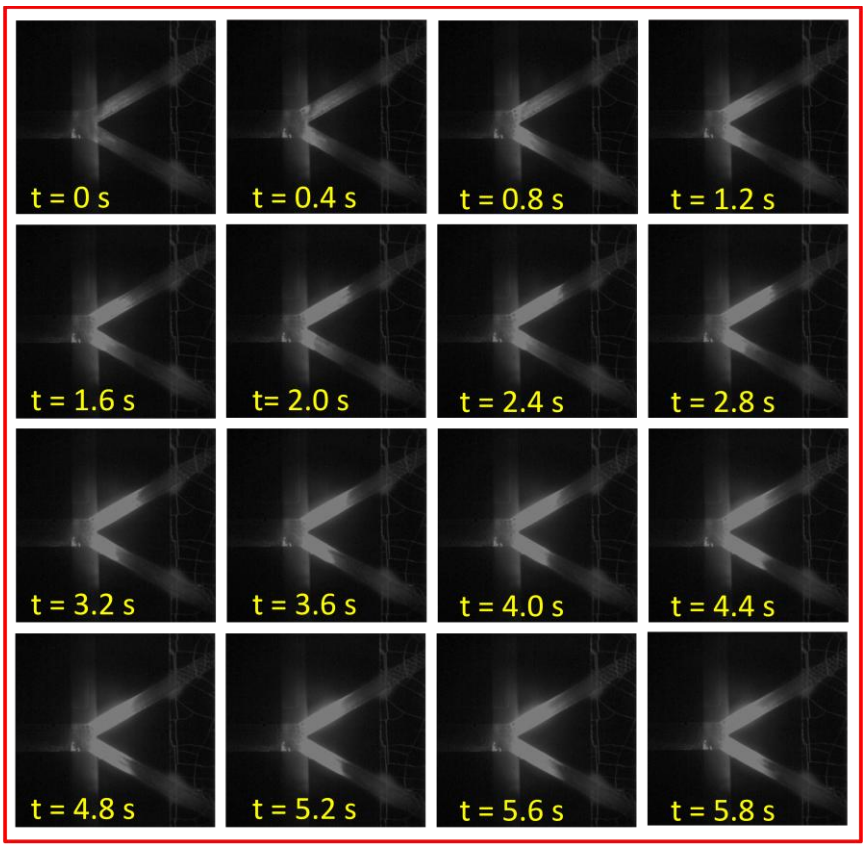

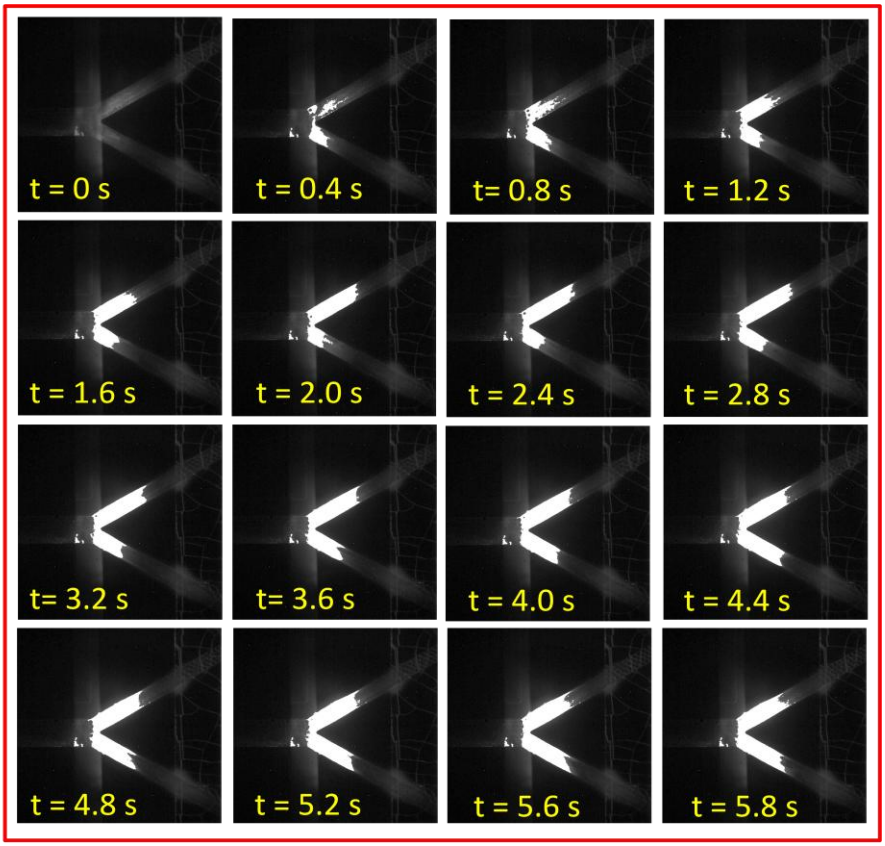
t = 0 s
t = 0.4 s
t= 0.8 s
t = 1.2 s
t = 1.6 s
t = 2.0 s
t = 2.4 s
t = 2.8 s
t= 3.2 s
t= 3.6 s
t = 4.0 s
t = 4.4 s
t = 4.8 s
t = 5.2 s
t = 5.6 s
t = 5.8 s

(b)

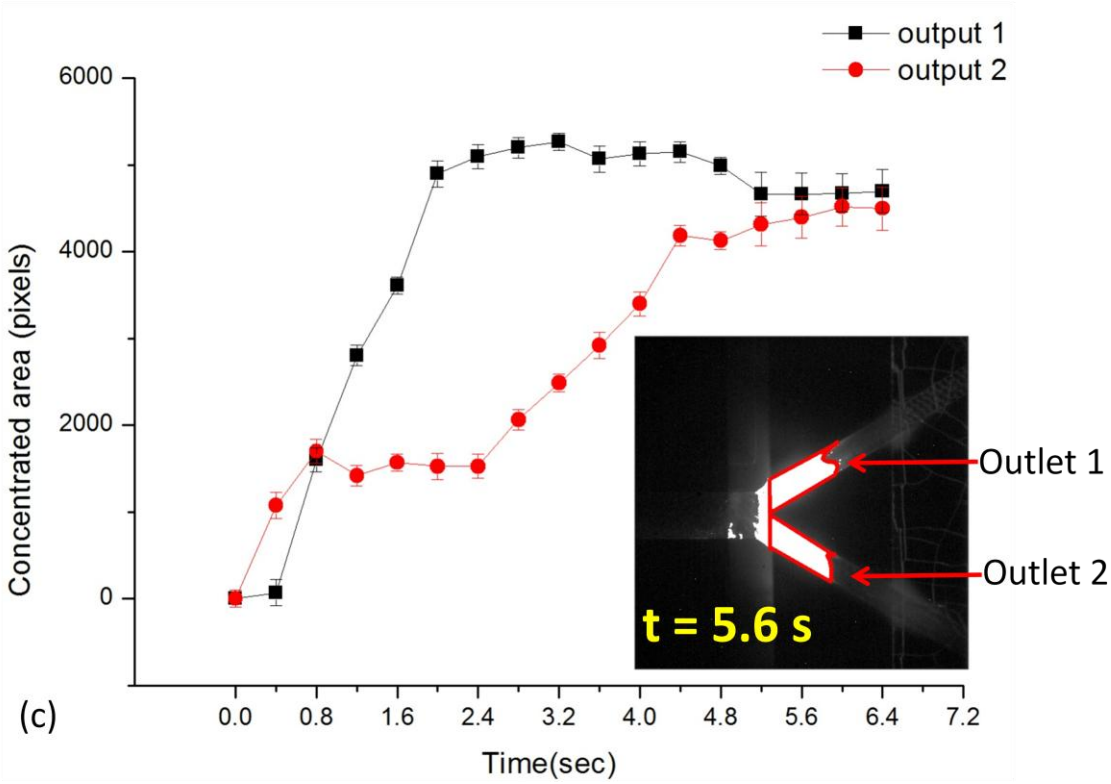
output 1
output 2
Concentrated area (pixels)
6000
4000
2000
0
0.0
0.8
1.6
2.4
3.2
4.0
4.8
5.6
6.4
7.2
Time(sec)
Outlet 1
Outlet 2
t = 5.6 s

(c)

Figure 60 (a) original images (b) converted images (using ImageJ, an open source image processing software) of the building up of the ion enrichment zone near the Nafion membrane at the Y junction. Conversion of the images is done by adjusting the threshold of the images and thereafter setting the brightness value of the altered images at 100. This step is necessary for highlighting the ion enrichment zones (c) plot of the area of ion enrichment zone along both outlet 1 and output 2 based on the area evaluation in (b) as shown in the inset figure.

5.3.2 Module II: Electrokinetic valve for the separation of oil droplets

This module consists of two outlets connected to the concentration polarization scheme in module I via a Y junction. When electric field is not applied, there exists an equilibrium between the rate of incoming and outgoing droplets and the droplets can exit through both the outlets 1 and 2. For this module, we used an external water phase flow rate of 0.15 ml/hr while the oil phase flow rate is kept at 0.02 ml/hr. Fig. 61(b) shows the trapped oil droplets in outlet 1 when electrodes V and G2 are connected to the power supply [Fig. 53(b)]. The greater the flow rate of the fluids at the inlet, the higher will be throughput of the device. In the previous chapter, the oil droplets were trapped at a much lower flow rate of 0.04 ml/hr. It needs to be noted that previously, we used an AC field only which produces two counter rotating vortices and pushed the droplets away from the electrode gap. However, in this case, we use a positive DC-biased AC field which produces an electrokinetic flow vortex directed from the ground towards the anode which in our case is against the incoming oil droplets, hence aids oil entrapment. Another factor is that that previously, our external phase consisted of DI water with a non-ionic

surfactant, Triton X-100, only as we observed rapid generation of bubbles in the presence of fluorescein ions at the ITO electrodes. In this case, the gold electrodes, being a noble metal and chemically inert in nature; are more stable in the presence of ions in our external water phase. The presence of fluorescein ions increases the difference in the polarizability between the non-polar oil droplets and the external water phase. So, the strength of DEP force is amplified as the Clausius-Mossotti factor increases. We applied an electric field of 78V +173sin(2π(100 Hz)) which is the same as we applied for inducing the concentration polarization at the Y junction near the nafion membrane in module I. The applied frequency is kept fixed at 100 Hz because previously[134], we found that the maximum entrapment efficiency was obtained at this particular frequency.

As shown in Fig. 62(b), we trapped the droplets at outlet 1 by connecting the electrodes V and G1 to the power supply. Alternately, we can also trap the droplets at outlet 2 and release the droplets via outlet 1. The use of micro-pillars is necessary so as to slow down the hydrodynamic force of the incoming oil droplets and essentially acts as speed barriers to the same. By reducing the distance between the micro-pillars as well as by increasing the diameter of the same, we can further increase the resistance to the incoming hydrodynamic pressure. In our experiments, the micro-pillars has a diameter of 110 microns.

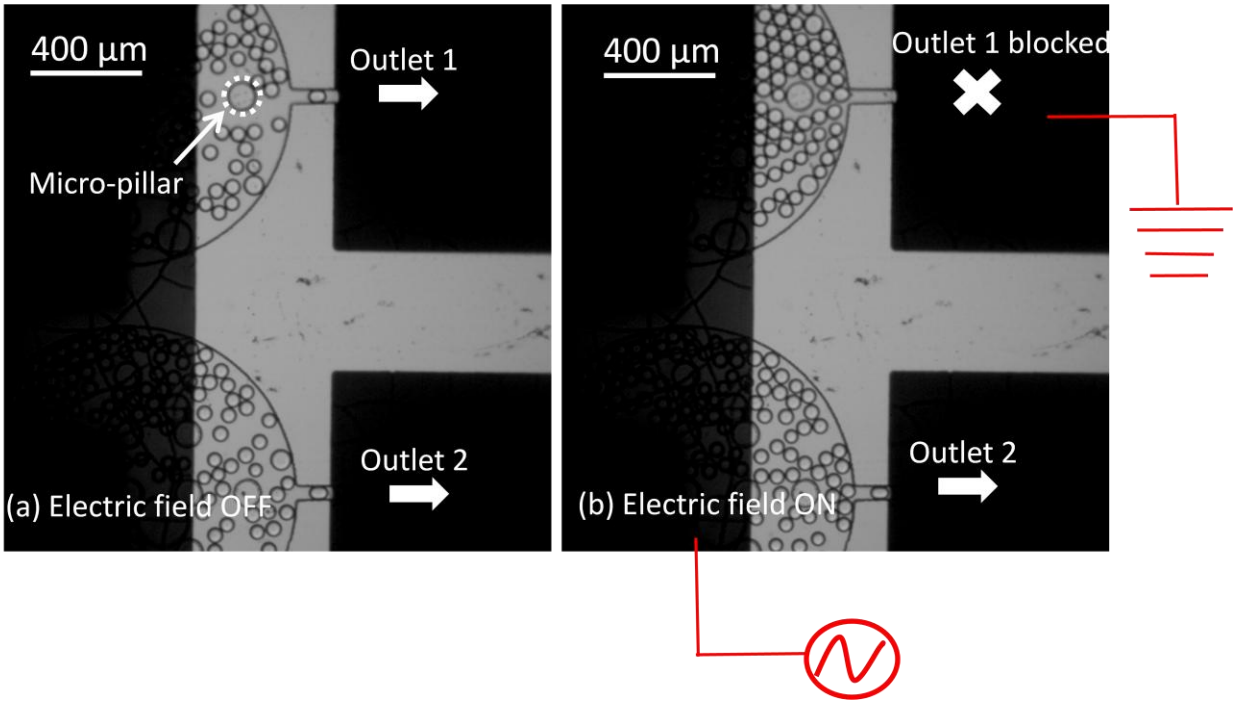

Figure 61 (a) Electric field is off and droplets exit out of both outlet 1 and 2 (b) t= 2 seconds after an electric field of 78V +173sin(2π(100 Hz)) is applied. Trapping zone at outlet 1 is saturated with oil droplets.

The significance of this module is that it can act as an electrokinetic valve for the separation of oil droplets from an O/W emulsion in a continuous flow reactor. As can be seen in Fig. 62, prior to the electric field is turned on, the total count of droplets released from outlet 1 and 2 are roughly the same. In the time interval when the electric field is turned on from t=1.5 sec to t=4.875 sec; the total number of droplets being released from outlet 1 is only 12 whereas 156 droplets escape from outlet 2. Although it is difficult to shut off the oil droplet flow completely in one of the two outlets, we managed to alter the oil droplets count escaping from the two outlets 1 and 2 from 1:1 to 1:13. After the electric field is turned off at t=4.875 sec, there is a sudden spike in the number of droplets released from outlet 1 as it is completely saturated with droplets [Fig.61 (b)]. In our

design, we can only trap the oil droplets to a certain extent until the trapping zone is saturated and the electrokinetic forces can no longer withstand the hydrodynamic pressure of the incoming fluids. However, by lowering the flow rate of the device and by using a stronger electric field; the trapping efficiency of the device can be vastly improved.

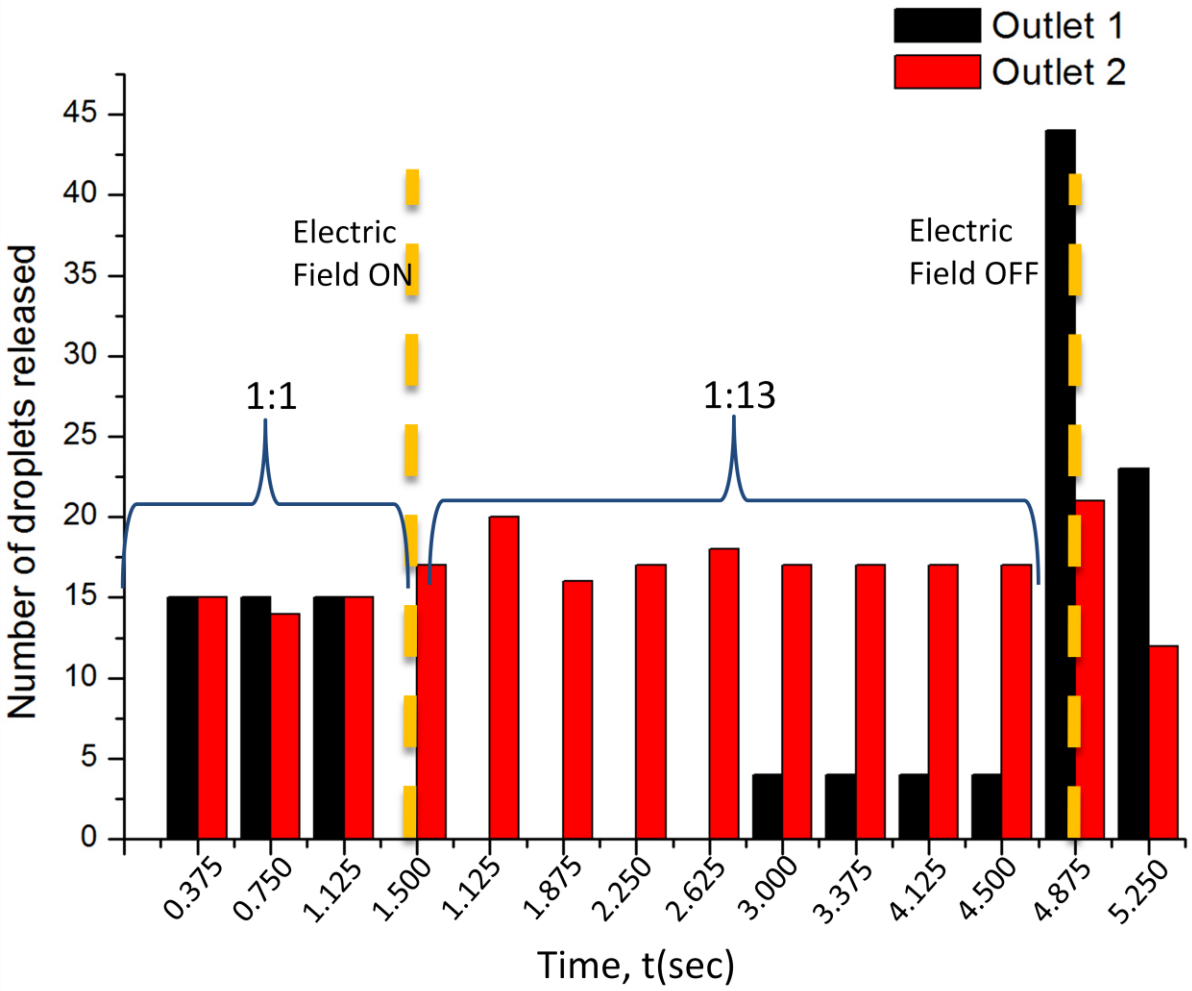

Figure 62 Count of the total number of droplets escaping from outlet 1 and outlet 2 before and after electric field is applied. Electric field is turned on at 1.5 sec and turned off at 4.875 sec.

5.4 Summary

We developed a novel device with dealing with O/W emulsion systems important implications for the environmental monitoring agencies. This device has two modules: for inducing concentration enrichment for the ions' presence in the external water phase and for the separation of oil droplets from the same O/W emulsion. A Nafion membrane of nanopores was embedded as a nanoporous junction for activating the concentration polarization effect. We applied a positive DC-biased AC electric field instead of the conventional DC electric field for the concentration effect as the oil droplets come under the influence of the EOF force and saturate the region between the nafion membrane and the anode under the DC field. Using a positive DC-biased AC electric field, a stable ion enrichment zone was achieved after 6 seconds at both outlets of the Y-junction near the nafion membrane and we obtained a 35.6% amplification in the grey scale value of the fluorescent signal in the region where the ion enrichment zone was produced. We also integrated this module with an oil droplet separation scheme using a Y-junction where we successfully used the same electric field for altering the oil droplet ratio in the water phase at the two outlets from 1:1 to 1:13.

6. Conclusions and Future Studies

6. 1 Contributions of this study

Following the objectives of this study, extensive and rigorous research is done with oil-in-water (O/W) emulsion systems using microfluidic platforms. The experimental investigations offer new insight into the potential realm of using continuous flow microfluidic devices for high throughput environmental monitoring applications. The study accomplishes objectives such as extraction of target analyte species from oil (liquid-liquid extraction, LLE)and O/W emulsion (membrane-based liquid-liquid-liquid extraction, LLLE), detection and separation of micron-sized oil droplets from water and pre-concentration of water soluble ions in O/W emulsion. All experiments are done following the surface modification of the device for hydrophilization of the microchannel walls. To sum up, the major contributions made during this study are as follows:

1. **Continuous droplet-based liquid-liquid extraction (LLE) of phenol from oil by emulsifying it in the form of droplets**

   A poly (methyl methacrylate) (PMMA)-based microfluidic device is presented for investigating the flow-dependent droplet-based liquid-liquid extraction (LLE) of phenol from oil. We used a suspension of phenol in silicone oil as a simulator of real-world oil samples containing poly aromatic hydrocarbons (PAH) from the environment. Continuous liquid-liquid extraction (LLE) of phenolic compounds from oil has potential

applications as a high throughput sample preparation method from the standpoint of extracting the ionic species in an organic phase. In this work, the dispersed phase of silicone oil, containing phenol, is emulsified into droplets with a uniform size distribution in an SDS surfactant solution which acts as the continuous phase using a cross-flow junction. We conclude that for the higher extraction efficiency of the target analyte species from a highly viscous organic donor phase such as silicone oil droplets onto a less viscous fluid, lower flow rate ratio of continuous to dispersed phase is to be preferred. Finally, we also integrate a hydrophobic polypropylene membrane into the device for liquid-liquid-liquid extraction (LLLE) of phenol molecules from silicone oil droplets onto the bottom phase via the continuous phase.

2. Continuous trapping and detection of micron-sized oil droplets using AC electroosmosis (ACEO)

A polydimethylsiloxane (PDMS) and indium tin oxide (ITO) glass based microchip is developed to continuously trap oil droplets from DI water by AC electroosmosis (ACEO). Two ITO electrodes are positioned in such a way that the escaping oil droplets will have to go over the electrode gap at the outlet from the circular shaped entrapment chamber. The droplets are pushed away from the electrode gap by the counter-rotating vortices of the ACEO flow field. The micro-pillars are also used in the entrapment zone to reduce the hydrodynamic drag force on the incoming oil droplets. Thereafter, experiments are performed to study the effect of frequency on the entrapment efficiency of the device. A size-dependent dielectrophoretic (DEP) force is also observed at the outlet which implies that the entrapment efficiency would be enhanced for larger sized

droplets. This work is significant in determining the electrode and microchannel configuration needed for the continuous trapping of oil droplets in water and hence can be considered useful for designing fully automatic schemes in the future.

3. **Continuous pre-concentration of water-soluble ions and separation of micron-sized oil droplets from oil-in-water (O/W) emulsions using positive DC-biased AC electrokinetic techniques**

A polydimethylsiloxane (PDMS) and gold electrode based microfluidic device with an embedded nanoporous membrane is presented in this study. To simulate the complexity of the real time O/W emulsions containing PAH ions in the water phase in our work, we used an emulsion of silicone oil droplets in an external deionized (DI) and solubilized fluorescein sodium salt in the DI water. The device has two modules. The first module is used for inducing the ion enrichment zone using the concentration polarization effect triggered by the nanoporous nafion membrane. This pre-concentration step may have future application as a method of identification of trace quantities of toxic ions in O/W emulsions. The identification may be done by aligning spectroscopic or electrochemical detectors[2] over the ion enrichment zones. In the second module, separation of oil droplets from water takes place by using a Y junction. The second module essentially acts as an electrokinetic valve for the separation of oil droplets from O/W emulsions. Both the modules are activated by the positive DC-biased AC electric field. For the first module, we applied a positive DC-biased AC electric field instead of the conventional DC electric field for the ion concentration polarization effect as the oil droplets come under the influence of the EOF force which is directed from the anode towards the ground and this saturated the region between the nafion membrane and the anode.

6.2 Recommendations for future studies

Based on the results presented in this study, recommendations for future research are listed below:

1. **Continuous trapping and separation of oil droplets in highly conductive fluids like saline water**

Due to the presence of ions present in saline water, there is rapid generation of chlorine and hydrogen gases in both anode and cathode, respectively. So, electrokinetics based trapping and separation using conventional metal electrodes is not viable. One alternative would be to dilute the saline water to reduce its ionic conductivity. But that would reduce the throughput of the microfluidic device. We propose the use of carbon-paste electrodes [138, 139] as they are resistant to fouling and can withstand a large potential drop. Another viable option is to combine electrokinetics with other force fields such as optics or magnetic field. Furthermore, such systems will also be able to detect cholesterol, lipids, etc in blood.

2. **Continuous separation of debris from oil-in-water (O/W) emulsions**

The ultimate necessity of sample preparation methods is the separation of debris from real-world samples as it can block the microchannels of the devices. Currently, separation of debris is done via filtration, sedimentation etc offline and off the chip. A future goal would be the continuous on-chip separation of debris from the working fluids via electrokinetic or flow cytometry systems in microfluidic channels. 3D conducting micro-pillar or blocks may also be constructed in the main channel for the continuous separation of debris using a dielectrophoretic (DEP) force.

3. Fusion of nano-sized oil droplets in water

Detection systems for oil droplets in water would greatly benefit from the fusion of nano-sized oil droplets. By continuously trapping the sub-micron droplets in an enrichment zone, followed by introducing a pH imbalance[140] can result in the fusion of oil droplets. Physical perturbations, for aiding the fusion process, may also be added to enrichment zone by providing an ACEO flow field.

4. Effect of polyelectrolyte coated microchannels on Faradaic charging mechanisms

In this work, two polyelectrolytes solutions of PSS and PAH are used for hydrophilizing the PDMS-glass and PDMS-PDMS microchannels. The surface coatings show great durability even upto 5 hours of continuous usage. A comparison of electroosmotic mobility and Faradaic charging[136] may be made between surface treated and untreated microchannels. Surface treated microchannels may be helpful in the fabrication of electrokinetic micro-mixers[132, 141] with higher efficiency as they inject additional ions into the electrolyte resulting in stronger net electroosmotic flow and generation of charge gradient in the direction of the applied electric field. In addition, effect of surface coatings on electrokinetic micro-pumps may also be investigated.

References

1. Mascarelli, A., *Deepwater Horizon: After the oil.* Nature, 2010. **467**: p. 22.
2. Marle, L. and G.M. Greenway, *Microfluidic devices for environmental monitoring.* TrAC Trends in Analytical Chemistry, 2005. **24**(9): p. 795-802.
3. marketsandmarkets.com. *Microfluidics Market by Material (Polymer, Glass, Silicon) Application (Pharmaceutical (Genomics, Proteomics, Capillary Electrophoresis) Diagnostic (POC, Clinical, Environmental, Industrial) Drug Delivery (Inhaler, Micropump)) - Global Forecast to 2020*. 2015; Available from: http://www.marketsandmarkets.com/Market-Reports/microfluidics-market-1305.html.
4. Mendoza, W.G., D.D. Riemer, and R.G. Zika, *Application of fluorescence and PARAFAC to assess vertical distribution of subsurface hydrocarbons and dispersant during the Deepwater Horizon oil spill.* Environmental Science: Processes & Impacts, 2013. **15**(5): p. 1017-1030.
5. Ortmann, A.C., et al., *Dispersed Oil Disrupts Microbial Pathways in Pelagic Food Webs.* PLoS ONE, 2012. **7**(7): p. e42548.
6. Watkins, M.B. *Disaster unfolds slowly in the Gulf of Mexico*. 2010; Available from: http://www.boston.com/bigpicture/2010/05/disaster_unfolds_slowly_in_the.html.
7. Carls, M.G., S.D. Rice, and J.E. Hose, *Sensitivity of fish embryos to weathered crude oil: Part I. Low-level exposure during incubation causes malformations, genetic damage, and mortality in larval pacific herring (Clupea pallasi).* Environmental Toxicology and Chemistry, 1999. **18**(3): p. 481-493.
8. Marlow, M. and R.J. Hurtubise, *Liquid–liquid–liquid microextraction for the enrichment of polycyclic aromatic hydrocarbon metabolites investigated with fluorescence spectroscopy and capillary electrophoresis.* Analytica Chimica Acta, 2004. **526**(1): p. 41-49.
9. Yazdi, A.S. and Z. Es'haghi, *Liquid–liquid–liquid phase microextraction of aromatic amines in water using crown ethers by high-performance liquid chromatography with monolithic column.* Talanta, 2005. **66**(3): p. 664-669.
10. Lambert, P., et al., *Field fluorometers as dispersed oil-in-water monitors.* Journal of Hazardous Materials, 2003. **102**(1): p. 57-79.
11. Lambert, P., *A literature review of portable fluorescence-based oil-in-water monitors.* Journal of Hazardous Materials, 2003. **102**(1): p. 39-55.
12. Kim, M., et al., *Hebei Spirit oil spill monitored on site by fluorometric detection of residual oil in coastal waters off Taean, Korea.* Marine Pollution Bulletin, 2010. **60**(3): p. 383-389.
13. Pu, Q., et al., *Ion-Enrichment and Ion-Depletion Effect of Nanochannel Structures.* Nano Letters, 2004. **4**(6): p. 1099-1103.
14. Christopher, G.F. and S.L. Anna, *Microfluidic methods for generating continuous droplet streams.* Journal of Physics D: Applied Physics, 2007. **40**(19): p. R319.
15. Ralf, S., et al., *Droplet based microfluidics.* Reports on Progress in Physics, 2012. **75**(1): p. 016601.
16. Ottino, J.M., *Mixing, Chaotic Advection, and Turbulence.* Annual Review of Fluid Mechanics, 1990. **22**(1): p. 207-254.
17. Gunther, A. and K.F. Jensen, *Multiphase microfluidics: from flow characteristics to chemical and materials synthesis.* Lab on a Chip, 2006. **6**(12): p. 1487-1503.

18. Seo, M., et al., *Continuous Microfluidic Reactors for Polymer Particles.* Langmuir, 2005. **21**(25): p. 11614-11622.
19. Zhang, H., et al., *Exploring Microfluidic Routes to Microgels of Biological Polymers.* Macromolecular Rapid Communications, 2007. **28**(5): p. 527-538.
20. Cramer, C., P. Fischer, and E.J. Windhab, *Drop formation in a co-flowing ambient fluid.* Chemical Engineering Science, 2004. **59**(15): p. 3045-3058.
21. Nie, Z., et al., *Emulsification in a microfluidic flow-focusing device: effect of the viscosities of the liquids.* Microfluidics and Nanofluidics, 2008. **5**(5): p. 585-594.
22. Baroud, C.N., F. Gallaire, and R. Dangla, *Dynamics of microfluidic droplets.* Lab on a Chip, 2010. **10**(16): p. 2032-2045.
23. Shelley L. Anna, H.C.M., *Microscale tipstreaming in a microfluidic flow focusing device.* Physics of Fluids, 2006. **18**(12): p. 12151.
24. Guillot, P., A. Colin, and A. Ajdari, *Stability of a jet in confined pressure-driven biphasic flows at low Reynolds number in various geometries.* Physical Review E, 2008. **78**(1): p. 016307.
25. Willaime, H., et al., *Arnold Tongues in a Microfluidic Drop Emitter.* Physical Review Letters, 2006. **96**(5): p. 054501.
26. Cheng-Tso, C. and L. Gwo-Bin, *Formation of Microdroplets in Liquids Utilizing Active Pneumatic Choppers on a Microfluidic Chip.* Microelectromechanical Systems, Journal of, 2006. **15**(6): p. 1492-1498.
27. Ozen, O., et al., *Electrohydrodynamic linear stability of two immiscible fluids in channel flow.* Electrochimica Acta, 2006. **51**(25): p. 5316-5323.
28. Ozen, O., et al., *Monodisperse Drop Formation in Square Microchannels.* Physical Review Letters, 2006. **96**(14): p. 144501.
29. Srisa-Art, M., A.J. deMello, and J.B. Edel, *Fluorescence Lifetime Imaging of Mixing Dynamics in Continuous-Flow Microdroplet Reactors.* Physical Review Letters, 2008. **101**(1): p. 014502.
30. Casadevall i Solvas, X., et al., *Mapping of Fluidic Mixing in Microdroplets with 1 μs Time Resolution Using Fluorescence Lifetime Imaging.* Analytical Chemistry, 2010. **82**(9): p. 3950-3956.
31. Mary, P., V. Studer, and P. Tabeling, *Microfluidic Droplet-Based Liquid−Liquid Extraction.* Analytical Chemistry, 2008. **80**(8): p. 2680-2687.
32. Wilke, C.R. and P. Chang, *Correlation of diffusion coefficients in dilute solutions.* AIChE Journal, 1955. **1**(2): p. 264-270.
33. Burns, J.R. and C. Ramshaw, *The intensification of rapid reactions in multiphase systems using slug flow in capillaries.* Lab on a Chip, 2001. **1**(1): p. 10-15.
34. Burns, J.R. and C. Ramshaw, *A Microreactor for the Nitration of Benzene and Toluene.* Chemical Engineering Communications, 2002. **189**(12): p. 1611-1628.
35. *Microfluidic flow focusing: drop size and scaling in pressure versus flow-rate-driven pumping.* Electrophoresis, 2005. **26**(19): p. 3716.
36. Thorsen, T., et al., *Dynamic Pattern Formation in a Vesicle-Generating Microfluidic Device.* Physical Review Letters, 2001. **86**(18): p. 4163-4166.
37. Kashid, M.N. and D.W. Agar, *Hydrodynamics of liquid–liquid slug flow capillary microreactor: Flow regimes, slug size and pressure drop.* Chemical Engineering Journal, 2007. **131**(1–3): p. 1-13.
38. Oh, K.W., et al., *Design of pressure-driven microfluidic networks using electric circuit analogy.* Lab Chip, 2012. **12**(3): p. 515-45.
39. Link DR, A.S., Weitz DA, Stone HA, *Geometrically mediated breakup of drops in microfluidic devices.* Phys. Rev. Lett., 2004. **92**(5): p. 054503.
40. Simon, M.G., et al., *A Laplace pressure based microfluidic trap for passive droplet trapping and controlled release.* Biomicrofluidics, 2012. **6**(1): p. 14110-1411013.

41. Crevillén, A.G., et al., *Real sample analysis on microfluidic devices.* Talanta, 2007. **74**(3): p. 342-357.
42. Kokosa, J.M., A. Przyjazny, and M.A. Jeannot, *Solvent Microextraction : Theory and Practice*. 2009: Wiley.
43. Wu, H.F., J.H. Yen, and C.C. Chin, *Combining drop-to-drop solvent microextraction with gas chromatography/mass spectrometry using electronic ionization and self-ion/molecule reaction method to determine methoxyacetophenone isomers in one drop of water.* Anal Chem, 2006. **78**(5): p. 1707-12.
44. Jeannot, M.A. and F.F. Cantwell, *Mass Transfer Characteristics of Solvent Extraction into a Single Drop at the Tip of a Syringe Needle.* Analytical Chemistry, 1997. **69**(2): p. 235-239.
45. Nernst, W., *Theorie der Reaktionsgeschwindigkeit in heterogenen Systemen.* Z. phys. Chem., 1904. **47**(1): p. 52-55.
46. Pedersen-Bjergaard, S. and K.E. Rasmussen, *Liquid−Liquid−Liquid Microextraction for Sample Preparation of Biological Fluids Prior to Capillary Electrophoresis.* Analytical Chemistry, 1999. **71**(14): p. 2650-2656.
47. Shen, G. and H.K. Lee, *Hollow Fiber-Protected Liquid-Phase Microextraction of Triazine Herbicides.* Analytical Chemistry, 2001. **74**(3): p. 648-654.
48. Rezaee, M., et al., *Determination of organic compounds in water using dispersive liquid–liquid microextraction.* Journal of Chromatography A, 2006. **1116**(1–2): p. 1-9.
49. Khalili Zanjani, M.R., et al., *A new liquid-phase microextraction method based on solidification of floating organic drop.* Analytica Chimica Acta, 2007. **585**(2): p. 286-293.
50. Ma, M. and F.F. Cantwell, *Solvent Microextraction with Simultaneous Back-Extraction for Sample Cleanup and Preconcentration: Quantitative Extraction.* Analytical Chemistry, 1998. **70**(18): p. 3912-3919.
51. García Sánchez, M.T., J.L. Pérez Pavón, and B. Moreno Cordero, *Continuous membrane extraction of phenols from crude oils followed by high-performance liquid chromatographic determination with electrochemical detection.* Journal of Chromatography A, 1997. **766**(1–2): p. 61-69.
52. Fernandez Laespada, M.E., J.L. Perez Pavon, and B. Moreno Cordero, *Automated on-line membrane extraction liquid chromatographic determination of phenols in crude oils, gasolines and diesel fuels.* J Chromatogr A, 1999. **852**(2): p. 395-406.
53. F.Probstein, R., *Physicochemical Hydrodynamics* 2005, Hoboken : John Wiley & Sons, Inc.
54. Bernard Betts, W., *The potential of dielectrophoresis for the real-time detection of microorganisms in foods.* Trends in Food Science & Technology, 1995. **6**(2): p. 51-58.
55. Kirby, B., *Micro- and Nanoscale Fluid Mechanics: Transport in Microfluidic Devices*. 2010: Cambridge University Press.
56. Hunter, R.J., *Foundations of Colloidal Science*. Vol. II. 1992: University University Press.
57. Chang, H.C. and L.Y. Yeo, *Electrokinetically driven microfluidics and nanofluidics / Hsueh-Chia Chang, Leslie Y. Yeo*. 2010: Cambridge ; New York : Cambridge University Press, 2010.
58. Kim, S.J., et al., *Direct seawater desalination by ion concentration polarization.* Nat Nano, 2010. **5**(4): p. 297-301.
59. Kwak, R., S.J. Kim, and J. Han, *Continuous-Flow Biomolecule and Cell Concentrator by Ion Concentration Polarization.* Analytical Chemistry, 2011. **83**(19): p. 7348-7355.
60. Phan, D.-T., Y. Chun, and N.-T. Nguyen, *A continuous-flow droplet-based concentrator using ion concentration polarization.* RSC Advances, 2015. **5**(55): p. 44336-44341.
61. Delgado, A.V., et al., *Measurement and interpretation of electrokinetic phenomena.* Journal of Colloid and Interface Science, 2007. **309**(2): p. 194-224.

62. Hunter, R.J. and J.V. Leyendekkers, *Viscoelectric coefficient for water.* Journal of the Chemical Society, Faraday Transactions 1: Physical Chemistry in Condensed Phases, 1978. **74**(0): p. 450-455.
63. Wang, J., *Electrochemical detection for microscale analytical systems: a review.* Talanta, 2002. **56**(2): p. 223-231.
64. Sierra-Rodero, M., J.M. Fernández-Romero, and A. Gómez-Hens, *Determination of fluoroquinolone antibiotics by microchip capillary electrophoresis along with time-resolved sensitized luminescence of their terbium(III) complexes.* Microchimica Acta, 2014. **181**(15): p. 1897-1904.
65. Wang, J., M.P. Chatrathi, and B. Tian, *Capillary electrophoresis microchips with thick-film amperometric detectors: separation and detection of phenolic compounds.* Analytica Chimica Acta, 2000. **416**(1): p. 9-14.
66. Hilmi, A. and J.H.T. Luong, *Micromachined Electrophoresis Chips with Electrochemical Detectors for Analysis of Explosive Compounds in Soil and Groundwater.* Environmental Science & Technology, 2000. **34**(14): p. 3046-3050.
67. Wu, J., et al., *Long-Range AC Electroosmotic Trapping and Detection of Bioparticles.* Industrial & Engineering Chemistry Research, 2005. **44**(8): p. 2815-2822.
68. Chiou, C.-H., et al., *Rapid whole-cell sensing chip for low-level arsenite detection.* Biosensors and Bioelectronics, 2011. **26**(5): p. 2484-2488.
69. Jesus-Perez, N.M. and B.H. Lapizco-Encinas, *Dielectrophoretic monitoring of microorganisms in environmental applications.* Electrophoresis, 2011. **32**(17): p. 2331-57.
70. Lewpiriyawong, N., et al., *Microfluidic characterization and continuous separation of cells and particles using conducting poly(dimethyl siloxane) electrode induced alternating current-dielectrophoresis.* Anal Chem, 2011. **83**(24): p. 9579-85.
71. Lewpiriyawong, N., C. Yang, and Y.C. Lam, *Continuous sorting and separation of microparticles by size using AC dielectrophoresis in a PDMS microfluidic device with 3-D conducting PDMS composite electrodes.* Electrophoresis, 2010. **31**(15): p. 2622-31.
72. Wang, H., et al., *Microfluidic acoustophoretic force based low-concentration oil separation and detection from the environment.* Lab on a Chip, 2014. **14**(5): p. 947-956.
73. Bauer, W.-A.C., et al., *Hydrophilic PDMS microchannels for high-throughput formation of oil-in-water microdroplets and water-in-oil-in-water double emulsions.* Lab on a Chip, 2010. **10**(14): p. 1814-1819.
74. Derzsi, L., et al., *Hydrophilic polycarbonate for generation of oil in water emulsions in microfluidic devices.* Lab on a Chip, 2011. **11**(6): p. 1151-1156.
75. Jankowski, P., et al., *Hydrophilic polycarbonate chips for generation of oil-in-water (O/W) and water-in-oil-in-water (W/O/W) emulsions.* Microfluidics and Nanofluidics, 2013. **14**(5): p. 767-774.
76. Jankowski, P. and P. Garstecki, *Stable hydrophilic surface of polycarbonate.* Sensors and Actuators B: Chemical, 2016. **226**: p. 151-155.
77. Piccin, E., et al., *Generation of water-in-oil and oil-in-water microdroplets in polyester-toner microfluidic devices.* Sensors and Actuators B: Chemical, 2014. **196**: p. 525-531.
78. Park, Y., et al., *Monodisperse Micro-Oil Droplets Stabilized by Polymerizable Phospholipid Coatings as Potential Drug Carriers.* Langmuir, 2015. **31**(36): p. 9762-9770.
79. He, M., et al., *Selective Encapsulation of Single Cells and Subcellular Organelles into Picoliter- and Femtoliter-Volume Droplets.* Analytical Chemistry, 2005. **77**(6): p. 1539-1544.
80. Shim, J.-u., et al., *Simultaneous Determination of Gene Expression and Enzymatic Activity in Individual Bacterial Cells in Microdroplet Compartments.* Journal of the American Chemical Society, 2009. **131**(42): p. 15251-15256.

81. Clausell-Tormos, J., et al., *Droplet-Based Microfluidic Platforms for the Encapsulation and Screening of Mammalian Cells and Multicellular Organisms.* Chemistry & Biology, 2008. **15**(5): p. 427-437.
82. Cai, L.F., et al., *Droplet-based microfluidic flow injection system with large-scale concentration gradient by a single nanoliter-scale injection for enzyme inhibition assay.* Anal Chem, 2012. **84**(1): p. 446-52.
83. Pei, J., Q. Li, and R.T. Kennedy, *Rapid and label-free screening of enzyme inhibitors using segmented flow electrospray ionization mass spectrometry.* J Am Soc Mass Spectrom, 2010. **21**(7): p. 1107-13.
84. Pei, J., J. Nie, and R.T. Kennedy, *Parallel electrophoretic analysis of segmented samples on chip for high-throughput determination of enzyme activities.* Anal Chem, 2010. **82**(22): p. 9261-7.
85. Ahn, K., et al., *Electrocoalescence of drops synchronized by size-dependent flow in microfluidic channels.* Applied Physics Letters, 2006. **88**(26): p. 264105-3.
86. Mazutis, L., et al., *Multi-step microfluidic droplet processing: kinetic analysis of an in vitro translated enzyme.* Lab Chip, 2009. **9**(20): p. 2902-8.
87. Roach, L.S., H. Song, and R.F. Ismagilov, *Controlling nonspecific protein adsorption in a plug-based microfluidic system by controlling interfacial chemistry using fluorous-phase surfactants.* Anal Chem, 2005. **77**(3): p. 785-96.
88. Srisa-Art, M., et al., *Monitoring of real-time streptavidin-biotin binding kinetics using droplet microfluidics.* Anal Chem, 2008. **80**(18): p. 7063-7.
89. Agresti, J.J., et al., *Ultrahigh-throughput screening in drop-based microfluidics for directed evolution.* Proc Natl Acad Sci U S A, 2010. **107**(9): p. 4004-9.
90. Zheng, B., L.S. Roach, and R.F. Ismagilov, *Screening of Protein Crystallization Conditions on a Microfluidic Chip Using Nanoliter-Size Droplets.* Journal of the American Chemical Society, 2003. **125**(37): p. 11170-11171.
91. Kreutz, J.E., et al., *Evolution of Catalysts Directed by Genetic Algorithms in a Plug-Based Microfluidic Device Tested with Oxidation of Methane by Oxygen.* Journal of the American Chemical Society, 2010. **132**(9): p. 3128-3132.
92. Holmberg, K., et al., *Surfactants and Polymers in Aqueous Solution*. 2002, John Wiley & Sons, Ltd.
93. Freer, E.M., H. Wong, and C.J. Radke, *Oscillating drop/bubble tensiometry: effect of viscous forces on the measurement of interfacial tension.* J Colloid Interface Sci, 2005. **282**(1): p. 128-32.
94. Vananroye, A., P. Van Puyvelde, and P. Moldenaers, *Effect of Confinement on Droplet Breakup in Sheared Emulsions.* Langmuir, 2006. **22**(9): p. 3972-3974.
95. *Droplet formation in microfluidic T-junction generators operating in the transitional regime. I. Experimental observations.* Physical Review E, 2012. **85**(1): p. 016322.
96. *Generation of geometrically confined droplets using microchannel arrays effects of channel and step structure.* Ind. Eng. Chem. Res., 2009. **48**(19): p. 8848.
97. Garstecki, P., H.A. Stone, and G.M. Whitesides, *Mechanism for Flow-Rate Controlled Breakup in Confined Geometries: A Route to Monodisperse Emulsions.* Physical Review Letters, 2005. **94**(16): p. 164501.
98. Griffiths, I.M. and H.A. Stone, *Axial dispersion via shear-enhanced diffusion in colloidal suspensions.* EPL (Europhysics Letters), 2012. **97**(5): p. 58005.
99. Akhmetov, D.G., *Vortex Rings [electronic resource] / by D. G. Akhmetov*. 2009: Berlin, Heidelberg : Springer-Verlag Berlin Heidelberg, 2009.
100. Shum, H.C., et al., *Droplet microfluidics for fabrication of non-spherical particles.* Macromol Rapid Commun, 2010. **31**(2): p. 108-18.

101. Golumbic, C., M. Orchin, and S. Weller, *Partition Studies on Phenols. I. Relation between Partition Coefficient and Ionization Constant.* Journal of the American Chemical Society, 1949. **71**(8): p. 2624-2627.
102. Kabalnov, A.S., *Can Micelles Mediate a Mass Transfer between Oil Droplets?* Langmuir, 1994. **10**(3): p. 680-684.
103. Peterson, C.H., et al., *Long-Term Ecosystem Response to the Exxon Valdez Oil Spill.* Science, 2003. **302**(5653): p. 2082-2086.
104. *Handbook of Environmental Fluid Dynamics : Systems, Pollution, Modeling, and Measurements*, H.J. Fernando, Editor. December 12, 2012, CRC Press. p. 587.
105. Hunter, R.J., *COLLOID SCIENCE*, in *Zeta Potential in Colloid Science*. 1981, Academic Press: New York. p. ii.
106. Yang, C., *Transport of Liquid in Rectangular Microchannels by Electroosmotic Pumping*, in *Microfluidics and BioMEMS Applications*, F.H. Tay, Editor. 2002, Springer US. p. 265-285.
107. Chuan-Hua, C. and J.G. Santiago, *A planar electroosmotic micropump.* Microelectromechanical Systems, Journal of, 2002. **11**(6): p. 672-683.
108. Islam, N. and J. Wu, *Microfluidic transport by AC electroosmosis.* International MEMS Conference, Journal of Physics: Conference Series 2006. **34**.
109. Pak Kin, W., et al. *An AC electroosmotic processor for biomolecules*. in *TRANSDUCERS, Solid-State Sensors, Actuators and Microsystems, 12th International Conference on, 2003*. 2003.
110. Bown, M.R. and C.D. Meinhart, *AC electroosmotic flow in a DNA concentrator.* Microfluidics and Nanofluidics, 2006. **2**(6): p. 513-523.
111. Gagnon, Z. and H.C. Chang, *Aligning fast alternating current electroosmotic flow fields and characteristic frequencies with dielectrophoretic traps to achieve rapid bacteria detection.* Electrophoresis, 2005. **26**(19): p. 3725-37.
112. Pohl, H.A., *Dielectrophoresis- The Behaviour of Neutral Matter in Nonuniform Electric Fields*. 1978, Cambridge(UK): Cambridge University Press
113. Denner, V. and H.A. Pohl, *Dielectrophoretic force in electrostatic fields.* Journal of Electrostatics, 1982. **13**(2): p. 167-174.
114. Nilsson, J., et al., *Review of cell and particle trapping in microfluidic systems.* Analytica Chimica Acta, 2009. **649**(2): p. 141-157.
115. Thomas, R.S., H. Morgan, and N.G. Green, *Negative DEP traps for single cell immobilisation.* Lab Chip, 2009. **9**(11): p. 1534-40.
116. Rosenthal, A. and J. Voldman. *Simple, Strong, size-selective dielectrophoretic traps for single-cell patterning*. in *Micro-Total Analysis Systems 2004, Proceedings of uTAS 2004*. 2004. Malmo, Sweden: Royal Society of Chemistry, Cambridge.
117. Donato, S.S., et al., *Metabolic viability of Escherichia coli trapped by dielectrophoresis in microfluidics.* Electrophoresis, 2013. **34**(4): p. 575-82.
118. Wang, X.B., et al., *Selective dielectrophoretic confinement of bioparticles in potential energy wells.* Journal of Physics D: Applied Physics, 1993. **26**(8): p. 1278.
119. Wang, W., C. Yang, and C.M. Li, *On-demand microfluidic droplet trapping and fusion for on-chip static droplet assays.* Lab Chip, 2009. **9**(11): p. 1504.
120. ZHANG, H.B., M.J. EDIRISINGHE, and S.N. JAYASINGHE, *Flow behaviour of dielectric liquids in an electric field.* Journal of Fluid Mechanics, 2006. **558**: p. 103-111.
121. Nuttawut, L., *Continuous separation and manipulation of particles and cells using dielectrophoresis.* . 2011, Nanyang Technological University, Singapore.
122. Conn, C.A., et al., *Visualizing oil displacement with foam in a microfluidic device with permeability contrast.* Lab Chip, 2014. **14**(20): p. 3968-77.

123. He, J., et al., *Damage study of ITO under high electric field.* Thin Solid Films, 2000. **363**(1–2): p. 240-243.
124. Delattre, C., et al., *Macro to microfluidics system for biological environmental monitoring.* Biosensors and Bioelectronics, 2012. **36**(1): p. 230-235.
125. Das, D., et al., *Continuous Droplet-based Liquid-Liquid Extraction of Phenol from Oil* Separation Science and Technology, 15 Jan, 2015. **50**(7): p. 7.
126. Soares, R.R.G., et al., *On-chip sample preparation and analyte quantification using a microfluidic aqueous two-phase extraction coupled with an immunoassay.* Lab on a Chip, 2014. **14**(21): p. 4284-4294.
127. Kuijt, J., et al., *Laser-induced fluorescence detection at 266 nm in capillary electrophoresis: Polycyclic aromatic hydrocarbon metabolites in biota.* Journal of Chromatography A, 2001. **907**(1–2): p. 291-299.
128. Phan, D.-T., et al., *Sample concentration in a microfluidic paper-based analytical device using ion concentration polarization.* Sensors and Actuators B: Chemical, 2016. **222**: p. 735-740.
129. Lee, J.H., Y.-A. Song, and J. Han, *Multiplexed proteomic sample preconcentration device using surface-patterned ion-selective membrane.* Lab on a Chip, 2008. **8**(4): p. 596-601.
130. MacDonald, B.D., et al., *Out-of-plane ion concentration polarization for scalable water desalination.* Lab on a Chip, 2014. **14**(4): p. 681-685.
131. Jännig, O. and N.-T. Nguyen, *A polymeric high-throughput pressure-driven micromixer using a nanoporous membrane.* Microfluidics and Nanofluidics, 2011. **10**(3): p. 513-519.
132. Ng, W.Y., et al., *DC-biased AC-electroosmotic and AC-electrothermal flow mixing in microchannels.* Lab on a Chip, 2009. **9**(6): p. 802-809.
133. Ng, W.Y., et al., *DC-biased AC-electrokinetics: a conductivity gradient driven fluid flow.* Lab on a Chip, 2011. **11**(24): p. 4241-4247.
134. Das, D., et al., *Continuous detection of trace level concentration of oil droplets in water using microfluidic AC electroosmosis (ACEO).* RSC Advances, 2015. **5**(86): p. 70197-70203.
135. Chen, W., R.H.W. Lam, and J. Fu, *Photolithographic surface micromachining of polydimethylsiloxane (PDMS).* Lab on a Chip, 2012. **12**(2): p. 391-395.
136. Ng, W.Y., Y.C. Lam, and I. Rodríguez, *Experimental verification of Faradaic charging in ac electrokinetics.* Biomicrofluidics, 2009. **3**(2): p. 022405.
137. Kim, S.J., et al., *Concentration Polarization and Nonlinear Electrokinetic Flow near a Nanofluidic Channel.* Physical Review Letters, 2007. **99**(4): p. 044501.
138. Sameenoi, Y., et al., *Poly(dimethylsiloxane) cross-linked carbon paste electrodes for microfluidic electrochemical sensing.* Analyst, 2011. **136**(15): p. 3177-3184.
139. Suea-Ngam, A., et al., *Electrochemical droplet-based microfluidics using chip-based carbon paste electrodes for high-throughput analysis in pharmaceutical applications.* Analytica Chimica Acta, 2015. **883**: p. 45-54.
140. Caschera, F., S. Rasmussen, and M.M. Hanczyc, *An Oil Droplet Division–Fusion Cycle.* ChemPlusChem, 2013. **78**(1): p. 52-54.
141. Chang, C.-C. and R.-J. Yang, *Electrokinetic mixing in microfluidic systems.* Microfluidics and Nanofluidics, 2007. **3**(5): p. 501-525.

Publications

1) **Das, D**., V. Kang, Y.; Chan, V.; Yang, C." A multi-module microfluidic platform for continuous pre-concentration of water-soluble ions and separation of oil droplets from oil-in-water (O/W) emulsions using a positive DC-biased AC electrokinetic technique." (under review, RSC Lab on a Chip).

2) **Das, D**.; Yan, Z.; Menon, N.V.; Kang, Y.; Chan, V.; Yang, C. (20 Aug, 2015). "Continuous detection of trace level concentration of oil droplets in water using microfluidic AC electroosmosis (ACEO)." RSC Advances, 5(86): 70197-70203.

2) **Das, D**.; Duraiswamy, S.; Yi, Z.; Chan, V.; Yang, C. (15 Jan, 2015) "Continuous Droplet-based Liquid-Liquid Extraction of Phenol from Oil". Separation Science and Technology, 50(7): 1023-1029.